Photo: Bruno Marty / IRD

Chapter 3

Observed and expected changes to the tropical Pacific Ocean

Alexandre S Ganachaud, Alex Sen Gupta, James C Orr, Susan E Wijffels, Ken R Ridgway, Mark A Hemer, Christophe Maes, Craig R Steinberg, Aline D Tribollet, Bo Qiu and Jens C Kruger

'The oceans are warming.' (Bindoff et al. 2007)[i]

i Bindoff et al. (2007) Observations: Oceanic climate change and sea level. In: S Solomon, D Qin, M Manning, Z Chen, M Marquis, KB Averyt, M Tignor and HL Miller (eds) *Climate Change 2007: The Physical Science Basis. Contribution of Working Group I to the Fourth Assessment Report of the Intergovernmental Panel on Climate Change.* Cambridge University Press, Cambridge, United Kingdom, and New York, United States of America, pp. 385–428.

Contents

	Page
3.1 Introduction	**103**
3.1.1 Use of climate simulations	104
3.2 Features of the tropical Pacific Ocean	**105**
3.2.1 Large-scale currents	105
3.2.2 Ocean temperature	110
3.2.3 Ocean eddies	120
3.2.4 Nutrient supply	123
3.2.5 Dissolved oxygen	127
3.2.6 Ocean acidification	129
3.2.7 Wave height	131
3.2.8 Sea level	135
3.2.9 Coastal circulation and island effects	137
3.3 Observed and projected changes in the tropical Pacific Ocean	**141**
3.3.1 Large-scale currents	141
3.3.2 Ocean temperature	143
3.3.3 Ocean eddies	149
3.3.4 Nutrient supply	150
3.3.5 Dissolved oxygen	157
3.3.6 Ocean acidification	159
3.3.7 Wave height	163
3.3.8 Sea level	164
3.3.9 Coastal circulation and island effects	167
3.4 Summary of present-day ocean features, and observed and projected changes	**169**
3.5 Recommendations to reduce uncertainties in projecting future changes to the tropical Pacific Ocean	**172**
3.5.1 SPCZ and ENSO	172
3.5.2 Integrating biogeochemical and physical models	173
3.5.3 Dynamical downscaling	173
3.5.4 Long-term observations and monitoring	173
References	**176**
Appendix	188

3.1 Introduction

The fish and invertebrates harvested from the tropical Pacific Ocean and the coastal waters of the region, and the ecosystems that support these species, are influenced not only by surface climate; they also depend intimately on the oceanic environment. Large- and small-scale circulation patterns influence larval dispersal and the migration of species; water temperature, salinity, nutrient availability, dissolved oxygen concentration and pH affect biological activity; and oceanic currents, waves and sea level shape coastal habitats. Together, these properties of the tropical Pacific Ocean[ii] have a profound effect on the productivity of oceanic and coastal fisheries, and coastal aquaculture.

Understanding how these features of the ocean vary is one of the primary keys to forecasting production from the fisheries sector. Resolving this puzzle is a major challenge, however, because the tropical Pacific Ocean varies across an enormous range of spatial and temporal scales. For example, within just a few days, cloud cover, local upwelling, surface mixing due to storms or oceanic eddies can substantially modify sea surface temperature, salinity, currents and nutrient supply at the scale of reefs and islands. On larger spatial scales, seasonal changes in nutrient upwelling have a significant effect on primary productivity (Chapter 4). Closer to the equator, key properties of the Pacific Ocean are dominated by the interannual variations of the El Niño-Southern Oscillation (ENSO) (Chapter 2). On longer time scales, variations in the strength of the mid-latitude westerly winds produce climate 'regime shifts', like those recorded in 1925 and 1943[1], and in 1976–1977[2]. Regime shifts are characterised by abrupt ENSO-like changes that can last for several decades, commonly associated with the Interdecadal Pacific Oscillation (IPO) or the closely related Pacific Decadal Oscillation (PDO)[3–5]. Profound changes over and above natural climate variability are also occurring, due to the build-up of anthropogenic greenhouse gas emissions in the atmosphere (Chapters 1 and 2).

The purpose of this chapter is to provide fisheries scientists and managers with fundamental information on the main features of the tropical Pacific Ocean, how these features have changed over the past few decades due to climate change (Chapter 2), and how they are projected to change as the levels of CO_2 increase and the earth continues to warm.

The oceanic features we examine include: large-scale currents, sea surface temperature and salinity, subsurface temperature, eddies, nutrients, dissolved oxygen, ocean acidification, wave height, sea-level rise and coastal and island effects.

ii Defined as the area 25°N to 25°S and 130°E to 130°W.

3.1.1 Use of climate simulations

To describe the features of the tropical Pacific Ocean listed above, and to make projections, we have drawn on published knowledge of the oceanography of the region and our analyses of a suite of coupled-atmosphere and ocean climate models from the Coupled Model Intercomparison Project Phase 3 (CMIP3) (Chapter 1). These state-of-the-art CMIP3 simulations formed the basis of the Intergovernmental Panel on Climate Change (IPCC) projections of future climate in the Fourth Assessment Report (AR4)[6]. They cover a large range of grid resolutions and use a diverse set of parameterisations to account for processes not simulated explicitly. The models often perform very differently with respect to their realism in simulating various features of the atmosphere and ocean. Before performing our analyses of future projections, we validated individual models against the observed (1980–1999) mean state of the ocean and assessed the ability of the models to reproduce ENSO-like behaviour – the dominant driver of interannual variability in the region (Chapter 2). To do this, we analysed the strength, spatial structure and temporal characteristics of the simulated ENSO, in conjunction with the results from previous studies[7–10].

As discussed in Chapter 2, while most models reproduce some form of ENSO-like variability, the level of realism differs markedly. A few, for example, produce an ENSO that occurs almost every second year. There are also considerable differences in the strength and seasonality of anomalies in sea surface temperature[7]. Of major concern is a systematic bias in the spatial structure of ENSO in almost all the models, whereby the maximum warming that occurs during El Niño events is displaced too far to the west. As a result, we retained 13 of the CMIP3 models (Appendix 3.1) that exhibited ENSO-like behaviour with a dominant frequency between 2 and 7 years, and a reasonable representation of the Warm Pool in the western Pacific (Chapter 2).

Even after model selection, some biases persisted. Where these biases did not occur across a large number of models, we used the 'multi-model mean' to 'average out' many of the biases in individual models. This averaging process generally gives a consistently more realistic representation of the real world than any individual model[11] (Chapter 1), but masks the possibility of more extreme changes. We used the multi-model mean to provide the best estimate of (1) the present state of the tropical Pacific Ocean centred on 1990 (1980–1999); and (2) future projections for the main features of the ocean described above of interest to fisheries in the tropical Pacific.

As outlined in Chapter 1, we considered the future projections for both a relatively low emissions (B1) and a relatively high emissions (A2) scenario for 2035 and 2100. To this end, we used 20-year segments of each model's output for 2025 to 2044 (hereafter referred to as 2035) and 2080 to 2099 (hereafter referred to as 2100)[iii], respectively, to define a mean climate and to average out any short-term variability. Most of the diagnostics are based on the mean of the selected subset of climate models (multi-model mean). Student's *t*-tests were used to determine whether the climate-driven

iii Some global climate models only make projections to 2099, so we have used the 20-year period 2080–2099 to represent 2100.

changes in oceanic features could be considered to be statistically significant. Although some long-term (multi-decadal to millennial) variability may be present in the simulations, resulting in a bias in mean-state estimates, this is essentially removed by using the multi-model mean.

3.2 Features of the tropical Pacific Ocean

3.2.1 Large-scale currents

Both large- and small-scale currents play a major role in the distribution and abundance of fish and invertebrates that support the oceanic and coastal fisheries of the tropical Pacific. The movement of tuna is linked to the horizontal displacement of water of a suitable temperature, and to vertical changes in the depth of the mixed layer that determines their surface habitat (Chapters 4 and 8). Areas where currents diverge or converge are of major importance because they are associated with the thermal fronts, upwelling and eddies described later in this chapter. These processes enhance local productivity and create good feeding areas for tuna (Chapter 4). For species reliant on coastal habitats, changes in currents can affect the distribution and abundance of corals and other invertebrates that create coral reef habitats (Chapter 5). Currents also influence the replenishment of key species supporting coastal fisheries at the end of their pelagic phase: postlarvae of fish and invertebrates use currents to find the habitats on which they depend as adults (Chapter 9).

3.2.1.1 Currents flowing into the region

The main currents in the tropical Pacific Ocean (Figure 3.1) are driven by the easterly trade winds[12] (Chapter 2). The primarily westward flow of these currents extends over the top few hundred metres of the ocean and reaches the western boundary of the basin. In the first few tens of metres, an interaction between the Coriolis force (associated with the rotation of the earth) and the trade winds cause 'Ekman transport' (Box 3.1), where the surface waters in the tropics move poleward in both hemispheres. Conversely, at latitudes poleward of 25°N and 25°S, the prevailing westerly winds force the surface waters towards the equator, resulting in a convergence of these waters between 15°–30°N and 15°–30°S. This convergence produces a build-up in sea surface height (SSH) around 10°–15°N to 10°–15°S. The sea-level slope is associated with pressure forces that drive two broad geostrophic westward flows (Box 3.1): the North Equatorial Current (NEC) and the South Equatorial Current (SEC) (Figure 3.1b). The NEC and SEC are the equatorial branches of two basin-scale circular circulation patterns: the large subtropical gyres in the northern and southern Pacific Ocean, with their poleward margins outside the domain at higher latitudes. Near the surface (0–80 m), frictional forces from the wind are superimposed on the geostrophic NEC and SEC, adding a component that is perpendicular to the local wind direction due to Ekman transport (see blue streamlines showing Ekman currents in Figure 3.1). For example, south of the equator the southeasterly trade winds bend the surface streamlines to the southwest.

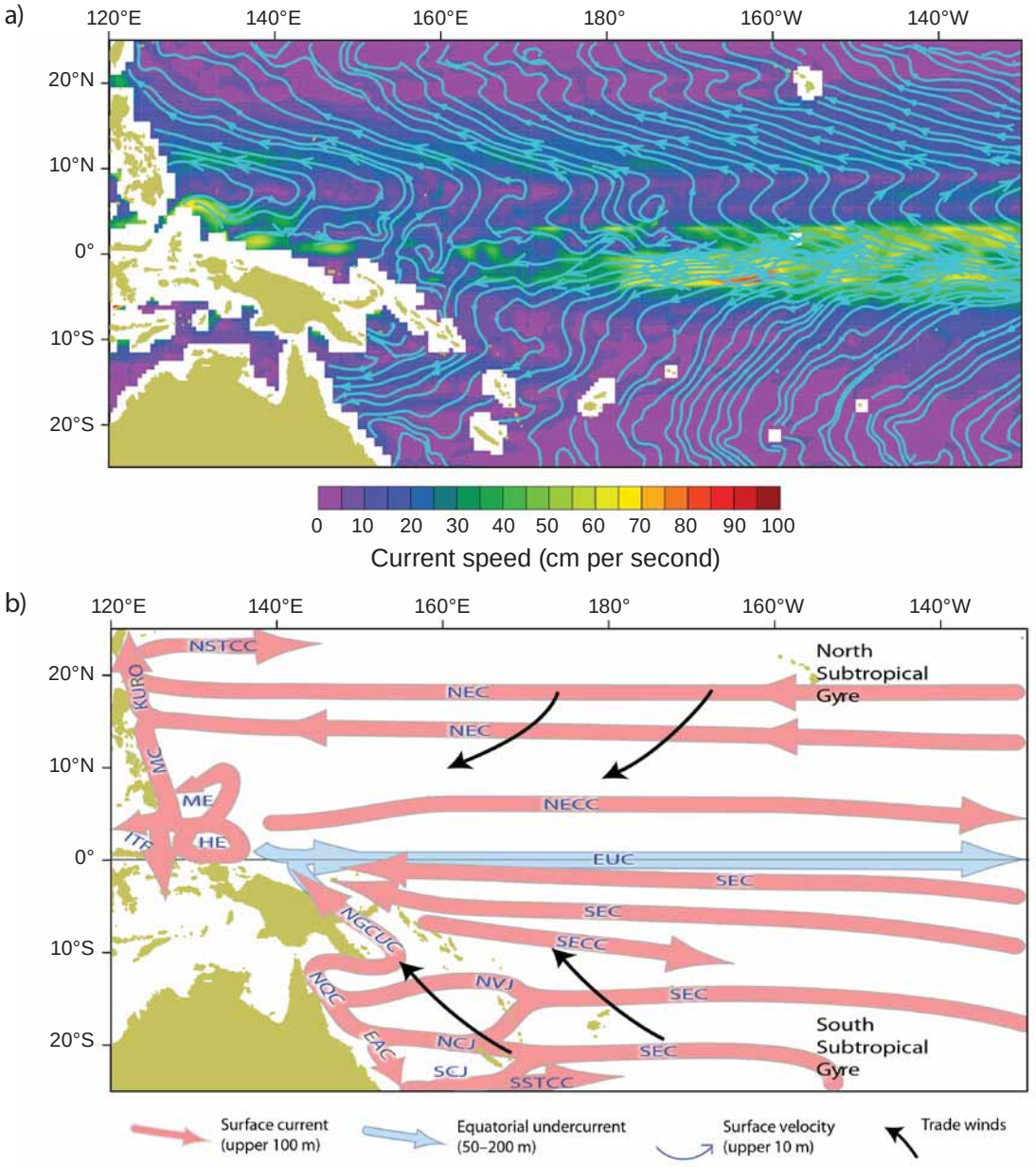

Figure 3.1 (a) Ocean surface currents in the tropical Western and Central Pacific Ocean, based on satellite data and *in situ* climatology (source: Sudre and Morrow 2008)[189]. As indicated by the stream lines, surface flow is generally directed to the left of the wind in the Southern Hemisphere, and to the right in the Northern Hemisphere, due to Ekman transport (Box 3.1). (b) The main ocean currents in the upper 100 to 200 m of the water column. Currents shown are: North Subtropical Counter Current (NSTCC); Kuroshio Current (KURO); Mindanao Current (MC); Mindanao Eddy (ME); Halmahera Eddy (HE); North Equatorial Current (NEC); North Equatorial Counter Current (NECC); Equatorial Undercurrent (EUC); Indonesian Throughflow (ITF); New Guinea Coastal Undercurrent (NGCUC); North Queensland Current (NQC); East Australian Current (EAC); North Vanuatu Jet (NVJ); North Caledonian Jet (NCJ); South Caledonian Jet (SCJ); South Equatorial Counter Current (SECC); South Equatorial Current (SEC) and South Subtropical Counter Current (SSTCC).

Box 3.1 Motion in the ocean

At any particular place in the ocean, a number of different forces act to create a current and determine its direction and strength. The main forces that cause water to move and generate currents are related to (1) the gravitational attraction by the moon and sun, causing tidal circulation; (2) the wind, which exerts a stress at the surface of the ocean and can directly drive currents in the upper few tens of metres; and (3) pressure gradients, which may be formed either through differences in sea surface height or via horizontal differences in water density. Once water is in motion, two additional forces also influence currents. The first is friction, which always retards motion. Friction is important mainly near coastlines and the bottom of the ocean, or where adjacent currents are moving at different speeds or in different directions. The second is the Coriolis force. This (apparent) force is a consequence of being on a rotating planet. The effect of the Coriolis force is to deflect water in motion to the left in the Southern Hemisphere and to the right in the Northern Hemisphere. The effect of the Coriolis force diminishes at the equator. This force results in the two ubiquitous but counter-intuitive types of current described below.

Ekman transport (see diagram below): Away from the equator, if a wind continues to blow on the surface of the ocean for an extended period, the resulting surface current does not flow in the direction of the wind as might be expected. Instead, the average flow is 90° to the left of the wind direction in the Southern Hemisphere, or to the right of the wind in the Northern Hemisphere, as a consequence of the Coriolis force. An important example of Ekman transport occurs on either side of the equator, where the easterly trade winds cause southward water motion in the Southern Hemisphere (i.e. 90° to the left of the direction of the wind) and northward water motion in the Northern Hemisphere (i.e. 90° to the right of the direction of the wind). The result is water flowing away from the equator on either side. To compensate for this surface divergence caused by Ekman transport, cool water is drawn up from the subsurface, a process known as 'upwelling'. At the equator, there is no Coriolis force and the surface water flows in the same direction as the wind.

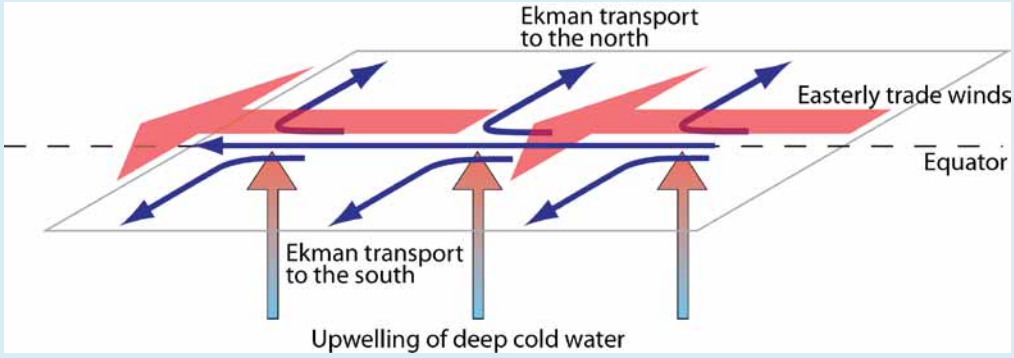

Geostrophic motion (see diagram below): Horizontal pressure differences exist in the ocean when there is a slope at the surface of the ocean (e.g. set up by a strong wind) or via lateral changes in water density (e.g. cold water abutting warm water). Where pressure differences like these occur, water does not flow directly from the high-pressure region to the low-pressure region as one might expect. Instead, it flows at 90° to the left of the pressure gradient force in the Southern Hemisphere (or to the right in the Northern Hemisphere) because of the Coriolis force. A result of geostrophic motion is that any horizontal change in water density (e.g. due to a front in temperature or salinity) will be associated with a current that is perpendicular to the front.

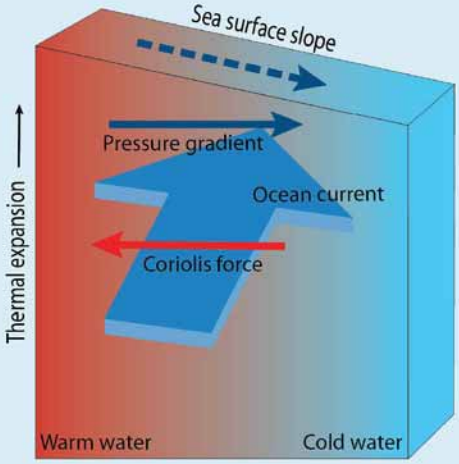

Different forces are important in different regions of the tropical Pacific Ocean. In the surface layer (i.e. the first few tens of metres), Ekman transport occurs and surface currents tend to move perpendicular to the wind direction. Away from the surface, and other oceanic boundaries, the flow tends to be geostrophic and is dictated by horizontal density gradients due to changes in temperature and/or salinity, or variations in sea surface height. If density gradients become very strong, or large current shears exist, flow can become turbulent and form eddies. The large-scale currents of the tropical Pacific Ocean are formed by the combination of the processes described above. Horizontal differences in the wind field drive surface Ekman currents, which change from location to location. These shifts cause upwelling and downwelling and ultimately pressure gradients that in turn lead to large-scale geostrophic currents that extend into the deep ocean.

3.2.1.2 Western boundary current system

The westward flowing NEC and SEC both encounter islands in their passage, and eventually the western boundaries of the basin. On average, the NEC occupies a broad region from 8°N to 20°N[13]. As the NEC reaches the western boundary, it divides to feed the Kuroshio Current to the north (called the 'Philippines Current' at this latitude[13]), and the Mindanao Current and Mindanao Eddy to the south (**Figure 3.1**). The average

latitude where the surface NEC bifurcates is 13.3°N (including Ekman transport) but this varies seasonally from 15°N in July to 17°N in December[13]. A similar process occurs in the southern Pacific, with the SEC splitting into the equatorward North Queensland Current and the poleward East Australian Current, with the bifurcation located at 16°S near the surface and 22°S at a depth of 1000 m[14,15]. The location of this bifurcation also varies seasonally by 1.25° latitude, with a displacement toward the equator in November to December[16].

When these broad currents encounter islands and land masses, the flow is diverted (Section 3.2.9). The pathways of the SEC are complicated by the presence of many islands and ridges in the western Pacific. As a result, the SEC splits into three jets, the South Caledonian Jet, the North Caledonian Jet and the North Vanuatu Jet[17–19] (Figure 3.1). The northern component of the bifurcation enters the Solomon Sea as the New Guinea Coastal Undercurrent and exits towards the equator through three narrow straits within Solomon Islands[20]. This latter flow, along with the Mindanao Current flow, converges towards the equator, feeding the Warm Pool (Section 3.2.2), the Indonesian Throughflow[21,22] and, at greater depth, the eastward flowing Equatorial Undercurrent[23] (**Figure 3.1**).

3.2.1.3 Eastward flowing counter currents

The westward-flowing NEC and SEC are also altered by the presence of the Intertropical Convergence Zone (ITCZ) and the South Pacific Convergence Zone (SPCZ) (Chapter 2). These convergence zones alter local wind conditions, generating horizontal shear ('curl') in the wind field. This wind curl produces two eastward-flowing, surface-intensified counter currents through Ekman transport and geostrophic processes (Box 3.1), known as the North Equatorial Counter Current (NECC) under the ITCZ[24], and the South Equatorial Counter Current (SECC) under the SPCZ[14,25] (Figure 3.2). Another modification to the flow comes from local changes in the trade winds as they interact with island topography. This interaction modifies the flow of water downwind of islands (Section 3.2.8). In the southern Pacific, similar counter currents occur in the Coral Sea west of Vanuatu[26] (**Figure 3.2**) and near the Marquesas Islands[27,28], causing the upwelling of nutrients. Near Hawaii, an eastward flowing current is created that flows against the NEC, named the Hawaii Lee Counter Current[29]. Eddies are formed at the boundaries where the westward flowing NEC and the eastward flowing NECC meet. These eddies also have the potential to bring nutrients to the surface waters[30].

3.2.1.4 Variability in large-scale currents

Currents in the central south Pacific remain fairly constant throughout the year, whereas currents in the western Pacific vary substantially in both intensity and direction (**Figure 3.3**). In the central eastern equatorial region, current direction actually reverses in different seasons. For example, there are strong seasonal variations

in the NEC, NECC, SEC and SECC associated with the migration of the SPCZ and ITCZ[31] (**Figure 3.3**). Variations in currents on interannual time scales can be even more dramatic, due to the influence of ENSO. A change in wind forcing in one location can have large effects that extend well outside the region directly affected by the wind. During El Niño events, there is a weakening or even a reversal of the southeast trade winds, particularly in the west of the Pacific basin. The resulting oceanic disturbance propagates eastward at high speed along the equator as equatorial waves[32] (Section 2.3.2.3). These waves can result in a reversal of the large-scale westward current direction, with eastward velocities reaching up to 50 cm per second[33].

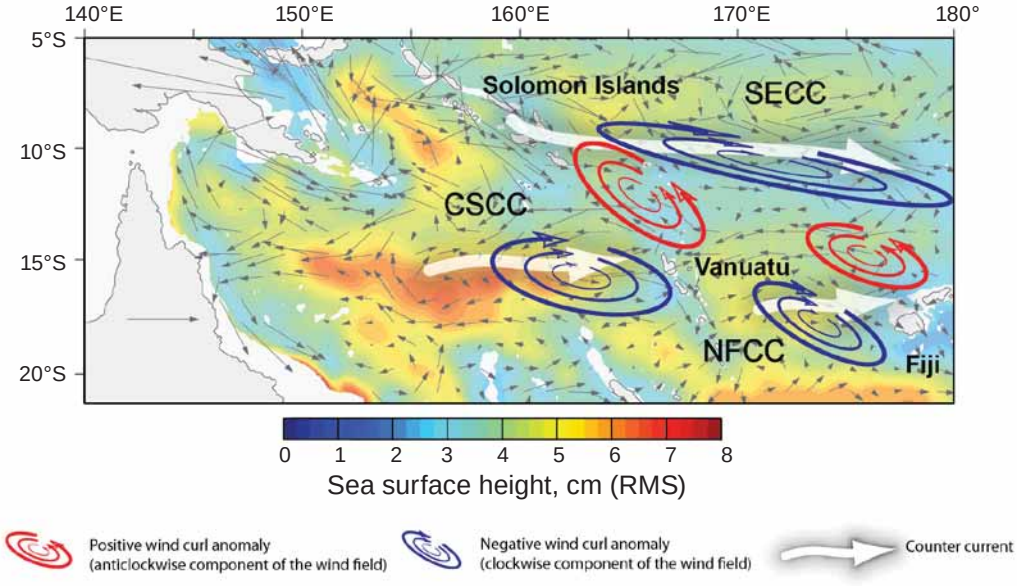

Figure 3.2 Formation of counter currents in the tropical Pacific Ocean. Weakening trade winds towards the north of the South Pacific Convergence Zone area create a clockwise forcing on the ocean by the wind field (negative wind curl). This generates pressure forces in the ocean that set in motion a counter current, the South Equatorial Counter Current (SECC) that flows against the broad westward South Equatorial Current (Figure 3.1). West of Vanuatu and Fiji, similar disruptions to the trade winds create wind stress curl dipoles that generate the Coral Sea Counter Current (CSCC) and the North Fiji Counter Current (NFCC). The presence of counter currents is also revealed by variability in sea surface height, as measured by satellite data (colour) over short time scales (180 days or less) (source: Qiu et al. 2009)[26], RMS = root mean square of sea surface height, in cm.

3.2.2 Ocean temperature

Water temperature is another key feature of the ocean that strongly affects the abundance and distribution of the fish and invertebrates supporting fisheries and aquaculture in the tropical Pacific. Each species has adapted to tolerate a specific range of temperatures under which it can optimise its growth and reproductive success (Chapters 8, 9 and 11). As a result, ocean warming is likely to have an effect

on egg production, which may be either positive or negative depending on whether the target species is close to its thermal optimum. However, increases in temperature above normal maxima are expected to have negative effects on the overall viability of some populations of fish and invertebrates. The effects of water temperature on the distribution and abundance of skipjack tuna are of special interest to Pacific Island countries and territories (PICTs) considering the strong influence that ENSO events have on this species (Chapter 8).

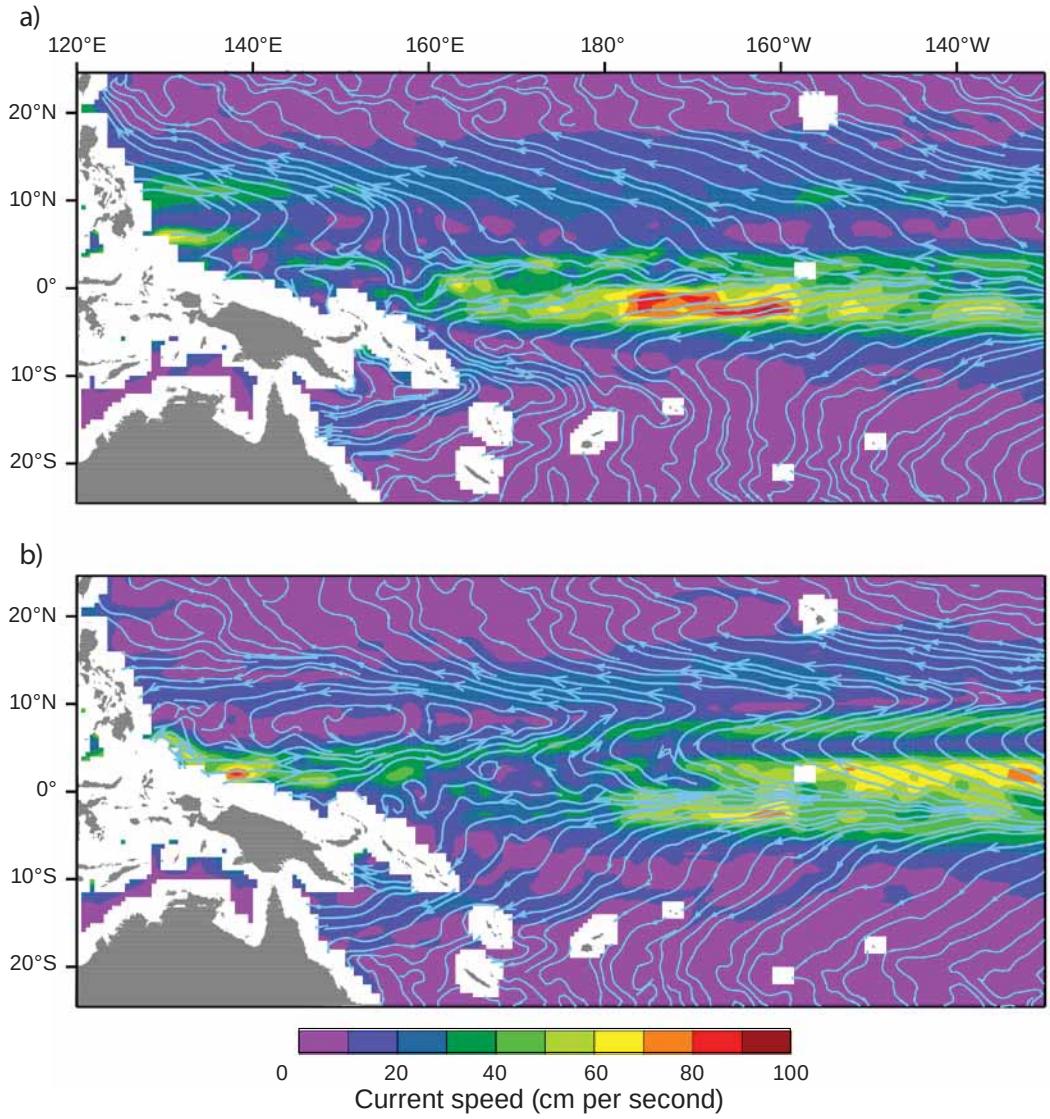

Figure 3.3 (a) Average seasonal variations in the speed of the surface currents of the tropical Pacific Ocean (1999–2007) from June to August, and (b) December to February, based on satellite data and *in situ* climatology (source: Sudre and Morrow 2008)[189]. The blue streamlines indicate the direction of currents.

3.2.2.1 Sea surface temperatures

As explained in Chapter 2, the sea surface temperature (SST) of the tropical Pacific Ocean varies spatially and temporally. More solar heat is absorbed by the ocean near the equator than at higher latitudes. This rise in temperature results in a pole-to-equator SST gradient (Chapter 2). However, there are regional deviations from this large-scale pattern. For example, the southeast trade winds push the warmest waters to the western side of the Pacific basin, forming the Warm Pool – a large heat reservoir intimately associated with ENSO. Along the equator and the coastline of South America, the prevailing winds cause equatorial and coastal upwelling, respectively, bringing cool, deep waters rich in nutrients to the surface. This process results in a relatively cool tongue of water extending from South America along the equator to the central Pacific, where it meets the eastern edge of the Warm Pool near the dateline. Sea surface temperature also varies seasonally. Away from the equator, SST varies by up to 7°C throughout the year; whereas seasonal changes in SST near the equator are weak and the largest variations (2 to 3°C) occur from one year to another. This interannual variability is mainly associated with ENSO (Chapter 2). Thus, SST at any given location and time depends on a broad range of processes, including diurnal and seasonal solar heating modulated by cloudiness, air-sea heat exchanges, heat transport by oceanic circulation, eddies (Section 3.2.3) and other local ocean processes, such as vertical mixing and upwelling (**Figure 3.4**).

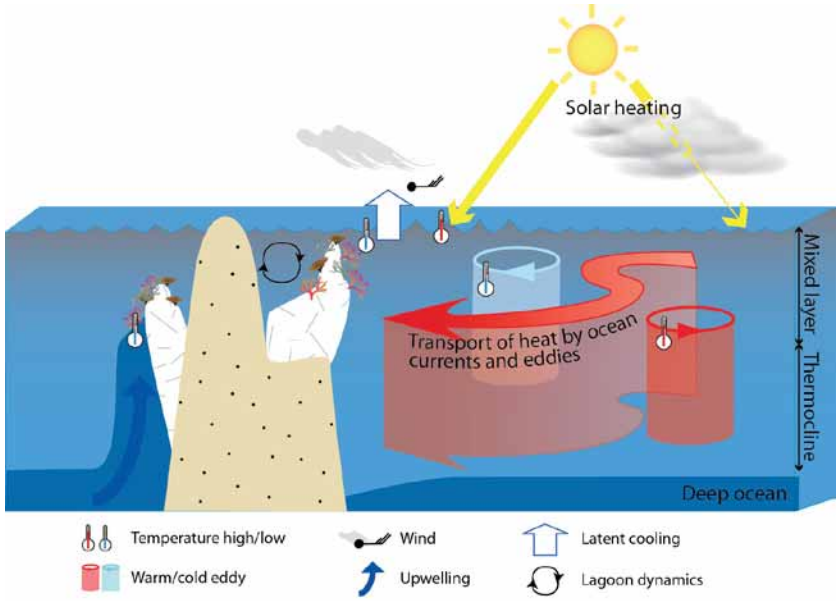

Figure 3.4 Factors affecting the temperature of the upper layer of the ocean. Surface waters are heated by incoming solar radiation, modulated by cloud cover. Winds create increased evaporation, which extracts latent heat from the ocean causing it to cool. Contact between the atmosphere and ocean also drives direct heat fluxes. The wind generates mixing with deeper and colder waters, resulting in cooling at the surface and more homogenised temperatures within the 'mixed layer' (Section 3.2.4). Currents, eddies and upwellings also transport warmer or colder water into or away from the upper layer of the ocean (Sections 3.2.3 and 3.2.9).

3.2.2.2 Vertical temperature structure

The temperature of the tropical Pacific Ocean also varies with depth – it declines as depth increases (**Figure 3.5**). This variation in temperature occurs because most of the sun's heat is absorbed near the surface, with little energy reaching below the first 100 m. The warmer surface water has lower density than the deeper cooler waters below and where these two layers meet at the 'thermocline', the water temperature changes rapidly. The thermocline is the part of the water column with the strongest vertical temperature gradient. In the tropical Pacific Ocean, the thermocline usually lies within the upper 500 m of the water column and the temperature drops by about 20°C. Below this layer, the ocean remains cold to abyssal depths.

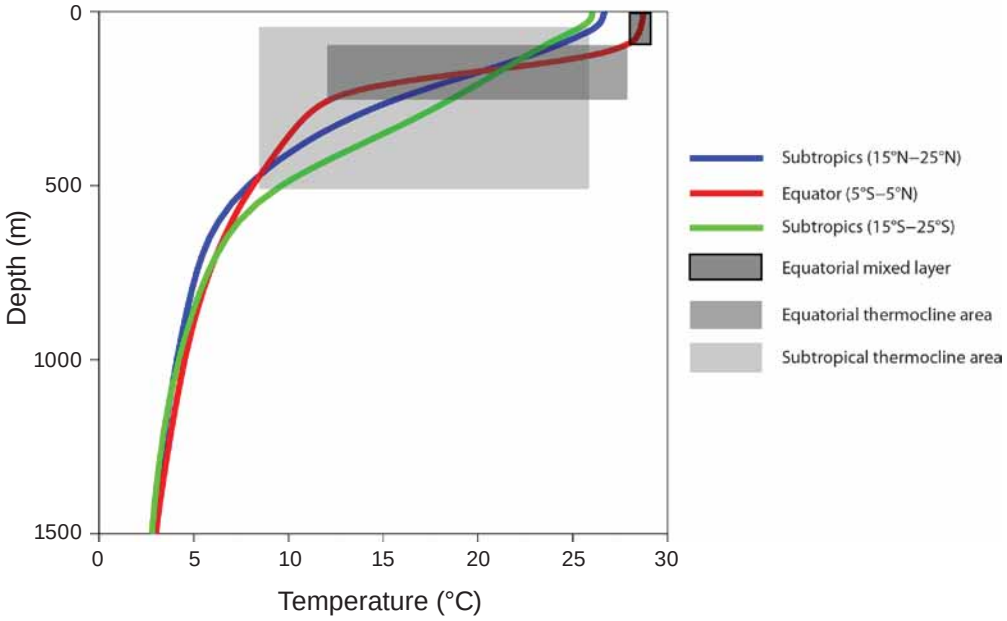

Figure 3.5 Average water temperature from the surface to a depth of 1500 m for three typical locations in the tropical Pacific: equator (red line); north subtropics (blue line); and south subtropics (green line). The equatorial thermocline area is indicated by the darker grey bar; the lighter grey bar indicates the area of the thermocline in the subtropics. All profiles are averaged between 160°E and 160°W (source: Climatological Atlas of Regional Seas, Ridgway and Dunn 2003)[190].

Because water density decreases with increasing temperature, and increases with increasing salinity (but to a lesser extent), 'stratification' occurs in the water column. That is, lighter surface water remains separated from the denser deeper layer, like a layer of oil sitting on water. Increased stratification makes the water column more stable because more energy, in the form of wind or buoyancy-driven convection, is needed to mix water between the two layers. This requirement has important implications for fisheries because when the water column is stable the transfer of nutrients to the sunlit (photic) zone where primary production occurs is inhibited.

The stratification across the tropical Pacific is generally strong but decreases with increasing latitude (**Figure 3.6**). The strongest stratification occurs below the main atmospheric convergence zones (ITCZ and SPCZ) (Chapter 2). Nevertheless, several processes occur in the surface layer of the ocean, which can act against stratification. In addition to generating surface currents (Box 3.1), wind causes strong mixing in the upper layer. Evaporation, and loss of heat from surface waters at night or during winter at higher latitudes, also causes strong convective mixing in the upper layer and weakens the stratification. These forms of turbulence and mixing homogenise temperature, salinity and other properties of the ocean in the first few tens of metres (**Figure 3.7**), resulting in the surface 'mixed layer'. This homogenisation of properties results in a very sharp gradient at the base of the mixed layer. Below this level, the properties of the water column are affected by deeper oceanic processes[34,35].

The depth of the mixed layer varies substantially on daily to interannual time scales and ranges from about 0 to 200 m at low latitudes[34,35]. In nutrient-poor (oligotrophic) waters, the mixed layer depth is vitally important because it determines the depth from which nutrients are brought up to support biological activity at the surface[34,35] (Box 3.2, Section 3.2.4).

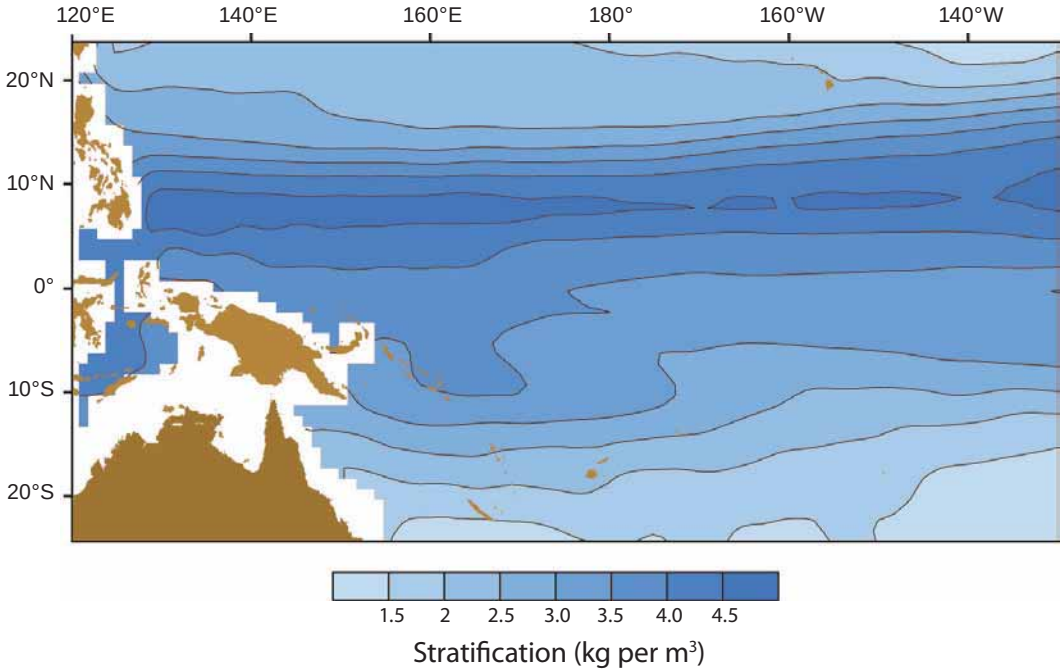

Figure 3.6 Average stratification of the tropical Pacific Ocean from 1980–1999 from the Simple Ocean Data Assimilation (SODA) (source: Carton et al. 2000)[191]. Stratification is defined here as the difference in water density (kg per m^3) between depths of 13 m and 200 m (13 m was chosen for compatibility with the common upper level of IPCC-AR4 model analyses). The highest vertical stratification is found under the Intertropical Convergence Zone and the South Pacific Convergence Zone.

The general vertical temperature structure described here varies with latitude. Deeper water within the thermocline is sourced from surface waters in the subtropics that are subducted into the thermocline to depths of around 200 m. This water then flows towards the equator where it eventually upwells. In the upper ocean, two warm water 'bowls' appear between 10°–20°N and 10°–20°S and extend to depths of 500 m (**Figure 3.8**).

These bowls are formed by the convergence of surface waters under the influence of Ekman transport (Box 3.1); the easterly trade winds drive the flow of warm surface water in the tropics poleward, whereas at 40°N–40°S westerly winds drive surface water towards the equator. This leads to a convergence that pushes the surface water downwards and creates the bowls of warmer water.

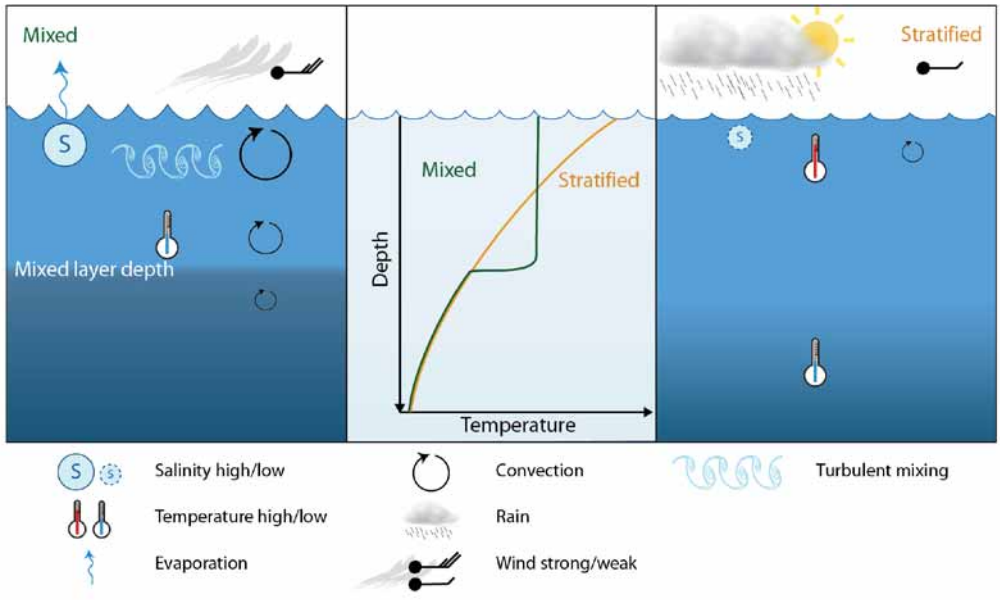

Figure 3.7 Factors affecting the mixed layer depth. The left panel shows a well-formed mixed layer with homogenised properties in the upper part of the water column; the right panel shows a smoothly stratified field. The corresponding temperature profiles are given in the middle panel. The formation of the mixed layer is enhanced by cooling, evaporation and strong winds, and weakened by heating, precipitation and slight winds.

In many parts of the tropical Pacific, the most important factor affecting water density, and therefore stratification, is temperature. However, in some regions, such as the Warm Pool, salinity becomes equally important (Section 3.2.2.3). The effects of temperature and salinity changes on density are significant because the motion of the ocean is controlled largely by spatial differences in water density (Box 3.1). For example, the downward tilt (towards the north) in the temperature structure below 100 m between 10° and 15°N (**Figure 3.8**) causes a westward flowing geostrophic

current – the NEC (Section 3.1). Similarly, the upward tilt (towards the north) in the deeper isotherms of the Southern Hemisphere is associated with the westward flowing, geostrophic SEC.

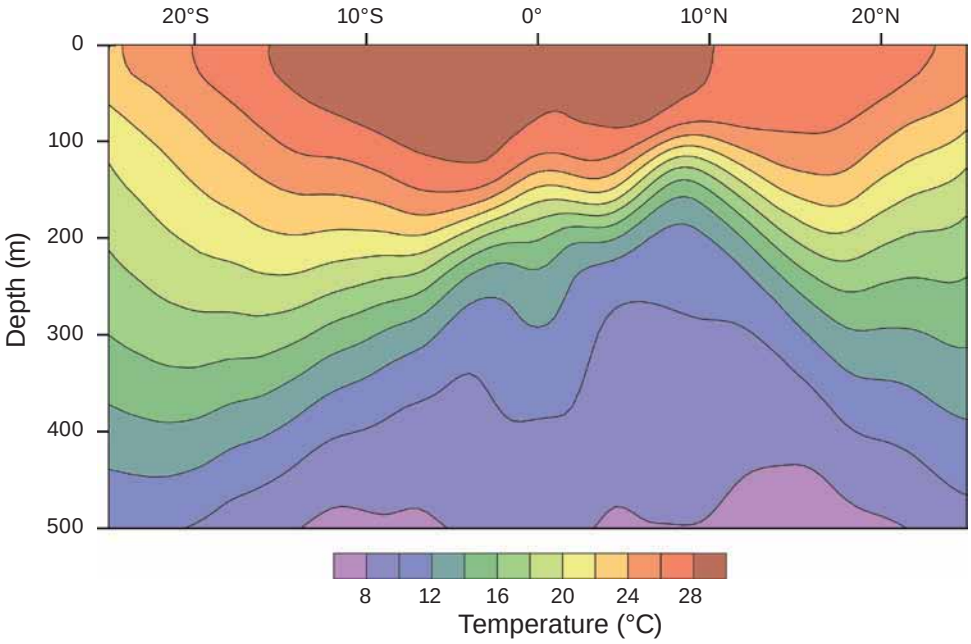

Figure 3.8 Vertical temperature structure (°C) of the water column, to a depth of 500 m, from 25°S to 25°N (averaged across the area from 160°E to 160°W). Note that warmer surface water penetrates to greater depths between 15°–20°N and 15°–20°S (source: Climatological Atlas of Regional Seas, Ridgway and Dunn 2003)[190].

3.2.2.3 The Warm Pool

The Western Pacific Warm Pool Province[36] (Section 3.2.2.4), is of major significance to tuna fisheries in the tropical Pacific (Chapter 8) and requires special attention in this description of ocean temperatures. The combined Warm Pool waters of the equatorial western Pacific Ocean and equatorial eastern Indian Ocean cover a vast area characterised by the world's warmest oceanic temperatures, the deepest atmospheric convection and the heaviest precipitation (Chapter 2). This Indo-Pacific Warm Pool is often defined by SSTs greater than a threshold value – usually 28°C. By this definition, it extends over ~ 12 million km^2 of the tropical Pacific Ocean (1.5 times the size of Australia) and ~ 6 million km^2 of the Indian Ocean. The interactions between the ocean and the atmosphere in this part of the world occur through radiative and latent heat transfers that drive vigorous convective clouds, winds and precipitation (Chapter 2). Small changes at the ocean-atmosphere boundary are enhanced through convection and can lead to self-amplification and eventually large changes in atmospheric circulation. The high precipitation levels above the Warm Pool strongly affect salinity, resulting in a relatively warm and fresh (less dense) pool of well-mixed water overlaying a cold and relatively saline (denser) ocean interior (**Figure 3.9**).

Box 3.2 Influence of the thermocline and mixed layer depth on transfer of nutrients to surface waters

In much of the subtropical northern and southern Pacific Ocean the potential for transferring nutrient-rich water from the deeper layers to the photic (sunlit) zone, where it can enhance the growth of phytoplankton (known as 'primary productivity') (Chapter 4), is constrained by stratification. Stratification is strongest at the depth of the pycnocline (the layer in the ocean where water density increases relatively rapidly with depth). As density is determined by temperature (and to a lesser extent salinity) the pycnocline depth usually corresponds to the depth of the thermocline, where temperature decreases relatively rapidly with depth (see panel a). Biological activity, commonly measured as Chlorophyll *a* (Chl-*a*) produced by phytoplankton, depends on both light (from above) and nutrients (from below), and is usually greatest in the lower part of the mixed layer.

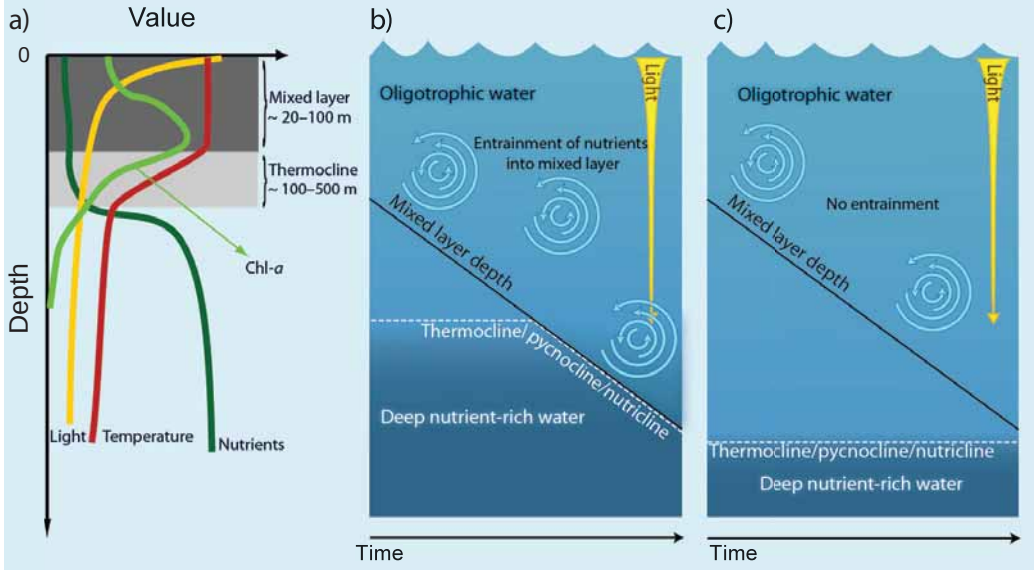

This vertical structure varies with time. Where the thermocline is shallow (panel b), mixing of the upper part of the water column by wind or convection reaches down to the nutrient-rich waters and transfers nutrients into the photic zone, where they are used for primary productivity. Where the thermocline is deep (panel c), nutrients remain out of reach below the mixed layer. The gradient in density at the thermocline/pycnocline also acts as a barrier to the downward penetration of the mixing, reinforcing the vertical structure. The time scales over which the processes that transfer nutrients occur vary from a few hours (e.g. strong wind events) to seasons (e.g. winter cooling and wind enhancements). The area of the water column where the maximum change in nutrients occurs with depth is called the nutricline and, like the thermocline, it is often co-located with the pycnocline.

The Warm Pool is at the heart of the ENSO mechanism (Chapter 2). Under 'normal' conditions, the trade winds generate surface currents that push and accumulate warm water to the west (Section 3.2.1), creating a large heat reservoir that maintains the easterly trade winds via the Walker circulation (Chapter 2). When an El Niño event occurs, the trade winds weaken, allowing the Warm Pool to spread eastwards across the equatorial Pacific over a period of ~ 2 months, along with its wind and precipitation systems. The displacement of the Warm Pool occurs through wave dynamics that set the speed and structure of the Warm Pool's motion to the east. After an El Niño event, westward propagating waves reset the system towards a 'normal' situation, replenishing and relocating the Warm Pool. Sometimes an 'overshoot' gives rise to a period of more extreme trade winds and a westward contraction of the Warm Pool – the Pacific shifts to a La Niña situation. El Niño events are associated with a 'shoaling' of the Warm Pool thermocline, which enhances primary productivity (Chapter 4). Conversely, the thermocline deepens during La Niña episodes, leading to lower productivity.

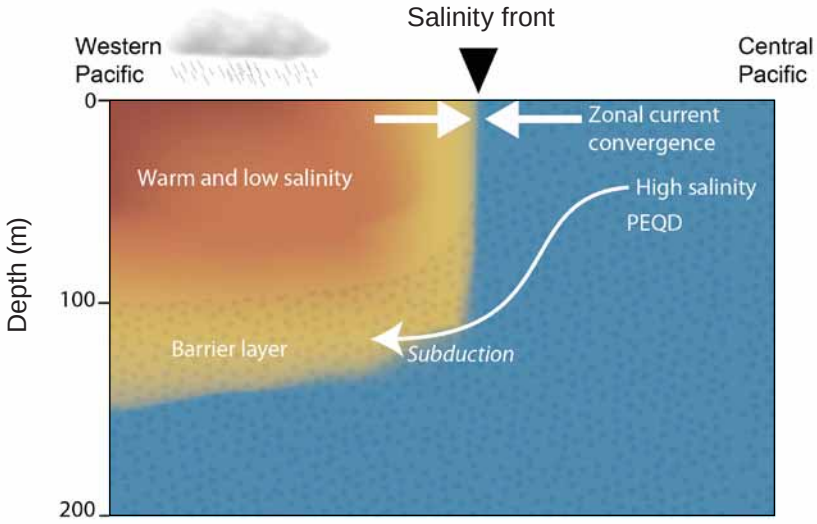

Figure 3.9 Temperature structure of the equatorial Pacific showing the Warm Pool. The thermally homogeneous waters of the Warm Pool, freshened by heavy rainfall in the western Pacific, converge with the colder, saltier waters originating in the Pacific Equatorial Divergence Province (PEQD) to the east. This convergence is one of the mechanisms that leads to the formation of a salinity-stratified layer in the lower part of the Warm Pool known as the 'barrier layer'. Upwelling occurs to the east of the salinity front, bringing nutrient-rich waters to the surface. In contrast, the Warm Pool has low nutrient levels.

At the eastern edge of the Warm Pool, there is a convergence zone where the incoming westward SEC weakens and there is a small eastward flow within the Warm Pool (**Figure 3.9**). The interannual movements of the Warm Pool (and its eastern edge) are controlled by the relative strength of these zonal currents and are subject to variations that are in phase with ENSO[37]. Because of the contrasting water properties to the east and west of this boundary, the convergence zone is characterised by a

sharp change in salinity (**Figure 3.9**). Displacements of this convergence zone are an intrinsic part of the ENSO system[38] and can reach several thousands of kilometres, between 140°W during El Niño conditions and as far west as 140°E during La Niña episodes[39]. These displacements also determine the boundary between the Pacific Equatorial Divergence Province (PEQD) (Section 3.2.2.4) and the Warm Pool[40].

The relative contributions of temperature and salinity to the density of sea water are similar in the Warm Pool – a situation that is uncommon in most other parts of the tropical Pacific Ocean, where temperature normally dominates. On average, temperature is homogeneous in the upper 60 m of the water column in the Warm Pool with a sharp thermocline below this surface layer. In contrast, the salinity 'halocline' in the Warm Pool is much shallower, resulting in a mixed layer (where both temperature and salinity are well-mixed), which is only about 30 m deep[41]. The stratified layer between the thermocline and the base of the mixed layer is called the 'barrier layer' (**Figure 3.9**). Within the barrier layer regions, any mixing driven by the wind is restricted so that the waters below the barrier layer are insulated from the influence of the atmosphere, and vice versa. This stratification acts as a barrier to the vertical exchanges of heat, fresh water and nutrients, and suppresses mixing[42]. The location and strength of the barrier layer are important to both ENSO dynamics[43,44] and biological production[45].

3.2.2.4 Boundaries of ecological provinces

Differences in water temperature, salinity and the convergence zones related to the major surface currents define five ecological provinces that cover the area of the tropical Pacific[36] (Chapter 4).

The Pacific Equatorial Divergence Province is generated by the diverging surface Ekman transports (**Figure 3.1**, Box 3.1), which drive upwelling of nutrient-rich water, creating the most productive surface waters in the region. The waters in this province are also characterised by a high salinity and high partial pressure of carbon dioxide (pCO_2). These nutrient-rich waters span much of the equatorial Pacific and drift westward and poleward before submerging at the convergence with the NECC (ca. 5°N) and SECC (ca. 6–8°S).

To the west, the Warm Pool forms a province by itself. In contrast to the PEQD, the surface waters of the Warm Pool are relatively nutrient-poor but, for reasons explained in Chapters 4 and 8, support high populations of tuna. At the equator, the salinity front marks the boundary between the Warm Pool and PEQD. Seasonal and interannual (ENSO) displacements define the extent of these two provinces.

On both sides of the equatorial band are the large oceanic gyres (**Figure 3.1**). These oligotrophic regions are associated with the convergence of warm surface water from the North Pacific Tropical Gyre (NPTG) and the South Pacific Subtropical Gyre (SPSG)[36] (Chapter 4).

The western part of SPSG is characterised by a large number of islands and shallow seamounts, referred to as the Archipelagic Deep Basins Province (ARCH). This province is subject to a range of mesoscale processes (Section 3.2.9), and the current regimes are complex because of the way islands, archipelagos or seamounts divert oceanic circulation. ARCH has a mixture of surface waters with different characteristics, and differs from the other provinces, which are generally dominated by more stable large-scale currents.

3.2.3 Ocean eddies

Eddies are large, horizontally-rotating vortices that can extend from the surface to considerable depths (**Figure 3.10**). Eddies in the ocean, and in coastal areas, affect the distribution and abundance of the species supporting fisheries in the tropical Pacific in two main ways. First, they help draw nutrient-rich water from the deeper layers of the ocean towards the surface, stimulating primary production (Chapter 4). This is important not only for oceanic fisheries, but also for the coastal fisheries around the islands in the generally nutrient-poor waters of the western Pacific (Section 3.2.4). Second, eddies help entrain the larvae of fish and invertebrates close to favourable habitats that support the spawning adults, increasing the probability that juveniles will recruit successfully[46]. This is particularly important for isolated PICTs, where stocks are usually dependent on self-replenishment.

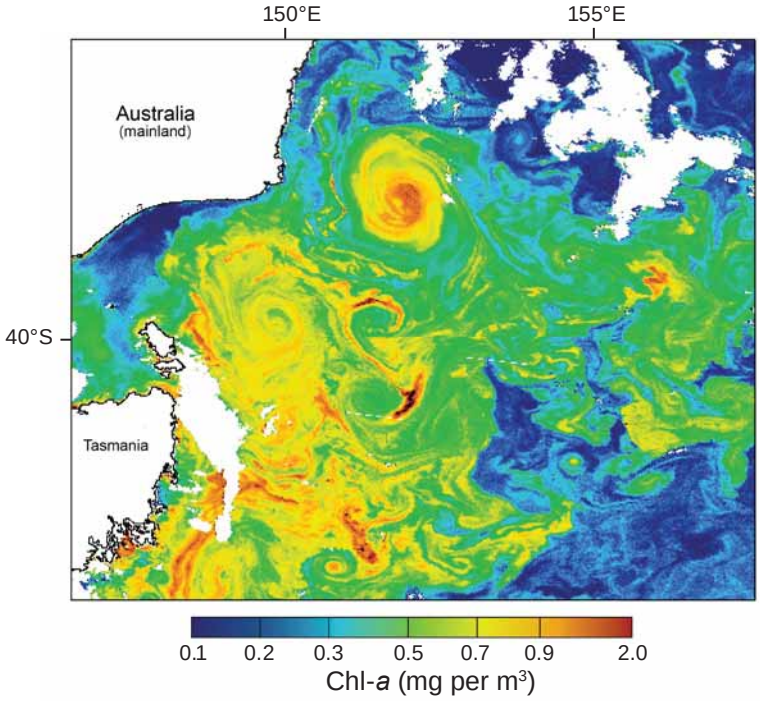

Figure 3.10 An example of mesoscale eddy activity in the southern Tasman Sea, illustrated by reconstructed Chlorophyll *a* concentration in mg per m^3 (see colour scale), from NASA SeaWiFS satellite data. White areas over the ocean correspond to data gaps.

Most of the energy in the ocean is not contained in the massive basin-scale circulations, but rather in pervasive, smaller-scale features, like eddies[47]. The energy that drives eddies and much of the other motion in the ocean is derived from the atmosphere (via wind and heat) or the sun (via radiation) (Box 3.1). Similar to the atmospheric mid-latitude depressions/anticyclones, mesoscale eddies are generated by instabilities in the large-scale flow, and occur throughout the ocean. The size of mesoscale eddies depends strongly on latitude – in the tropical Pacific they range from ~ 150 to 300 km across[48]. As a result of the Coriolis force, mesoscale eddies tend to propagate to the west in the Pacific at speeds ranging from 5 cm per second at 25°N–25°S to 10 cm per second at 10°N–10°S[49,50].

On larger scales (up to ~ 1000 km), horizontal water displacements associated with Rossby waves are also evident away from the equator[51]. Rossby waves are generated by large-scale fluctuations in the surface winds. Like eddies, Rossby waves only travel in a westward direction as a consequence of the Coriolis force.

The passage of mesoscale eddies and Rossby waves is associated with important variations in local currents, sea level and the vertical structure of the water column. A warm, anticyclonic eddy raises sea level in the order of 10 cm over a horizontal distance of a few tens of kilometres[52] and depresses the thermocline (**Figure 3.11**). A cold, cyclonic eddy has the opposite effects.

The impact of eddies can be dramatic. For example, an anticyclonic eddy delivers warm water that can boost the energy of an ongoing cyclone. Cold eddies, through their capacity to reduce the depth of the thermocline, can bring nutrients into the photic zone (Section 3.2.4.1). The passage of Rossby waves also enhances the availability of nutrients in a similar way, and 5% to 20% of the variability in ocean productivity is associated with these phenomena[53].

Because eddies result in changes in sea surface height, areas of vigourous variation in sea surface height correspond to places of intense eddy activity. Satellite images of such variability reveal that eddies are distributed unevenly across the tropical Pacific[54] (**Figure 3.12**). Near the equator, variability in sea surface height is dominated by ENSO.

Away from the equatorial region, five areas of relatively high variability occur close to strong currents and in the places where currents and counter currents interact (1) near Australia at 25°S, which is the northern end of the high energy zone associated with the EAC[55,56]; (2) east of Solomon Islands, in the wake of the SECC; (3) near 6°N in the NECC, and in two bounding areas where surface counter currents intrude into the domain; (4) south of 20°S and between 160°E and 150°W in the South Pacific Subtropical Counter Current; and (5) near 22°N in the North Pacific Subtropical Counter Current[57,58] (**Figure 3.1**, Section 3.2.1).

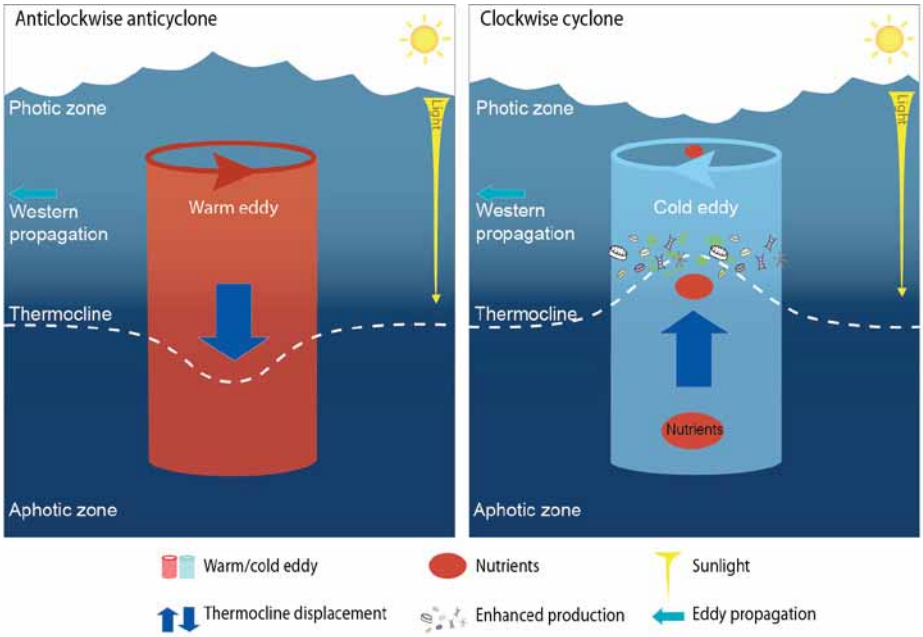

Figure 3.11 Effects of an oceanic eddy on the vertical temperature structure of the water column in the Southern Hemisphere. In the case of an anticlockwise warm eddy (left panel), the thermocline is pushed downwards and the sea surface is slightly raised within the eddy as it propagates westward. A cold eddy, on the other hand, which rotates in a clockwise direction (right panel), raises the thermocline, potentially making nutrients available for enhanced biological production. In the Northern Hemisphere, the direction of rotation is reversed but the thermocline displacements are in the same direction.

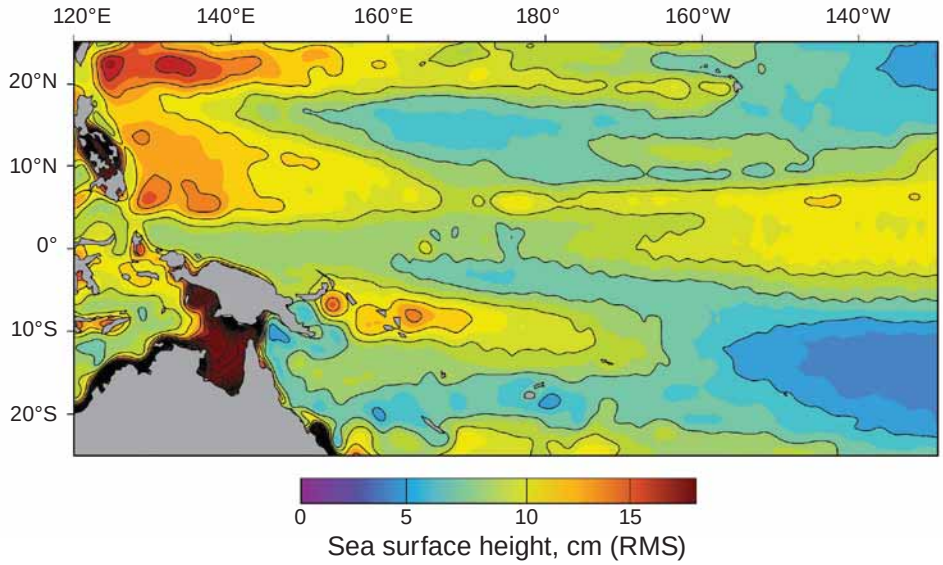

Figure 3.12 Eddies in the tropical Pacific Ocean, shown as variability (standard deviation) in sea surface height (SSH) anomaly from a merged satellite altimetry dataset (including Topex/Poseidon, Jason, ERS and Envisat from 1992–2007) (source: Ridgway 2007)[192]. Contour interval is 2.5 cm. Note that passing eddies cause a temporary change in sea level.

3.2.4 Nutrient supply

The availability of nutrients in the ocean is of great significance to fisheries. Together with sunlight, nutrients underpin the primary productivity associated with phytoplankton at the base of the food webs that support the stocks of tuna and other large pelagic fish harvested throughout the tropical Pacific Ocean (Chapter 4). The main nutrients associated with biological productivity are nitrates, phosphates and silicates. The maintenance of this productivity can be fragile, however, because nutrients are not distributed evenly – they are depleted near the surface, where they are needed, but abundant in the deeper ocean. This variation occurs because the phytoplankton use up the available nutrients in the photic zone, where there is sufficient light for photosynthesis and, although a small part of the nutrients pass down the food web, most of them eventually sink as organic matter into the deep ocean. There, bacteria remineralise the organic matter, releasing nutrients. As a result, concentrations of nutrients are much greater below the pycnocline than they are at the surface (**Figure 3.13**). The sinking of organic material is also one of the main ways that CO_2 is transferred into the deep ocean from the atmosphere and is known as the 'biological pump'[59].

Ocean circulation, or deep mixing of the water column, is needed to transfer the nutrients back to the surface layers. The strong density stratification (pycnocline) usually associated with the thermocline (Box 3.2) effectively inhibits the vertical exchange of water (and therefore nutrients) between the deep and shallow layers of the ocean. Molecular mixing is too weak to transport significant amounts of nutrients towards the surface. The main processes that can overcome the stratification barrier and deliver nutrient-rich water to the upper layers – turbulence in the mixed layer, wind-driven upwelling and eddies – are outlined below.

3.2.4.1 Mechanisms that make nutrients available

- **Turbulence in the mixed layer:** The strong mixing in the upper ocean (Section 3.2.2.2) entrains nutrient-rich deeper waters and circulates them within the photic zone. The extent of nutrient input is determined by the depth of mixing in relation to the depth of the nutricline (Box 3.2). A strong wind, for example, may deepen the mixed layer to 100 m in several hours and entrain the nutrient-rich deep waters from greater depths. On seasonal time scales, and at subtropical latitudes, the mixed layer deepens during winter because of stronger winds and surface cooling, and becomes shallower during summer as surface warming acts to stratify the water column (**Figure 3.14**). In oligotrophic waters, the maximum mixed layer depth determines the depth from which nutrient-rich waters can be mixed to the surface to replenish nutrient supplies depleted by biological activity in the photic zone. Thus, mixed layer depth is a useful indicator of biological production[60].

  Maximum yearly mixed layer depth in the tropical Pacific Ocean ranges from 70 to 80 m in the highly stratified Warm Pool (**Figure 3.15**), where warm water accumulates over the cold waters of the Equatorial Undercurrent, to more than

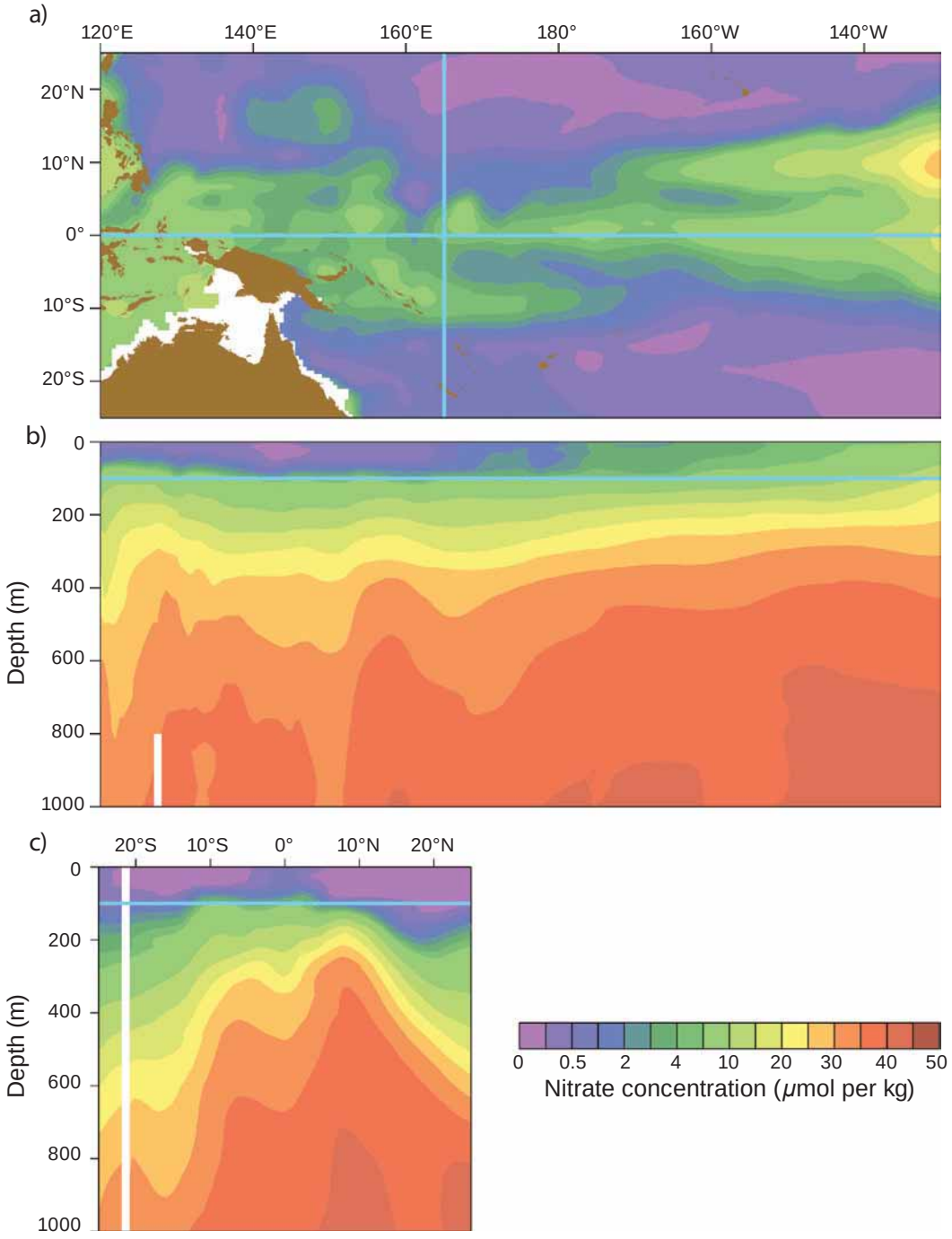

Figure 3.13 (a) Average dissolved nitrate concentration (μmol per kg) in the tropical Pacific Ocean at a depth of 100 m; and average dissolved nitrate concentrations for vertical sections of the water column to depths of 1000 m at (b) the equator, and (c) 165°E. The positions of the vertical sections are indicated as blue lines on (a); horizontal blue lines in (b) and (c) represent values at a depth of 100 m as shown in (a) (source: CARS 2006 CSIRO climatology, Ridgway and Dunn 2003)[190]. White areas in (b) and (c) correspond to topography.

200 m in the low rainfall regions at the centre of the two gyres (NPTG and SPSG), where relatively high-salinity waters are cooled during the winter, causing convection and much deeper mixing.

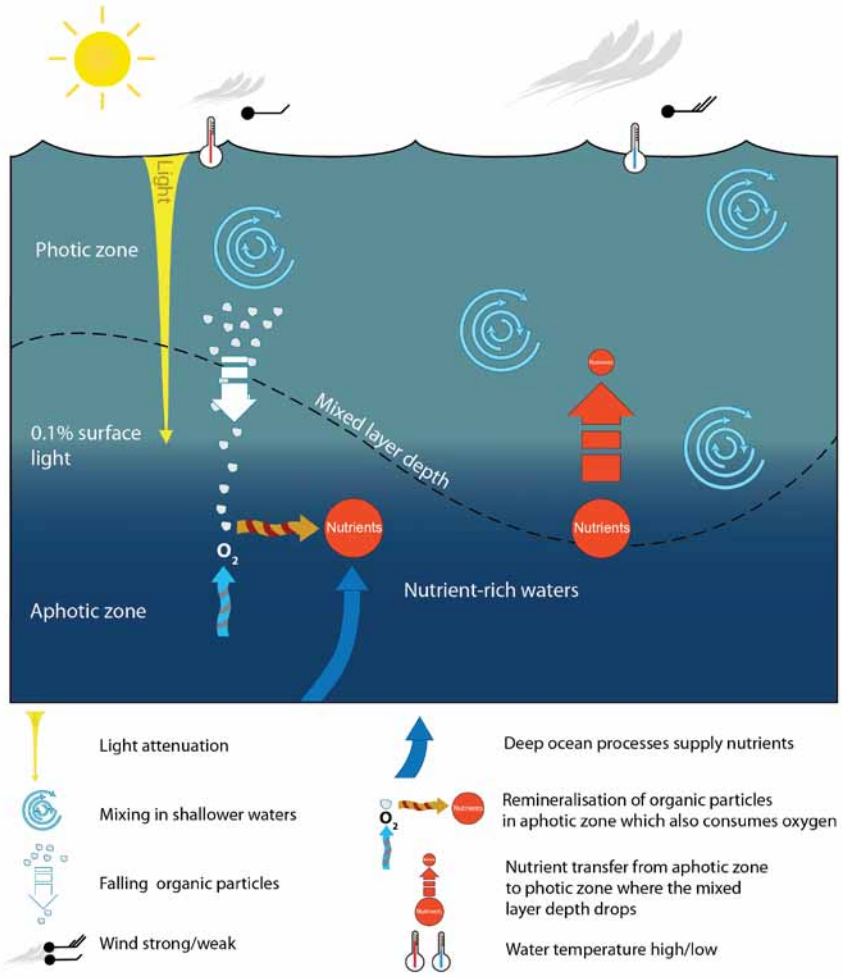

Figure 3.14 Factors contributing to nutrient concentration in the surface waters of the tropical Pacific Ocean. A deeper mixed layer, caused by stronger winds and lower surface temperatures during winter, helps to transfer nutrients to the photic zone, where they are available to contribute to biological production. Advection by ocean currents and decomposition of organic matter by bacteria (remineralisation) maintains a reservoir of nutrients below the mixed layer (see Chapter 4 for more details).

- **Upwelling:** As explained in Section 3.2.2.1, upwelling of deep, nutrient-rich waters is created by the divergence of surface water, when wind-driven surface currents move in opposite directions (e.g. at the equator), or when surface water is pushed away from the coast (e.g. near islands, or along the Peru-Chile coast). The surface divergence 'draws' deeper waters towards the surface, creating an 'upwelling'. If these waters originate from a sufficient depth, they deliver nutrients into the mixed layer. This occurs in PEQD, where strong upwelling occurs within

4 to 5° of the equator driven by the easterly trade winds (Chapter 4). In contrast, the subtropics (NPTG and SPSG) are dominated by convergence of surface waters and downwelling, making them areas of low productivity. Weak upwelling is found, however, near the poleward edge of the SPCZ and ITCZ, and near islands in NPTG and SPSG, where sharp changes in the direction of ocean currents or the wind can lead to local upwelling events that enrich surface waters. The local influence of coasts and islands is more pronounced in ARCH, where boundary currents, jets, wind-driven upwelling, enhanced internal waves or tidal mixing activity more commonly bring nutrients into the photic zone (Section 3.2.9) (Chapter 4).

- **Eddies:** Surface divergence associated with oceanic eddies and Rossby waves, both within the eddies or waves (mesoscale) and at their edges (submesoscale) (Section 3.2.3), can raise the thermocline temporarily and bring nutrient-rich waters into the photic zone[52,61,62] (**Figure 3.11**) to increase primary productivity (Chapter 4). Because oceanic eddies are ubiquitous in the subtropics (**Figure 3.12**), they are believed to be the main nutrient supply system along with frontal processes in NPTG and SPSG[53,59,63–66].

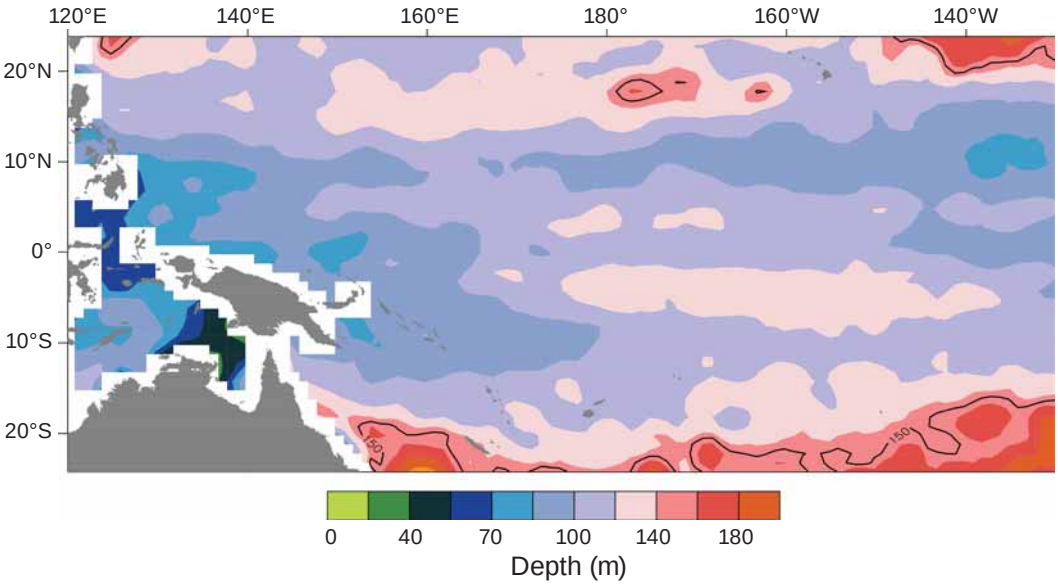

Figure 3.15 Maximum mixed layer depths across the tropical Pacific Ocean for the period 1980–1999, based on the Simple Ocean Data Assimilation (SODA) (source: Carton et al. 2000)[191]. The mixed layer depth (MLD) is defined as the depth at which the density of the water increases by 0.1 kg per m^3 with respect to the density at the surface (source: Sarmiento et al. 2004)[60]. The 150 m MLD contour is shown in black.

Overall, the supply of nutrients to the photic zone in the tropical Pacific Ocean is the result of the interplay between mixed layer depth, upwelling and eddies against the background of the stratification and nutrient structure of the particular province (Box 3.2). Upwelling, for example, driven by the easterly trade winds, plays an important

part in supplying nutrients in PEQD, where the thermocline is shallow. In addition, ENSO-related equatorial waves can lead to displacements in the thermocline, which affect the supply of nutrients (Section 3.2.2.2). Following a westerly wind burst in the western Pacific (an important precursor to El Niño events), a 'downwelling' equatorial wave moves across the basin to the east deepening the thermocline on its way and suppressing upwelling. The strength and depth of the EUC is another important factor controlling productivity in the tropical eastern Pacific as it provides a source of iron, which is the element that limits primary production in that region[45,67] (Chapter 4).

The sporadic nature of phytoplankton blooms in the tropical Pacific Ocean (Chapter 4) suggests that occurrence and coincidence of the various processes affecting biological production along the equator are highly irregular. A single biological bloom associated with a La Niña episode can dominate the average conditions over a 5-year period[45].

3.2.5 Dissolved oxygen

Adequate levels of dissolved oxygen (O_2) throughout the water column are essential for the growth and survival of the zooplankton and micronekton in the food webs for tuna, and for tuna themselves (Chapters 4 and 8). Where the concentrations of dissolved oxygen are too low, the distributions of these animals are restricted because they require O_2 for energy, and for oxidising organic substrates, such as carbohydrates.

The levels of dissolved oxygen in surface waters are determined by the rate at which oxygen is transferred from the atmosphere (which is highly dependent on SST and surface mixing), the rate it is produced from photosynthesis by phytoplankton, and the rate at which the oxygen-rich surface waters are submerged via ocean currents and mixing. At high latitudes, some cold surface waters rich in O_2 are pushed dynamically to lower latitudes, below lighter subtropical waters – a process called 'subduction'. These waters gradually lose O_2 as it is used up in the decomposition of organic matter by bacteria, a process termed 'remineralisation'. Therefore, dissolved oxygen concentration at any point in the water column is a balance between the original O_2 content, the effect of remineralisation of organic matter, and the rate at which water is replaced through ocean circulation. As a result, vertical O_2 concentration is usually inversely related to nutrient levels in the upper 500 m (compare **Figures 3.13** and **3.16**).

In regions of high remineralisation, consumption of O_2 can exceed replenishment from ocean circulation, causing part of the water column to become depleted in oxygen. This depletion results in anoxic conditions (see for example the areas around 10°N and 5°S in **Figure 3.16**). Unlike CO_2 (Section 3.2.6), changes in the dissolved oxygen content in surface waters are insensitive to changes in atmospheric O_2 concentrations because such changes are negligible relative to total oxygen concentration.

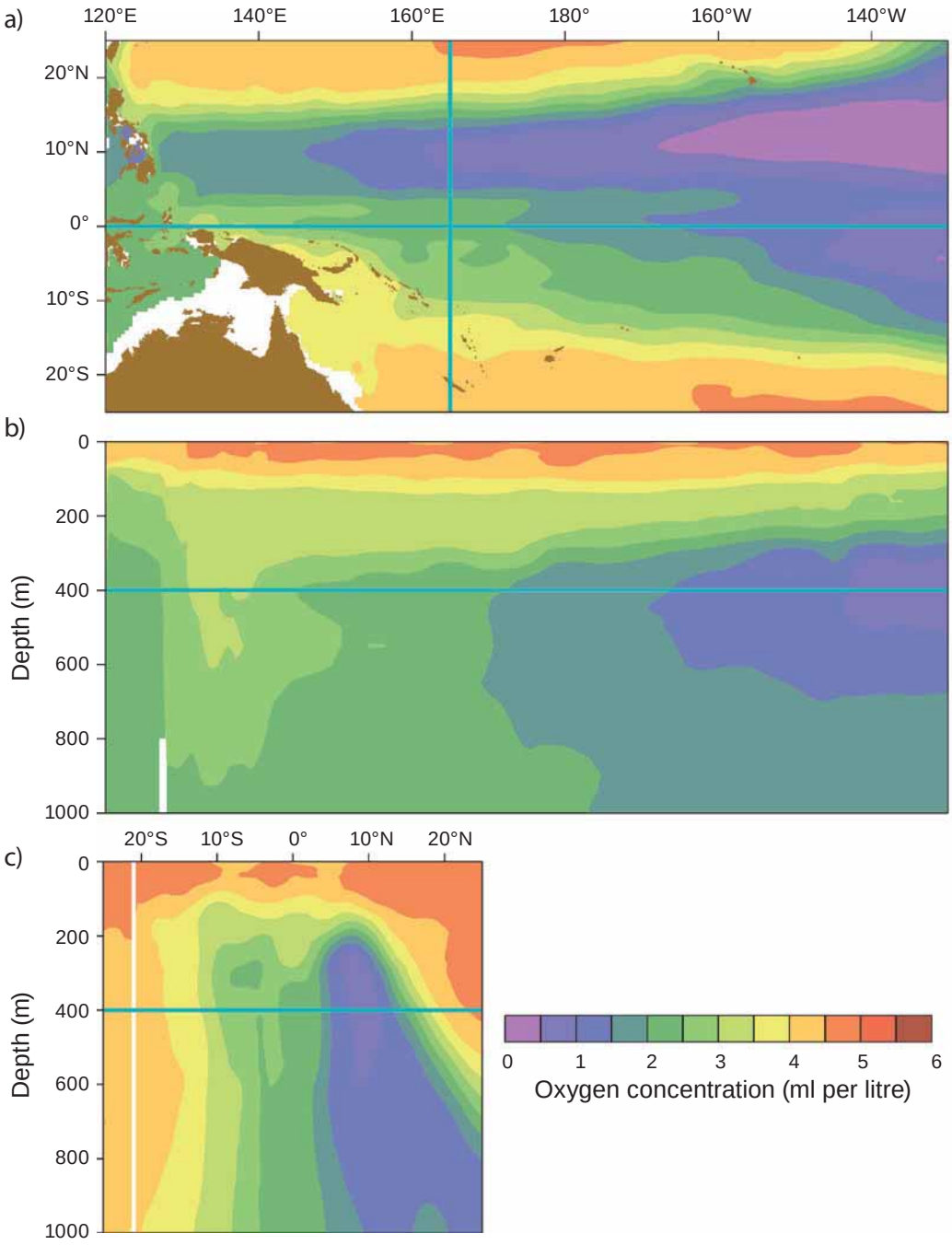

Figure 3.16 (a) Average dissolved oxygen (O_2) concentration (ml per litre) in the tropical Pacific Ocean at a depth of 400 m; and average O_2 concentrations for vertical sections of the water column to depths of 1000 m at (b) the equator, and (c) 165°E. The positions of the vertical sections are indicated as blue lines in (a); horizontal blue lines in (b) and (c) represent values at a depth of 400 m as shown on (a) (source: CARS 2006 CSIRO climatology, Ridgway and Dunn 2003)[190]. White areas in (b) and (c) correspond to topography.

3.2.6 Ocean acidification

The acidity of the open ocean has been relatively stable for millions of years. Due to this stability, carbonate ions (CO_3^{2-}) are so naturally abundant that the common pure minerals of calcium carbonate ($CaCO_3$) in the ocean (aragonite and calcite) are formed in surface waters and do not dissolve. This availability of carbonate ions is important to the corals and other calcifying organisms that build the reefs that support coastal fisheries (Chapters 5 and 9). Carbonate ion availability is also important to a range of organisms in the food webs for tuna (Chapter 4), and for many of the invertebrates that are collected for food and income by villagers throughout the tropical Pacific (Chapter 9). These organisms extract calcium (Ca^{2+}) and CO_3^{2-} from sea water to secrete the $CaCO_3$ they use to build their skeletons and shells.

The stability of ocean acidity and the supply of carbonate ions are likely to be threatened by increasing levels of anthropogenic CO_2. The problem is that the increased concentration of CO_2, much of which dissolves in the ocean (**Figure 3.17**), is changing the chemistry of sea water (Box 3.3). The consequence is that less CO_3^{2-} is expected to be available for use by calcifying organisms, reducing their growth and their chances of survival. Although the responses of species are likely to vary, depending on their physiology and the composition of their skeletal material (aragonite, calcite)[68,69], there is serious concern that ocean acidification will cause difficulties for the growth of corals and the maintenance of the essential habitats they provide for coastal fisheries. Indeed, a decrease of 0.3 units in oceanic pH is expected to inhibit formation or limit the growth of many marine organisms[70–76]. If CO_3^{2-} declines sufficiently, aragonite (the most common form of calcium carbonate used by marine species) actually begins to dissolve[70,76,77] (Box 3.3).

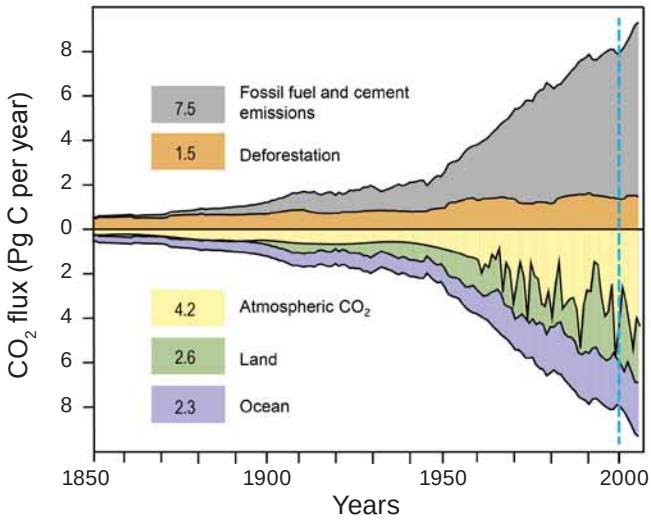

Figure 3.17 Sources of anthropogenic emissions of carbon dioxide (CO_2) and the 'sinks' that absorb CO_2, including the atmosphere. The flux is expressed in 10^{15} g of carbon (C) per year (Pg C per year); numbers in the colour legend represent the 2000–2007 average of the yearly flux for each component of the anthropogenic emissions (the period to the right of the dashed blue line) (source: IPCC-AR4 and Canadell et al. 2007)[193].

Box 3.3 The chemistry of ocean acidification

When carbon dioxide (CO_2) is dissolved in the surface waters of the ocean, certain chemical reactions take place. In particular, CO_2 combines with water to form carbonic acid (see Equation 1 below). The carbonic acid (H_2CO_3) dissociates into hydrogen ions (H^+) and bicarbonate ions (HCO_3^-) (Equation 2). The bicarbonate can also split into a further hydrogen ion and a carbonate ion (CO_3^{2-}) (Equation 3).

$$CO_2 + H_2O \leftrightarrows H_2CO_3 \quad (1)$$

$$H_2CO_3 \leftrightarrows H^+ + HCO_3^- \quad (2)$$

$$HCO_3^- \leftrightarrows H^+ + CO_3^{2-} \quad (3)$$

Rather than creating a chain reaction, these equations represent two-way reactions that equilibrate continuously so that three dissolved inorganic carbon species occur simultaneously: carbonic acid, bicarbonate and carbonate (with relative concentrations of about 1%, 91% and 8%, respectively). These contributions shift, however, depending on the physical, chemical or biological conditions of the ocean. The fourth component in these reactions is the hydrogen ion. If there are more H^+, the water becomes more acid, i.e. its pH (= $- \log_{10}[H^+]$) decreases.

Fortunately, these chemical reactions self-regulate in such a way as to minimise the changes in pH. For example, if extra CO_2 is dissolved in the surface ocean (as is presently occurring) the balance shifts via chemical reactions (1) and (2) to higher concentrations of HCO_3^- and H^+, thus reducing pH. However, some of the excess hydrogen ions are removed as they combine with free CO_3^{2-} via reaction (3). This greatly reduces the rate at which acidification of the ocean occurs (although not entirely), but there is an environmental 'cost' because free carbonate ions are removed from the water. This tempering of the pH by free carbonate ions is known as 'carbonate buffering'. However, as more CO_2 is added to the ocean, the number of free carbonate ions decreases. As a result, the capacity for buffering will be reduced and pH is expected to continue to decline.

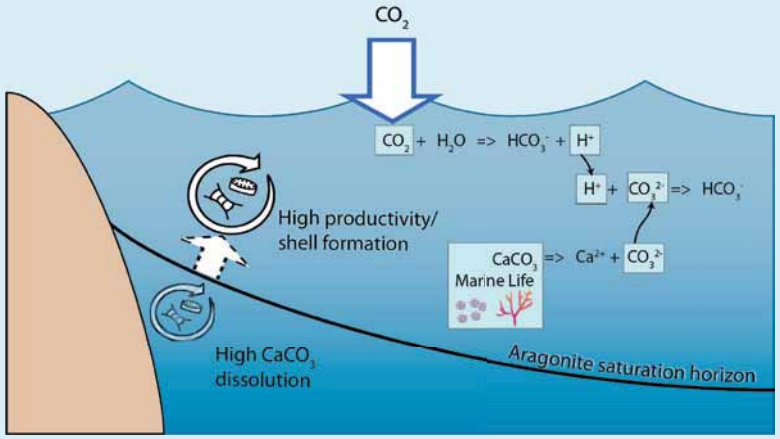

Both increased acidity (lower pH) and lower CO_3^{2-} concentration ('carbonate saturation') can have adverse effects on the growth and survival of marine organisms, especially those that build their shells and skeletons from $CaCO_3$, which is formed when calcium combines with carbonate ($Ca^{2+} + CO_3^{2-} \Leftrightarrows CaCO_3$). As concentrations of CO_3^{2-} decrease, such species find it more difficult to secrete $CaCO_3$. At some 'saturation' concentration of carbonate, the ambient water becomes corrosive to $CaCO_3$ and the shells and skeletons of organisms actually begin to dissolve. This saturation level is sensitive to ocean temperatures, however, and cold high-latitude regions reach 'undersaturation' before tropical and subtropical waters. Also, as depth increases, a threshold is reached where $CaCO_3$ starts to dissolve due to increased pressure. This threshold is known as the 'aragonite saturation horizon'.

Organisms whose growth is naturally limited by the availability of CO_2, such as some phytoplankton and benthic microalgae, may benefit from rising levels of CO_2 in sea water. For example, the cryptic, bioeroding microalgae on coral reefs grow faster under elevated CO_2 concentrations, which exacerbate reef erosion through chemical dissolution[78]. Chemical dissolution in reef carbonate sediments can also increase due to enhanced bacterial activity under higher CO_2 levels[68,69,79].

Average ocean pH is now about 8.1, but it varies both seasonally and spatially by ~ 0.3 units across the oceans of the world due mainly to changes in SST and the upwelling of deep waters rich in CO_2 in the open ocean. Higher temperatures reduce the amount of CO_2 that can be dissolved in sea water, so that where the ocean is warmer, CO_2 is released and pH increases. Upwelling affects pH because concentrations of CO_2 are higher in deep water due to the remineralisation of the organic matter that accumulates there (Chapter 4). Where deep water upwells, for example, in PEQD, the pH of surface waters is reduced. This process is also affected by seasonal and spatial changes in biological productivity[80].

3.2.7 Wave height

The height (or energy) and direction of waves affect the ecosystems that support fisheries and aquaculture. For example, waves have a major influence on ocean surface mixing[81], sediment suspension and transport[82]. They also affect the structural complexity of coral reefs[83–85] (Chapter 5) and the extent and form of mangrove and seagrass habitats (Chapter 6), which provide shelter and feeding areas for the fish and shellfish that sustain coastal fisheries (Chapter 9). Where the wave climate is too strong, these ecosystems may be damaged by the direct force of the waves, and by turbidity resulting from coastal erosion or resuspension of sediments (Chapters 5 and 6). Wave height and direction also determine the locations where the infrastructure needed to support oceanic and coastal fisheries and aquaculture can be located securely, and where fishers can operate safely.

3.2.7.1 The nature of waves in the region

The waves on the surface of the ocean are generated by wind. Depending on location, they vary in length or period, from ripples (centimetres) to long swells (hundreds of metres). The period of a wave is measured as the time taken for two consecutive wave crests to pass the same point. The average wave conditions, or 'wave climate' of an area

can consist of waves of many periods and heights, collectively called the 'wave spectrum'. The height of waves is usually recorded as 'significant wave height' (SWH), which is the average height (trough to crest) of the highest one-third of the waves over a given time.

The height and period of surface ocean waves are a function of wind energy, the distance over which the wind blows (fetch), the length of time the wind has been blowing and, in shallow water, the water depth (see below). Waves generated by local winds are called 'wind-sea waves', and generally have periods of < 8 seconds. Longer-period waves, which have travelled from remote regions where they were generated by storms, are known as 'swell'. These larger swell waves may traverse many thousands of kilometres in less than a day before they reach shallow waters and break on the shore. Most swells that arrive in the tropical Pacific are generated by storms in higher latitudes (**Figure 3.18**). However, the tropical cyclones described in Chapter 2 cause the local generation of much larger waves than those produced by remote storms.

In the tropical Pacific Ocean, long-term *in situ* wave data are generally lacking, and we rely on model re-analyses, i.e. a model simulation that is constrained by observations[86] and satellite data[87]. Such re-analysis suggests that the average SWH ranges from 1.5 to 2.5 m, but generally decreases to the west[86] (**Figure 3.18**). The wave spectrum is dominated by two types of waves: (1) short period 'wind-sea' waves generated locally by the trade winds, which have a westward direction but also move towards the equator (**Figure 3.18**); and (2) long-period swell waves generated by storms at mid to high latitudes in the band of easterly winds, which enter tropical regions with a dominant south-eastward direction in the north and a north-eastward direction in the south.

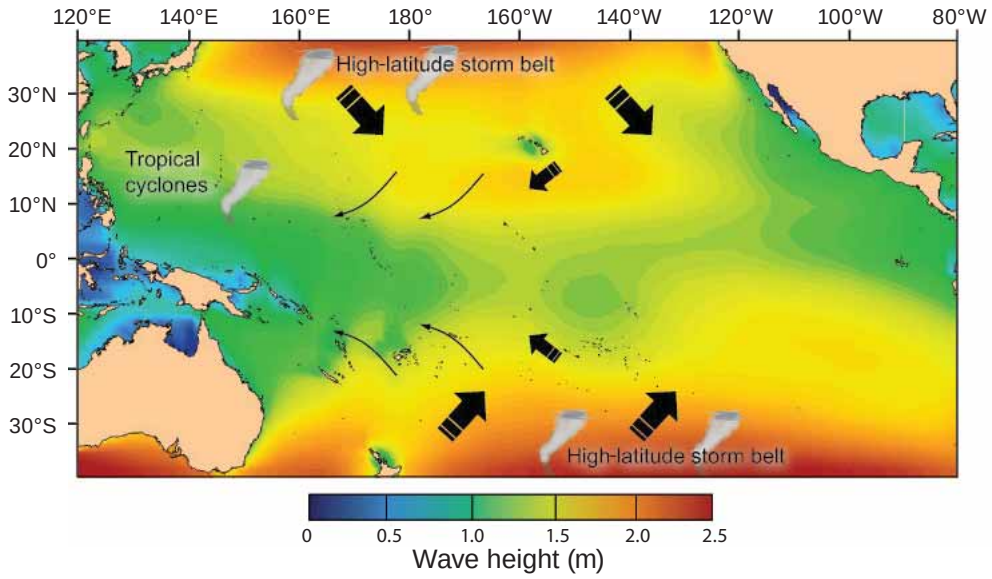

Figure 3.18 Long-term (1958–2002) average annual significant wave heights (SWH) in the tropical Pacific Ocean. Block arrows show the dominant wave direction. Size of block arrows indicates approximate relative wave height. Curved black arrows represent the trade winds (source: Sterl and Caires 2005)[86].

3.2.7.2 Effect of waves coming ashore

When swell waves enter water that is shallow compared with their wavelengths (i.e. equal to or less than about half the wavelength) they interact with the bottom. The waves slow, and their amplitude increases, to conserve energy (**Figure 3.19**). This causes the steepness of the wave to increase and, when the wave height reaches about 80% of the water depth (ignoring wind effects), the wave begins to break. The wave energy is then released, generating currents, sediment transport, and an increase in local sea level. Because longer wavelength swells interact with the bottom at greater depth, they generally break further offshore compared with wind-sea waves, which break closer to reefs. Thus, wind-sea waves penetrate further over the reef. This means that a 2 m wind-sea wave can actually cause the same damage on the inner parts of the reef as a 6 m swell which has broken further offshore[88].

The persistent arrival and breaking of waves on the shore creates an increase in water level over reef flats, which is about 20% of the offshore SWH. This increase is known as 'wave setup' (**Figure 3.19**)[89]. For enclosed lagoons and atolls, the lagoon water level can remain above the average ocean height throughout the tidal cycle, and rise significantly during large wave events[90]. Wave setup can create additional habitat space, enabling the vertical growth of a reef above the mean height of living corals[91,92]. Wave setup also creates a water level gradient sloping towards the less energetic side of an atoll, resulting in wave-driven flushing of lagoons[93]. For example, a swell event in Aitutaki, Cook Islands with a SWH of 4.5 m and a wave period of 15 seconds, resulted in a water level gradient of 30 cm across the lagoon. This caused a tripling of current speeds inside the lagoon[94]. Therefore, both average wave conditions, as well as individual events, can have important implications for the renewal of lagoonal water.

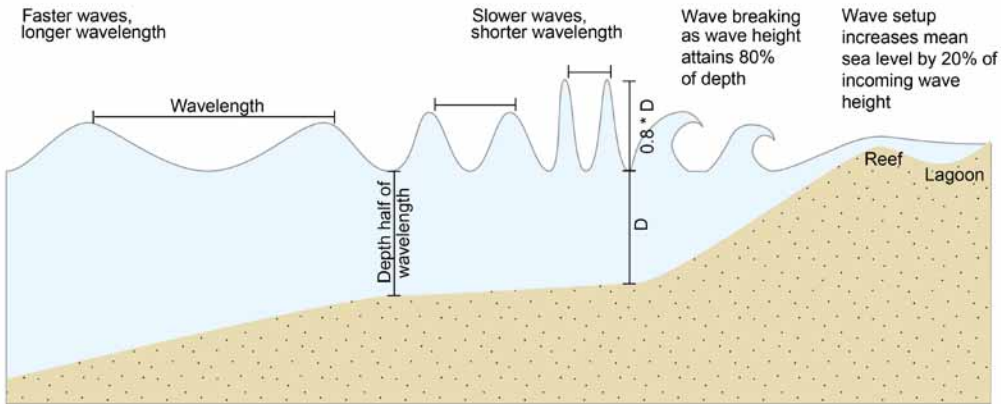

Figure 3.19 Changes in the characteristics of waves as they approach the shore. Waves approaching a reef interact with the bottom – their speed decreases, wavelength shortens and height increases. When the wave height reaches about 80% of the water depth the wave breaks, producing an accumulation of water that increases the mean sea level near the reef and over the lagoon. As a result, longer wavelength swells break earlier than shorter wavelength wind waves, and do not penetrate as far into reef and lagoon waters.

3.2.7.3 Variability in wave height

There are large natural variations in the wave conditions of the tropical Pacific Ocean. As the formation of waves is driven by wind, SWH and wave period in the region can be related to large-scale climate patterns (Chapter 2). ENSO events are a major source of this variability. An El Niño event is associated with higher waves east of about 170°E during the austral summer (Figure 3.20). West of 170°E, waves generally decrease during El Niño. The opposite occurs during La Niña events. The larger El Niño waves in the central southern Pacific also tend to come from a more southerly direction than normal[87]. During the rest of the year, the pattern of increase in the east and decrease in the west is shifted towards the west (**Figure 3.20**).

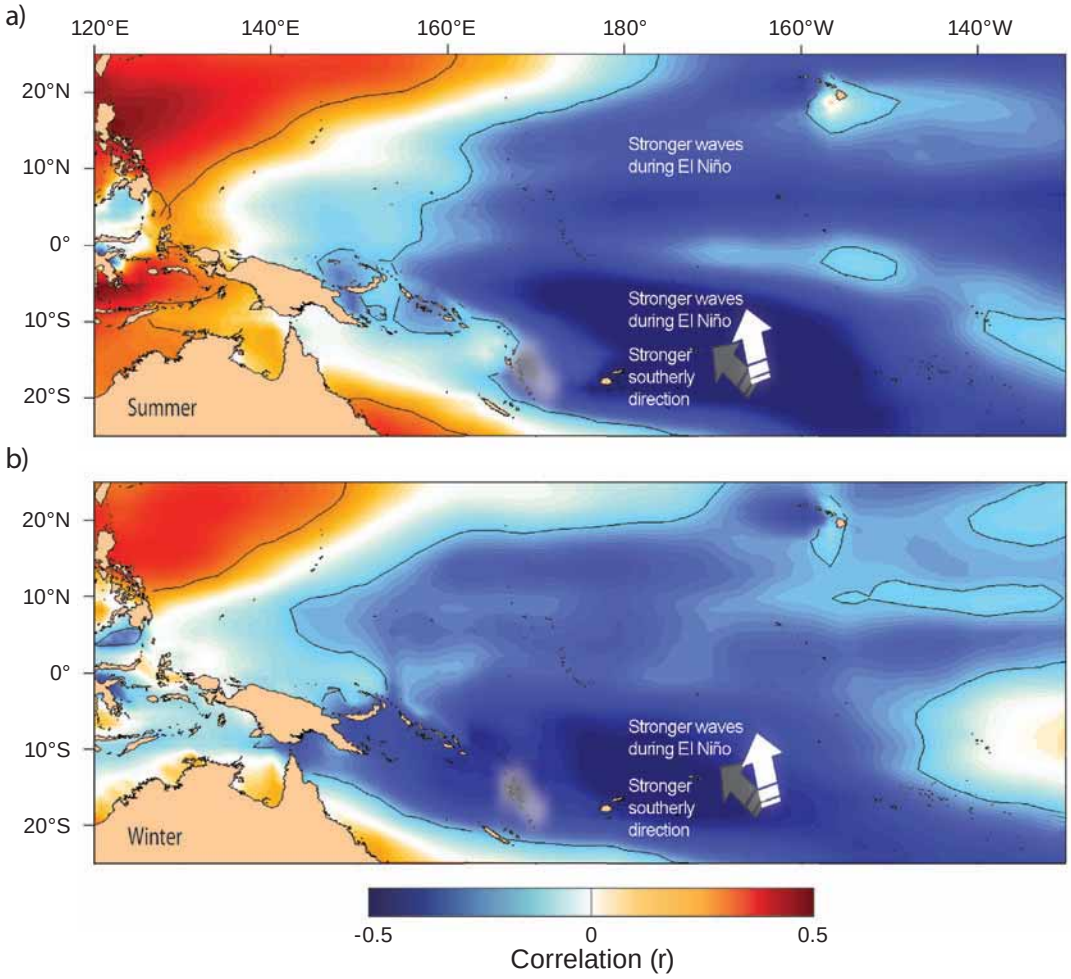

Figure 3.20 Effect of El Niño on wave height and direction (arrows) in the tropical Pacific Ocean during (a) austral summer (December to February) and (b) austral winter, which also represents the remainder of the year. The colour scale represents the (dimensionless) correlation coefficient between mean significant wave height (after annual mean cycle is removed) and the Southern Oscillation Index for the period 1958–2002 (source: Sterl and Caires 2005)[86]. Regions of negative correlation correspond to higher waves during El Niño conditions (a rotation from the grey arrow to the white arrow), or to lower waves during La Niña, with a less southerly direction.

Variation in the intensity and position of storms outside the region to the south also influences SWH in the tropical Pacific Ocean. Storm activity in the mid-latitudes is related to another characteristic climate pattern – the Southern Annular Mode (SAM)[87] (Chapter 2). A positive (negative) SAM is associated with stronger (weaker) mid-latitude westerly winds and increased (decreased) storm activity. The SAM has undergone a robust trend towards a more positive state over recent decades[95].

In the northern Pacific, there is also a strong relationship between wave conditions in Hawaii and ENSO[96]. During El Niño years, high swell events (SWH > 4 m) can occur. This difference is related to a combination of different storm generation regions, intensities and trajectories. During El Niño events, the central northern Pacific experiences the highest winter wave heights north of the equator. In contrast, during La Niña episodes, the region with the highest waves is nearer to the coast of North America[96].

3.2.8 Sea level

Several PICTs are acutely aware that land they depend on may be lost unless there is urgent mitigation of CO_2 emissions to prevent the inundation of low-lying islands. In the worst case scenarios of projected rises of sea level, large-scale relocation of infrastructure and human populations is likely to be required. But the effects of sea-level rise are not limited to the potentially tragic effects on human settlements – they also extend to altering the ecosystems that support the coastal fisheries on which many Pacific people depend for food security and livelihoods (Chapters 5, 6 and 9). Rising sea level will allow damaging waves to penetrate further inshore. It will also change the shape of coastlines and the tidal regimes in some areas as shallow basins are created. In some places, rising sea level may promote increased cover of mangroves and seagrass; in other areas, the extent of these ecosystems will be reduced (Chapter 6).

3.2.8.1 Sea level components and variations

Sea level at a given location is determined by a number of factors (**Figure 3.21**), and the interaction of these factors causes substantial variation on a broad range of time scales (**Figure 3.22**). Tides affect sea level on a predictable periodic basis; storms and eddies are episodic with effects lasting from hours to days; and circulation changes, like those associated with ENSO, can cause large year-to-year variation. The steady driver of global sea-level rise, however, is related to the long-term warming of the ocean and atmosphere which causes the melting of land-based ice and thermal expansion of sea water. Both processes increase the volume of the ocean.

During the peak of the last ice age, when ice sheets covered large parts of the Northern Hemisphere, the additional storage of water on the land led to a drop in sea level of ~ 120 m. Conversely, during the Pliocene ~ 3 million years ago, when global average temperatures were thought to be 2 to 3°C above today's temperatures, sea level was at least 15 to 20 m above present-day values[97].

Today, the main ice sheets are in Greenland and Antarctica, supplemented by ice caps (small ice sheets) such as the one in Iceland, and glaciers. If the major ice sheets were

to melt completely, sea level would increase by about 70 m[98]. In contrast, complete melting of the ice caps and glaciers would increase sea level by only about 70 cm. The melting of floating sea ice does not affect sea level.

Regional changes in sea level due to ENSO events can be as great as 20 to 30 cm (**Figure 3.22**)[99]. This high degree of natural variability makes it difficult to extract robust long-term trends from the relatively short-term records for the region. Combining the information from individual tide gauges to produce estimates for the entire tropical Pacific requires advanced statistical methods[100], particularly because of differences in the way ENSO affects sea level in different locations. In general, an El Niño episode will tend to lower the sea level in the west, and raise it in the east, along the equator. In contrast, a La Niña event can significantly raise the sea level to the west. Over long time periods, sea-level rise due to El Niño events balances the fall due to La Niña episodes. Based on the long-term data series from tide gauges in the tropical Pacific, sea level is rising by between 0 and 3 cm per decade, depending on location (**Figure 3.23**).

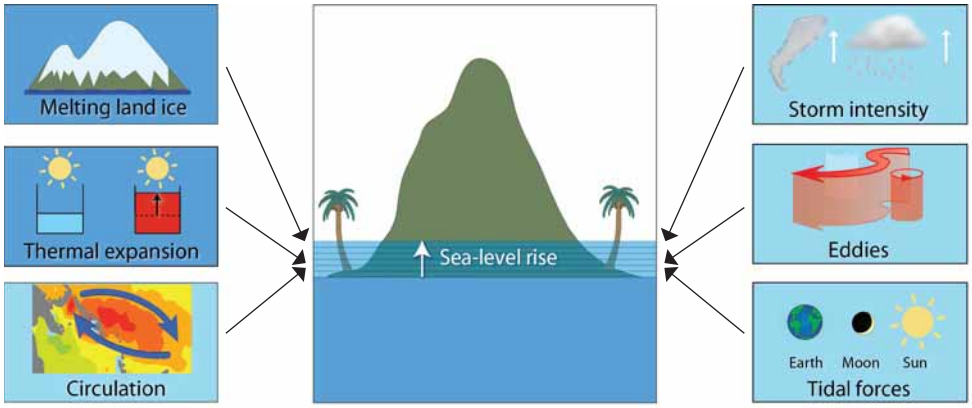

Figure 3.21 Factors determining sea-level rise at any given time and location: melting of land ice, thermal expansion of the ocean, large-scale ocean circulation, atmospheric pressure and storm surges, transient eddies (or ENSO-type waves at the equator) and tides. Melting of land ice and thermal expansion of the ocean are the most important of these factors.

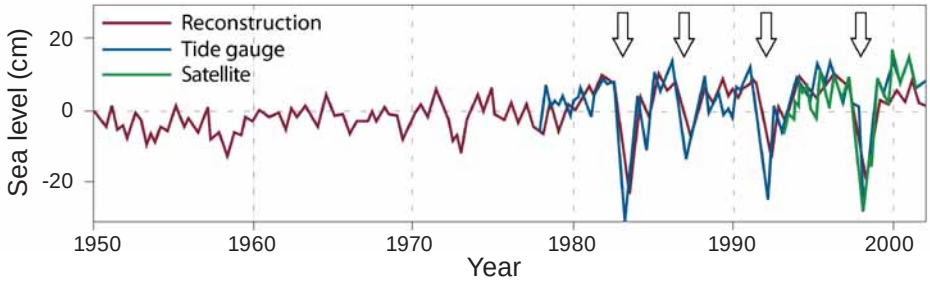

Figure 3.22 Time series (1950–2004) from Funafuti, Tuvalu, showing variation in sea level. Data are from tide gauge (blue), satellite (green) and reconstructions based on the empirical relationship between spatial patterns of variations and tide gauge data (red). Major drops in sea level occur during El Niño events (see arrows). A gradual long-term upward trend can be seen which is particularly pronounced in the second half of the record (source: Church et al. 2006)[99].

Changes in large-scale currents can also alter sea level. An acceleration of the subtropical gyre in the Southern Hemisphere due to long-term changes in the wind field has led to modified sea levels, with local increases or decreases of ~ 10 cm over several years[101]. Oceanic eddies (Section 3.2.3) can alter sea level by ~ 10 cm for several days[102]. Decreases in atmospheric pressure raise sea level by 1 cm for each millibar decrease. This effect is most extreme during cyclones, when the low atmospheric pressure at their centre can draw the water column up by 30 to 50 cm. The amplitudes of each process affecting sea level are usually smaller than those of tides, but they can act in concert. For example, storm surges associated with higher sea levels during cyclones allow destructive waves to penetrate further into coastal habitats.

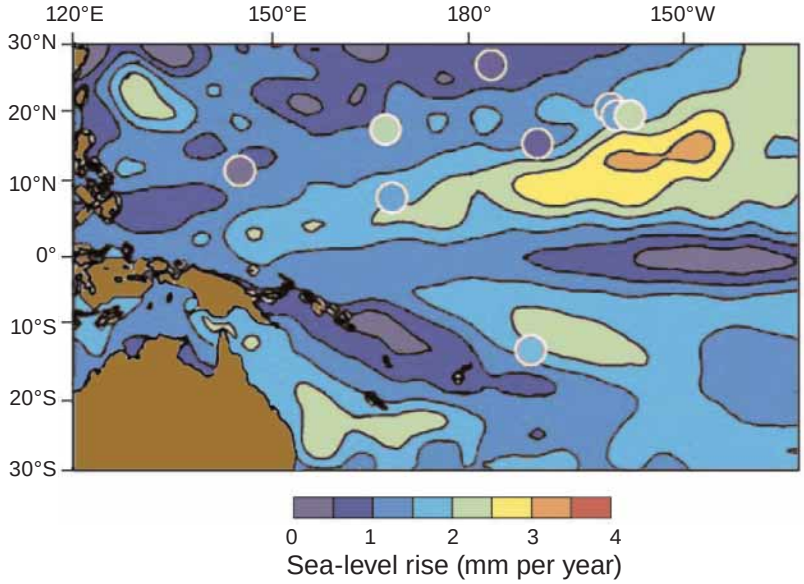

Figure 3.23 Sea level trends from 1950–2001, reconstructed from tide gauge data at several locations across the tropical Pacific Ocean (coloured dots). Recent satellite data have been used to determine the relationship between localised tide gauge data and the rest of the ocean. The longer time-series of tide gauge data are then projected over the region (source: Church et al. 2006)[99].

3.2.9 Coastal circulation and island effects

The description of the tropical Pacific Ocean above has focused largely on the effects of processes in the open ocean that are likely to affect the distribution and abundance of species supporting the important oceanic fisheries of the region. Because coastal fisheries are also vital to the food security and livelihoods of many people in the tropical Pacific (Chapters 1 and 9), it is also important to examine the oceanic processes that influence the productivity of fish and invertebrates close to the coast. We have discussed briefly the effects of waves and sea-level rise on the habitats (coral reefs, mangroves, seagrasses) that support fisheries. Here, we look at the regional oceanic processes that occur along coastlines and around islands, and how these influence the local primary productivity that underpins coastal fisheries production.

These processes generally occur on different scales in the tropical southern and northern Pacific Ocean, largely because the topography in the south is much more complex than in the north. In the south, there are several archipelagos, ranging from rugged high islands to a myriad of coral atolls (Chapter 1). There are also oceanic ridges and many seamounts in the southern and northern Pacific Ocean[103].

The topographic complexity in the south allows the islands there to support rich ecosystems, despite the fact that many of them are located in oligotrophic waters (Section 3.2.4). The presence of islands alters oceanic circulation to bring deep nutrients into the photic zone through at least four processes (**Figure 3.24**), as described below.

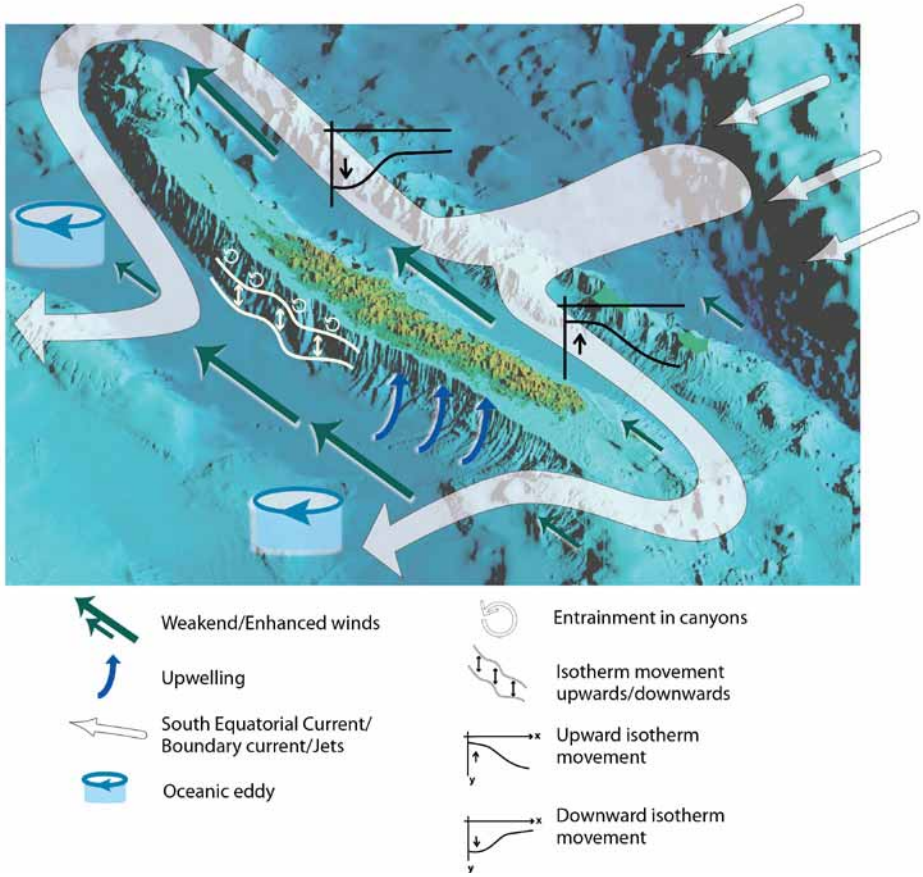

Figure 3.24 The four processes associated with islands that alter ocean circulation and nutrient supply, illustrated over the topography of New Caledonia (1) islands act as obstacles to large-scale currents, generating boundary currents on their eastern sides and eddies downstream, which cause the thermocline to become either deeper or shallower; (2) winds blowing parallel to the coast create local upwelling which enhances nutrient supply; (3) internal waves and tides interact with the topography, generating either temporary upwelling or enhanced mixing that transfers nutrients to the surface (this has been observed at other islands but not at New Caledonia); and (4) orographic effects of high islands that create disturbances to the large-scale winds downstream of an island, resulting in counter currents, upwelling and more intense eddy activity (source: Lefevre et al. 2010 and New Caledonia Remote Sensing and Geomatics Service)[116].

3.2.9.1 Islands as obstacles to flow

Where islands lie in the path of large-scale westward flowing ocean circulation, boundary currents are formed on their eastern coasts. On large islands and coasts (e.g. Australia and PNG), the strong boundary currents formed there have a direct effect on nutrient supply; an equatorward current, such as the North Queensland Current, will deepen the thermocline locally (Section 3.2.2) and restrict access to nutrients. Conversely, a poleward current reduces the depth of the thermocline, facilitating access to deep nutrients[104]. Local counter currents, bottom friction and turbulent interaction with canyons can also result in enhanced mixing of surface and deeper nutrient-rich waters adjacent to the shelves.

An oceanic current encountering an island can also trigger eddy formation 'downstream', reducing the depth of the thermocline in its wake and enhancing nutrient supply and biological production[105–108].

A snapshot of the SST and current velocity around Vanuatu and New Caledonia (**Figure 3.25**) illustrates how the westward flowing SEC interacts with the different islands. Strong boundary currents form on the east coast of New Caledonia, which eventually continue westwards as jets flowing around the northern and southern tips of the New Caledonia shelf. The complex topography leads to the formation of eddies in the lee of islands, or the modification of passing eddies[61]. These eddies are associated with either anomalously warm (anticlockwise on **Figure 3.25**) or cold (clockwise) surface temperatures.

3.2.9.2 Wind-driven upwelling

When the wind blows parallel to the coast, local upwelling can occur that enhances nutrient supply to the surface waters. The snapshot shown in **Figure 3.25** represents the situation during an episode of strong southeast trade winds parallel to the coastline of New Caledonia. The trade winds push surface waters to the southwest by Ekman transport (Box 3.1) away from the coast, resulting in an upwelling of deep water. Such upwelling produces the 'cold patch' to the southwest of New Caledonia and occasionally brings nutrients from deep waters to the surface[109–111].

3.2.9.3 Internal waves

Tidal currents affect the full water column and when they interact with features on the seafloor such as seamounts, they can generate strong vertical displacements of water. Such tidal-bathymetry interactions, as well as quick vertical displacements of water generated by other processes, create 'internal waves'. These subsurface waves can travel large distances away from their source region, and eventually dissipate in areas of rugged topography. The Pacific islands are a major dissipation region for internal waves[112], where their energy is released to produce oceanic mixing. Internal waves can displace water vertically from tens to hundreds of metres, over periods

ranging from minutes to several hours. Near islands, vertical movements of water as great as 270 m have been observed[113]. Such displacements can deliver nutrients from the deep ocean to the trenches and channels at the base of coral reefs, a depth of about 50 m. Because of the large amount of mixing occurring at such places, nutrients can then be brought to the surface within just a few minutes. This process provides an efficient mechanism for nutrient enrichment of coastal waters and results in greater biological productivity where it occurs. In summary, internal waves interact with topography, generating either temporary upwelling or enhanced mixing.

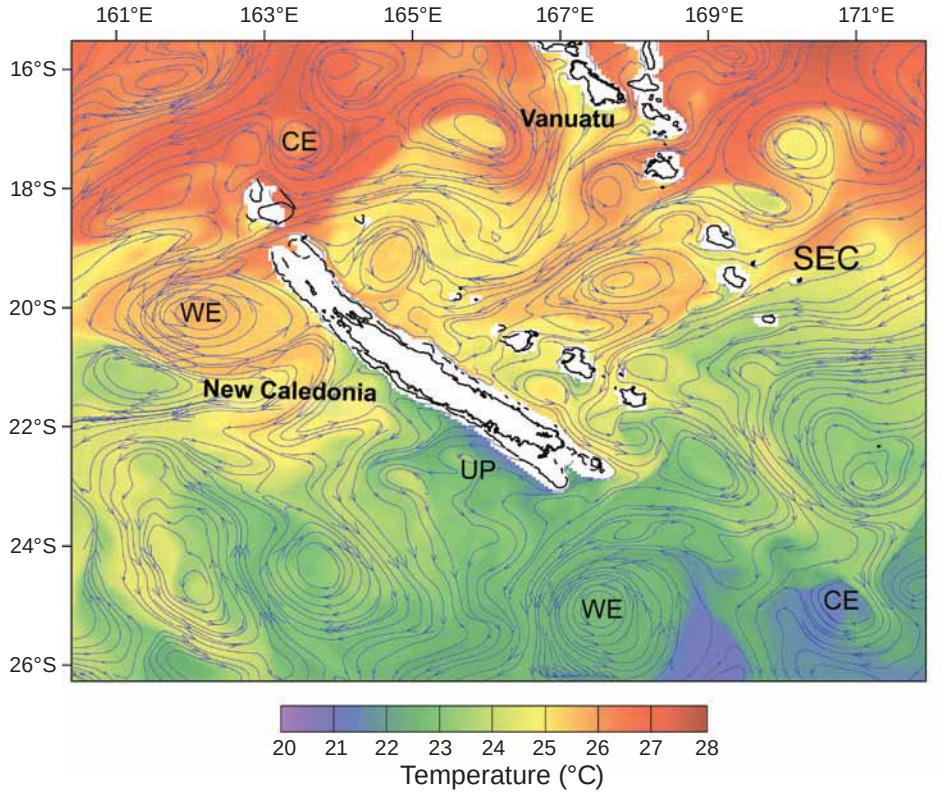

Figure 3.25 Sea surface temperature and surface velocity fields (blue streamlines) on November 9, 2004 near New Caledonia and Vanuatu from a high resolution numerical simulation forced with observed winds. The large-scale easterly flowing South Equatorial Current (SEC) encountering the islands is divided into multiple branches by eddies and islands, and finally splits against the east coast of New Caledonia. This snapshot demonstrates the high variability associated with oceanic eddies that either arrive from the east, or form by interaction with topographic features. Against the southwest coast of New Caledonia, a cold patch of surface water reveals an upwelling event; WE = warm eddy; CE = cold eddy; UP = upwelling (source: Lefèvre et al. 2010)[116].

3.2.9.4 Orographic effects

High islands also modify large-scale wind patterns, creating disturbances 'downstream' which can generate counter currents and more intense eddy activity[27–30] to deliver more nutrients to surface waters. For example, the Hawaiian Islands split

the northeast trade winds and induce a westerly oceanic counter current in their wake[114,115]. Similarly, the mountain range with several major peaks running along New Caledonia disrupts the southeast trade winds. This results in areas of both enhanced and weakened surface winds well away from the island, which affect current circulation patterns both in the lagoon and nearby open ocean[116].

3.3 Observed and projected changes in the tropical Pacific Ocean

The features of the tropical Pacific Ocean described above are undergoing changes due largely to the recent observed alterations in atmospheric conditions, particularly surface temperatures and their associated effects on winds in the region, and the increased emissions of CO_2 (Chapter 2). Future changes to surface climate and atmospheric concentrations of CO_2 are also expected to drive profound changes in many features of the tropical Pacific Ocean, including currents, SST, eddies, availability of nutrients, dissolved oxygen, acidification, wave height, sea level and coastal processes. In this section, we outline the changes that have already been observed and those that are projected to occur.

3.3.1 Large-scale currents

3.3.1.1 Observed changes

Substantial changes in the South Pacific Subtropical Gyre (**Figure 3.1**) have been recorded between 1993 and 2003. These changes are thought to be associated with an intensification of the SAM, with the southwesterly winds in the Southern Hemisphere shifting southwards and increasing in intensity[101,117]. There has been an increase in the intensity of the gyre's circulation, the SEC and, as a consequence, the height of the sea surface at its centre (40°S, 170°W) has increased by about 12 cm[101]. In addition, the East Australian Current has intensified over the past 60 years, generating substantial warming of the Tasman Sea[118]. The North Pacific Subtropical Gyre also intensified between 1993 and 2003 but with weaker amplitude[119].

3.3.1.2 Projected changes

The currents of the upper water column across much of the tropical Pacific Ocean are expected to change in the future, particularly as a result of weakened wind regimes at low latitudes[120] and strengthened winds in the subtropical Southern Hemisphere[121,122]. Multi-model mean projections for large-scale surface currents show relatively small absolute changes away from the equatorial band 12°S–10°N. However, major changes occur near the equator.

For the SECC, which flows eastward from the area around Solomon Islands to about 160°W, 10°S (**Figure 3.1**), these changes will take time to appear – in the upper 50 m flow is projected to be ~ 8% weaker under the B1 and A2 scenarios in 2035. However,

by 2100 under B1 the strength of the surface SECC is projected to decrease by 28% and by a dramatic 60% in 2100 under A2 (**Figure 3.26**). The surface flow also tends to turn towards the south, reducing the penetration of the SECC to the east. Nearby, at 12°S, the upper 50 m of the SEC is projected to increase in a thin zonal band. In the Northern Hemisphere, a decrease is projected in the eastern half of the surface NECC (180°–130°W; 7°N–10°N), with a slight decrease in the NEC just north of this region (at 140°W–130°W).

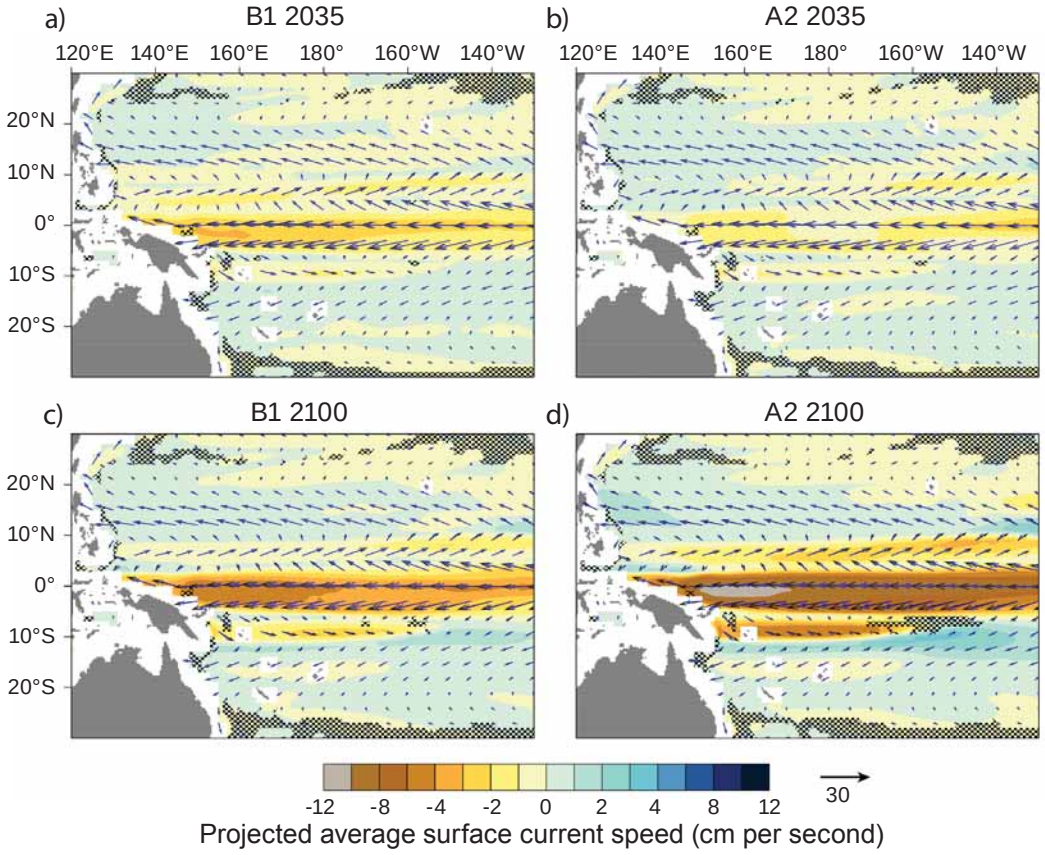

Figure 3.26 Multi-model means of recent and projected average surface current speed (cm per second) down to a depth of 50 m for (a) the B1 scenario in 2035; (b) A2 in 2035; (c) B1 in 2100; and (d) A2 in 2100. Black arrows represent averaged 1980–1999 currents; blue arrows are the projections. The size of the arrows reflects velocity. Shaded areas indicate where either current speed or the change in direction is below the 90% confidence level; white areas represent regions where one or several models have no data.

Within 3° of the equator, the westward flowing SEC also decreases in strength with global warming. Its initial flow, which averages between 30 and 50 cm per second in the upper 50 m, is projected to decrease by only 2 to 3 cm per second in 2035 under both scenarios, and then by about 5 cm per second under B1 and 10 cm per second under A2 in 2100. The corresponding projected reductions in SEC transport (volume of water moved) compared with its average present value between 160°E to 130°W

(~ 28 Sv, Figure 3.27) (1 Sv = 1 Sverdrup = 10^6 m^3 per second) are -0.5 to -1 Sv (3–5%) in 2035, -2 Sv (9%) under B1 in 2100 and -4.5 Sv (18%) under A2 in 2100. A vertical section along the equator shows that just below the SEC the eastward EUC is projected to move progressively upwards by about 10 m under B1 and A2 in 2035 and B1 in 2100, and then by 20 m under A2 in 2100 (Figure 3.27). The eastward EUC is also expected to increase in strength and transport over the 21st century (Figure 3.27), reducing the depth to which the SEC penetrates.

Changes in current strengths are likely to affect biological production and fisheries through the various processes that supply nutrients discussed below. They will also affect the dispersal of larvae and connectivity among populations[123]. Changes to the EUC may have consequences because of the important role of this undercurrent in the transport of iron, sourced from the New Guinea Coastal Undercurrent, to the eastern and central Pacific[124], where iron concentrations limit primary productivity (Chapter 4). Therefore, changes to the depth and strength of the EUC may also have important effects on fisheries in the region.

3.3.2 Ocean temperature

3.3.2.1 Observed changes

As a result of its large heat capacity, the ocean has absorbed most of the additional heat due to recent global warming – about 30 times more anthropogenic heat has entered the ocean than the atmosphere since the 1960s[125]. Globally, SST is estimated to have warmed ~ 0.67°C from 1901 to 2005[126]. In the Pacific basin, warming of SST of 1 to 1.5°C has occurred at the western coastal boundary south of the equator and in the east, north of the equator, during the past 50 years[127,128].

Separating long-term warming of SST from the natural variability of the tropical Pacific Ocean has not been straightforward. For example, ENSO has accounted for ~ 30% of the variability (excluding the seasonal cycle) during the past 100 years, with ~ 10% attributable to global warming[127,129], and the remaining ~ 60% being due to decadal and other modes of variability. But the warming trend is conspicuous, even below the surface – it has been detected in all oceans and at increasing depths since the 1950s[125,130–132].

Over the past 50 years, the water column between the surface and about 200 m in the tropical and subtropical Pacific has warmed by up to 2°C (Figure 3.28). Counter-intuitively, south of 8°N, a consistent and broad-scale cooling has occurred in the central and lower thermocline that extends south to at least 25°S (Figure 3.28), which is most pronounced at around 200 m in the equatorial region. This cooling appears to be related to changes in the surface winds that can raise the thermocline. Despite the addition of heat to the system, the upward displacement of the strongest vertical temperature gradient associated with the thermocline leads to net cooling[133].

(~ 28 Sv, Figure 3.27) (1 Sv = 1 Sverdrup = 10^6 m^3 per second) are -0.5 to -1 Sv (3–5%) in 2035, -2 Sv (9%) under B1 in 2100 and -4.5 Sv (18%) under A2 in 2100. A vertical section along the equator shows that just below the SEC the eastward EUC is projected to move progressively upwards by about 10 m under B1 and A2 in 2035 and B1 in 2100, and then by 20 m under A2 in 2100 (Figure 3.27). The eastward EUC is also expected to increase in strength and transport over the 21st century (Figure 3.27), reducing the depth to which the SEC penetrates.

Changes in current strengths are likely to affect biological production and fisheries through the various processes that supply nutrients discussed below. They will also affect the dispersal of larvae and connectivity among populations[123]. Changes to the EUC may have consequences because of the important role of this undercurrent in the transport of iron, sourced from the New Guinea Coastal Undercurrent, to the eastern and central Pacific[124], where iron concentrations limit primary productivity (Chapter 4). Therefore, changes to the depth and strength of the EUC may also have important effects on fisheries in the region.

3.3.2 Ocean temperature

3.3.2.1 Observed changes

As a result of its large heat capacity, the ocean has absorbed most of the additional heat due to recent global warming – about 30 times more anthropogenic heat has entered the ocean than the atmosphere since the 1960s[125]. Globally, SST is estimated to have warmed ~ 0.67°C from 1901 to 2005[126]. In the Pacific basin, warming of SST of 1 to 1.5°C has occurred at the western coastal boundary south of the equator and in the east, north of the equator, during the past 50 years[127,128].

Separating long-term warming of SST from the natural variability of the tropical Pacific Ocean has not been straightforward. For example, ENSO has accounted for ~ 30% of the variability (excluding the seasonal cycle) during the past 100 years, with ~ 10% attributable to global warming[127,129], and the remaining ~ 60% being due to decadal and other modes of variability. But the warming trend is conspicuous, even below the surface – it has been detected in all oceans and at increasing depths since the 1950s[125,130–132].

Over the past 50 years, the water column between the surface and about 200 m in the tropical and subtropical Pacific has warmed by up to 2°C (Figure 3.28). Counter-intuitively, south of 8°N, a consistent and broad-scale cooling has occurred in the central and lower thermocline that extends south to at least 25°S (Figure 3.28), which is most pronounced at around 200 m in the equatorial region. This cooling appears to be related to changes in the surface winds that can raise the thermocline. Despite the addition of heat to the system, the upward displacement of the strongest vertical temperature gradient associated with the thermocline leads to net cooling[133].

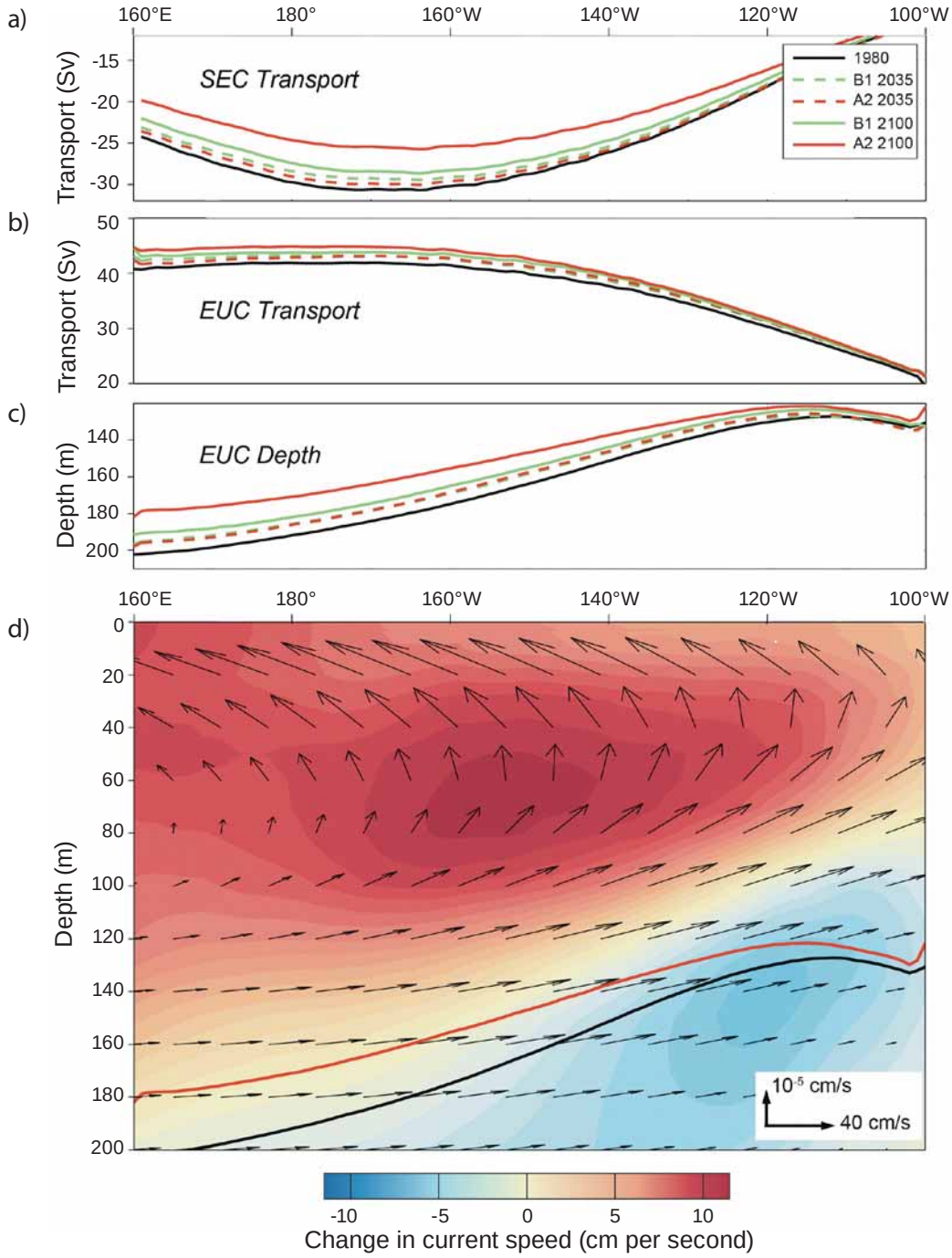

Figure 3.27 Projected changes in (a) transport volume (Sv = 10^6 m^3 per second) of the South Equatorial Current (SEC) as a function of longitude across the equator; (b) transport volume of the Equatorial Undercurrent (EUC); (c) depth of the EUC; and (d) eastward velocity (cm per second) for the A2 scenario in 2100 (2080–2099) minus (1980–1999), with mean velocity vectors superimposed as arrows (averaged between 2°S and 2°N with vertical velocity scale accentuated). Black and red lines indicate the mean position of the EUC core for 1980–1999, and for the A2 scenario in 2100, respectively.

Changes have also been observed in the Warm Pool, which is subject to interannual and longer-term (decadal) fluctuations[134]. Since 1956, a reduction in salinity ('freshening') of 0.1 to 0.4 PSU (practical salinity unit: 1 PSU = 1 g per kg of sea water) has occurred in the Warm Pool[128,135]. The observed freshening, and the intensified surface warming trends described above, combine to reduce the near-surface density of water near the surface of the ocean. Along with the deeper cooling, these trends cause increased stratification (Section 3.2.2.2) and an associated reduction in depth of the thermocline in the Warm Pool. This has important consequences for the availability of nutrients (Box 3.2) (Section 3.2.4). These processes may also cause further increases in SST locally because absorbed heat now warms a thinner surface layer. Such changes in the vertical structure of water density also affect the onset and intensity of ENSO[44].

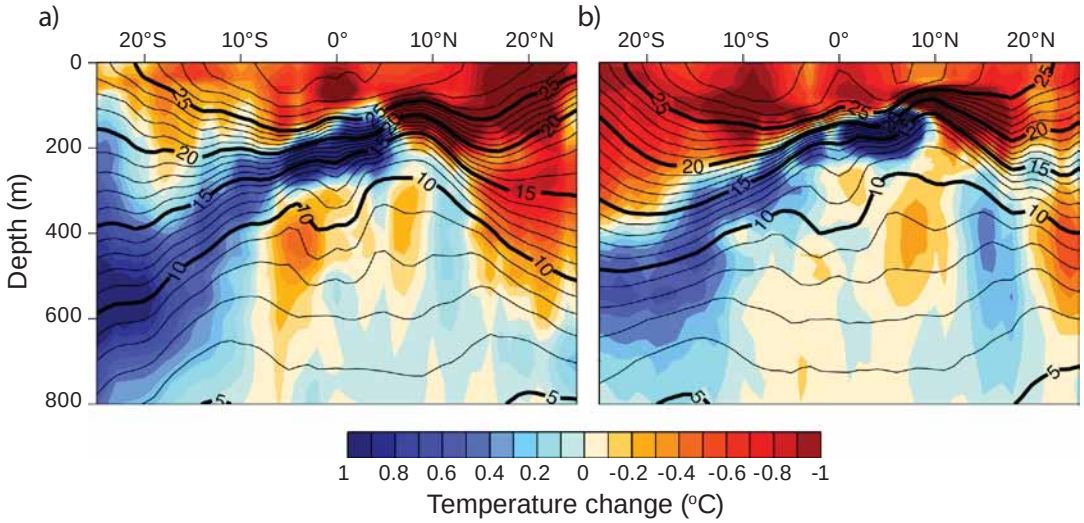

Figure 3.28 Temperature changes in the tropical Pacific Ocean over the past 50 years for a vertical meridional section at (a) 160°E and (b) 160°W. Average temperature is overlayed as black contours (fine lines are 1°C intervals; thick lines 5°C intervals) (source: Durack and Wijffels 2010)[194]. The warming reaches 2°C in dark red areas.

3.3.2.2 Projected changes

Sea surface temperature of the tropical Pacific Ocean is projected to increase under the B1 and A2 emissions scenarios. For both scenarios, annually averaged warming across the region, relative to the 1980 to 1999 average, is projected to increase within a range of 0.5 to 1.0°C by 2035. In 2100, the increase in SST is expected to be within the range of 1.0 to 1.5°C greater under B1, and to increase by 2.5 to 3.0°C under A2 (**Table 3.1**). The greatest warming is projected to occur in the Pacific Equatorial Divergence Province and the least warming at the eastern boundary of the South Pacific Subtropical Gyre (Section 3.2.2.4).

Both scenarios and time periods show a similar spatial and vertical pattern of warming. The increase is greatest near the equator, with warming decreasing with depth. Maximum warming is expected to approach 1°C at the surface and 0.5°C at 80 m by 2035 in both scenarios (**Figure 3.29**). Under B1 in 2100, the multi-model mean

projects warming of up 1.5°C at the surface and 1°C at 80 m. Projected warming for the A2 scenario is about twice as great, i.e. up to 3°C at the surface and 1.8°C at 80 m (**Figure 3.29a**). These trends are similar to those observed over the past 50 years (~ 2°C per century at the surface) (**Figure 3.28**). Below 100 m, and west of about 150°E, a distinct cooling pattern is projected to occur, which gets stronger over time: two cooling centres occur north and south of the equator (**Figure 3.29b,c**) at ~ 160 m depth and within 10°N–10°S. This pattern is also similar to the observed temperatures over the past 50 years (**Figure 3.28**) and is probably associated with the projected changes in the overlying wind field, and a shoaling of the thermocline[133] (Section 3.2.2). In 2100, the maximum subsurface cooling is projected to reach about 0.5°C under the B1 emissions scenario and 1°C under A2.

The 28°C isotherm along the equator is projected to deepen in the west by ~ 10 m for the B1 scenario and ~ 15 m for A2, with most of this increase occurring after 2035 (**Figure 3.29**). Poleward of 10°N–10°S, the projected warming penetrates to considerably greater depths than at the equator, with a warming of ~ 0.5°C down to 250 m under both scenarios by 2035. This deep projected warming increases to ~ 1°C under B1 and ~ 1.5°C under A2 in 2100. The uneven warming of the water column increases stratification strongly across most of the region, with associated negative effects on vertical mixing and nutrient uptake, as discussed in Section 3.2.4.

By averaging over multiple climate models, we have removed the more extreme changes that are nonetheless feasible. Individual models show that the projected warming may reach 3.6°C at the surface and that the +2°C contour may deepen to 100 m at the equator by 2100. Also, by examining 20-year averages, we are purposely removing the effect of any year-to-year variations to isolate the global warming signal. In the real world, there is a high degree of interannual variability in this region, associated with ENSO in particular. Thus, in some years we would expect considerably warmer temperatures than the mean values projected here. Based on our multi-model mean for the A2 scenario in 2100, a relatively strong ENSO event (2 standard deviations) is expected to produce year-to-year variations in surface temperature of ~ 2°C.

Simulation of the projected features of the Warm Pool remains a major challenge for the IPCC models due to difficulties in realistically simulating SST, precipitation and salinity. In particular, the tropical Pacific is generally too cold, with the east Pacific cold tongue extending too far into the western basin. The models tend to produce a SPCZ that is zonally elongated and that extends too far to the east in a symmetrical pattern of high precipitation about the equator, forming a 'double ITCZ'[136]. This distortion creates a spurious pattern of rainfall south of the equator, limiting the ability of many models to represent tropical precipitation patterns and ocean surface salinity accurately[137–139]. While the IPCC models used produce ENSO-like variability, they also have biases in ENSO behaviour, e.g. the region of greatest SST variability is displaced far towards the west. We present the following projections for the extent of the Warm Pool, bearing in mind these biases.

The edge of the Warm Pool (as defined by the 29°C isotherm) is projected to move ~ 5000 km eastward in 2100 under the A2 scenario (**Figure 3.29a**). The surface extent

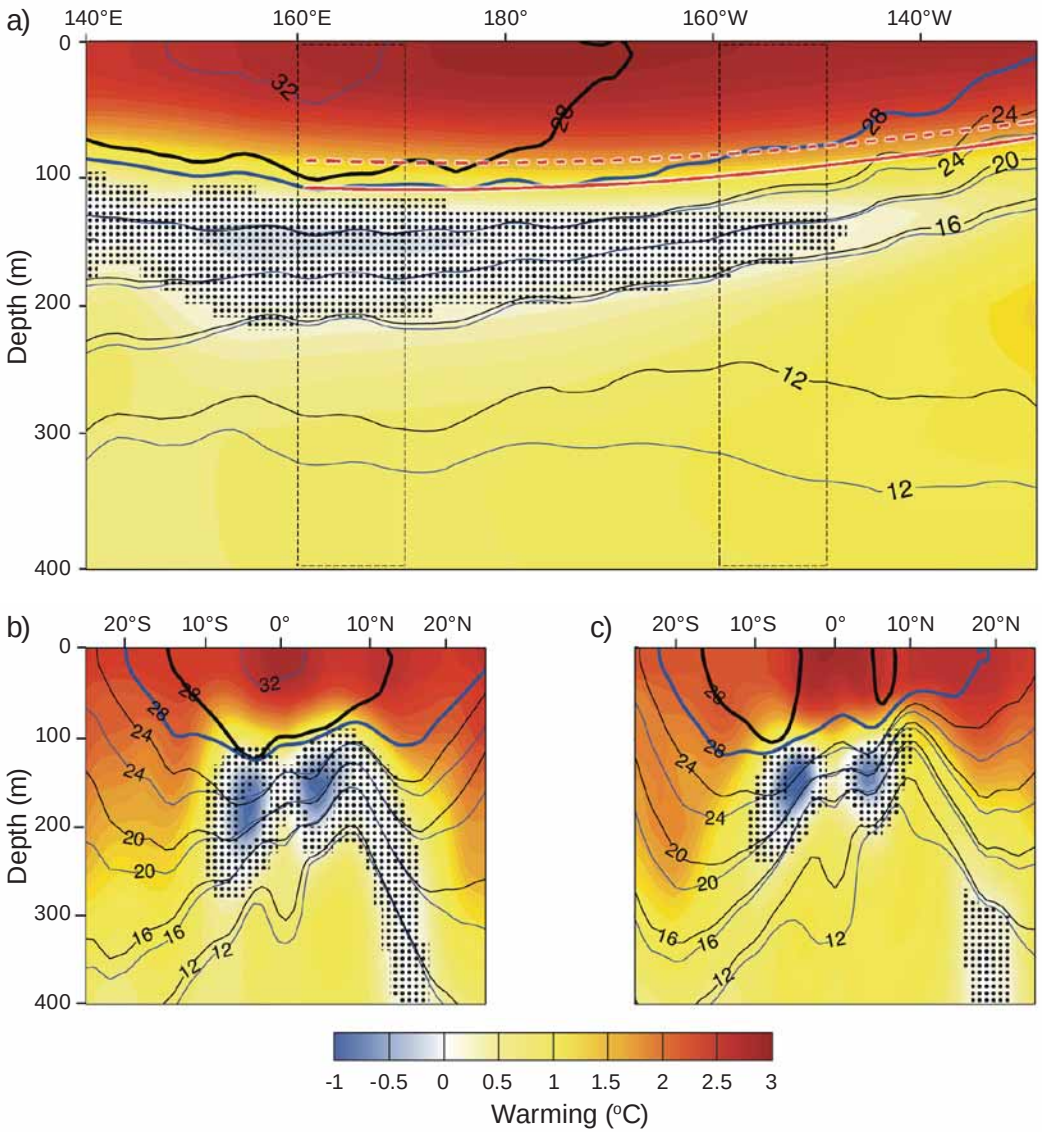

Figure 3.29 Projected warming in the upper 400 m of the tropical Pacific Ocean under the A2 emissions scenario in 2100 (a) along the equator (averaged between 2°S and 2°N); (b) along 165°E (averaged between 160°E and 170°E); and (c) along 155°W (averaged between 160°W and 150°W). Colour shading shows the multi-model mean projected warming in 2100 for the A2 scenario, relative to 1980–1999. Grey mottling indicates areas where warming is not significant at the 90% confidence level. Black contours show mean present day temperatures (based on the CARS 2006 CSIRO climatology) and the blue line represents the mean temperatures projected for 2100 (calculated relative to the CARS 2006 data), with the 28°C isotherms thickened. The red lines in (a) indicate the depth of the thermocline during 1980–1999 (solid) and the depth projected for 2100 (dashed). Thermocline depth is estimated as the depth where temperature is 2.5°C below the temperature at the surface.

of the area comprising the Warm Pool is expected to have an eastern boundary around 170°W in 2035 under both emissions scenarios. This area is projected to increase by a factor of eight, and the eastern limit of the 29°C isotherm is expected to be around 150°W for the B1 scenario in 2100. For A2 in 2100, the area increases by a factor of nine, reaching 61 million km^2. By that time, the 29°C waters are projected to spread across the Pacific basin at the equator, reaching the coast of central America.

Table 3.1 Projected changes to selected key features of the tropical Pacific Ocean, relative to 1980–1999, for 2035 (2025–2045) and 2100 (2080–2099) under the B1 and A2 emissions scenarios, based on a multi-model mean. The confidence intervals provided at 90% confidence for each projection (see key below); percentage change for the multi-model mean is indicated.

Ocean feature	1980–1999	2035		2100	
		B1	A2	B1	A2
Mean equatorial SEC transport (Sv) (160°E–130°W)	28	26–28 (-5%)	26–29 (-3%)	25–27 (-9%)	22–25 (-18%)
Strength of SECC in upper 50 m* (cm.s^{-1})	6.20	4.9–6.5 (-8%)	3.9–6.2 (-18%)	3.2–5.7 (-28%)	0–5.1 (-60%)
SECC zonal component isotach* 5 cm per second	187°E	186°E (2°W)	184°E (3°W)	181°E (6°W)	174°E (13°W)
Zonally averaged zonal windstress* (10^{-2} Nm^{-2}) (2°S to 2°N)	-3.3	-3.26 to -3.06 (-5%)	-3.24 to -3.08 (-5%)	-3.23 to -2.91 (-8%)	-3.20 to -2.73 (-10%)
Pacific basin SST (°C)**	27.4	28.0–28.2 (+0.7)	28.0–28.2 (+0.7)	28.6–29.0 (+1.4)	29.6–30.1 (+2.5)
Maximum Warm Pool temperatures (°C)[a,**]	29.6	30.3–30.5 (+0.7)	30.4–30.6 (+0.8)	30.9–31.3 (+1.5)	32.0–32.5 (+2.6)
29°C Warm Pool area*** (x 10^6 km^2)[b]	7	20–26 (+230%)	22–27 (+250%)	36–46 (+480%)	58–65 (+770%)
Warm Pool salinity front[c]	~ 166°E	166°E–172°E	166°E–169°E	167°E–172°E	170°E–179°E

* Average eastward velocity between 165°C and 160°W and 8.5°S to 7.5°S which corresponds to the maximum of the multi-model-mean contour line of constant velocity; ** for region 130°E–130°W, 25°S–25°N; *** for region 105°E–160°W, 30°S–30°N; a = temperature based on the maximum long-term monthly mean sea surface temperatures in the warmest 10% of the region (higher temperatures can be expected in individual years – particularly those associated with ENSO); b = '29°C pool' defined as area with temperature above 29°C; c = defined as the position of the 34.8 salinity at the equator; SEC = South Equatorial Current; SECC = South Equatorial Counter Current; SST = sea surface temperature.

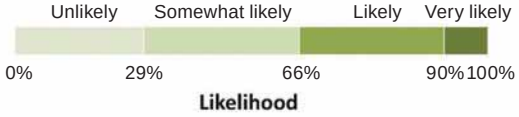

The position of the Warm Pool is intimately tied to ENSO dynamics and the boundary of intense convective rainfall. However, because warming occurs across the whole basin, changes in the 29°C isotherm may not be the best way to identify the edge of the Warm Pool in the future. A more relevant boundary may be the position of the salinity front that highlights the area of strong rainfall occurring over the Warm Pool. At the equator, this front is projected to move east by ~ 1400 km under the A2 scenario by 2100 (**Table 3.1, Figure 3.30**), which is likely to alter the distribution of tuna (Chapter 8).

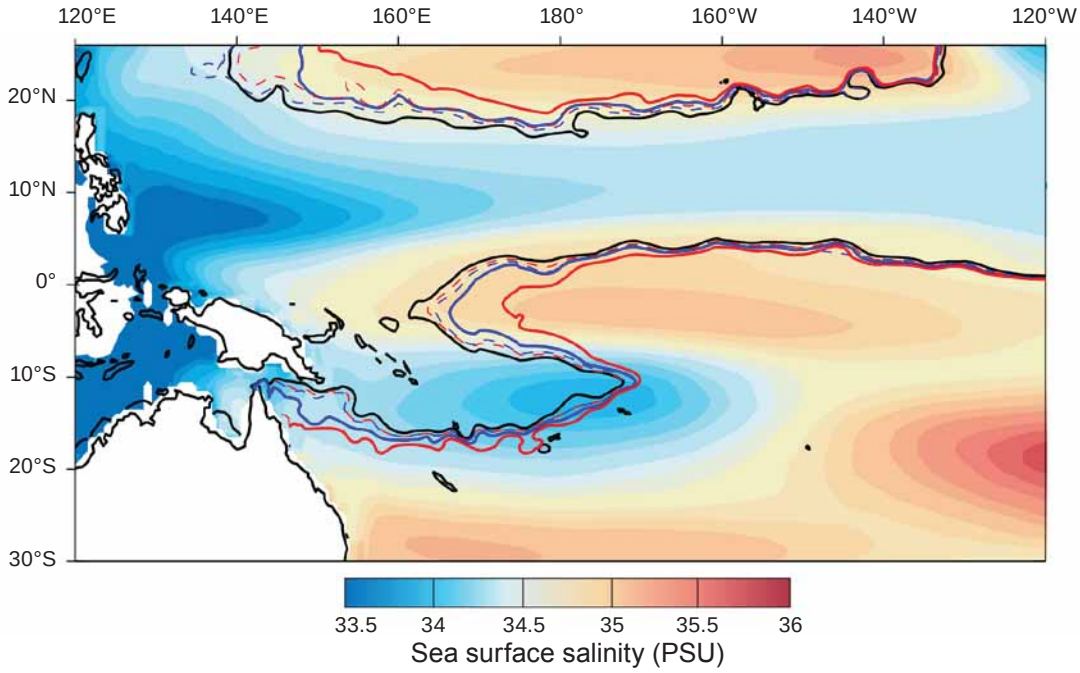

Figure 3.30 Sea surface salinity (SSS), derived from the multi-model mean. The 34.8 contour used to characterise the edge of the Warm Pool at the equator is shown by the black line for the period 1980–1999. The other lines indicate the projected 34.8 contour for 2035 under the B1 (dashed blue) and A2 scenarios (dashed red); and for 2100 under B1 (solid blue) and A2 (solid red). The black line also represents the position of the observed SSS front and the projections are anomalies relative to the observed SSS.

3.3.3 Ocean eddies

3.3.3.1 Observed changes

Energy is generated for eddies when there are strong horizontal density gradients, e.g. when the thermocline is tilted[25,26]. Consequently, eddy activity changes on seasonal, decadal and longer time scales, as the density structure of the ocean varies (Section 3.2.3). Changes in water density are mirrored by those for sea level (e.g. high density/cold patches of water are associated with depressed sea level). As a result, observation of large-scale patterns of eddy activity can be made from satellite data

for sea surface height. These altimetric data have been used to reveal important seasonal[52] and interannual[140] variations in eddy activity. Between 1993 and 2001, eddy activity varied by 15–30% in the tropical Pacific Ocean. An extension of the satellite time-series until 2008 revealed even larger interannual variability in strength and distribution of eddies (**Figure 3.31**), with some of the 'high-energy' regions during 1998 to 2002 disappearing between 2003 and 2008. The limited period that satellite observations have been available does not allow us to determine whether this represents natural interannual changes in eddies or a long-term trend.

3.3.3.2 Projected changes

The coarse spatial scales of the CMIP3 climate models do not resolve oceanic eddies. Therefore, projections of future eddy activity can only be qualitative. As eddies are generated at thermal fronts where there are strong oceanic currents (Section 3.2.3), future eddy activity may also be linked to projected changes in ocean currents (Section 3.3.1). The multi-model average suggests that little change in circulation is likely poleward of 15°N–15°S (Section 3.3.1). Nevertheless, significant changes are projected within 15° of the equator in 2100 (**Figure 3.26**). East of Solomon Islands, the SECC is projected to decrease (Section 3.3.1), which may cause a decline in eddy activity[52,141]. At 12°S, the SEC is projected to increase in a thin zonal band. In the Northern Hemisphere, eddy activity can be expected to increase or decrease in association with projected changes in strength in parts of the NEC and NECC (Section 3.3.1), if the same dynamical link between flow strength and eddy activity applies there[52]. Based on **Figure 3.26**, the amplitude of changes in both circulation and eddy activity is expected to be small in 2035.

Rossby waves of planetary scales are resolved in climate models. Because of their sensitivity to the thermal structure of the ocean, the propagation speeds of Rossby waves are expected to increase by up to 35% relative to pre-industrial times under the A1B scenario[142]. Any change in the activity of eddies and Rossby waves may have important consequences for the supply of nutrients to the photic zone, because they are associated with increased vertical water transport.

3.3.4 Nutrient supply

3.3.4.1 Observed changes

The availability of nutrients in the photic zone, and consequently the biological productivity that sustains fisheries, is sensitive to changes in the circulation and stratification of the ocean (Section 3.2.4). Strong variations in the supply of nutrients have been observed as a result of climate variability on decadal time scales[143]. One of the two existing long-term time-series of nutrient levels collected over the past 30 years indicates small net decreases in nutrient supply to the photic zone of the tropical Pacific Ocean. However, poor spatial and temporal data coverage before the satellite era means that any assessment across the region is uncertain.

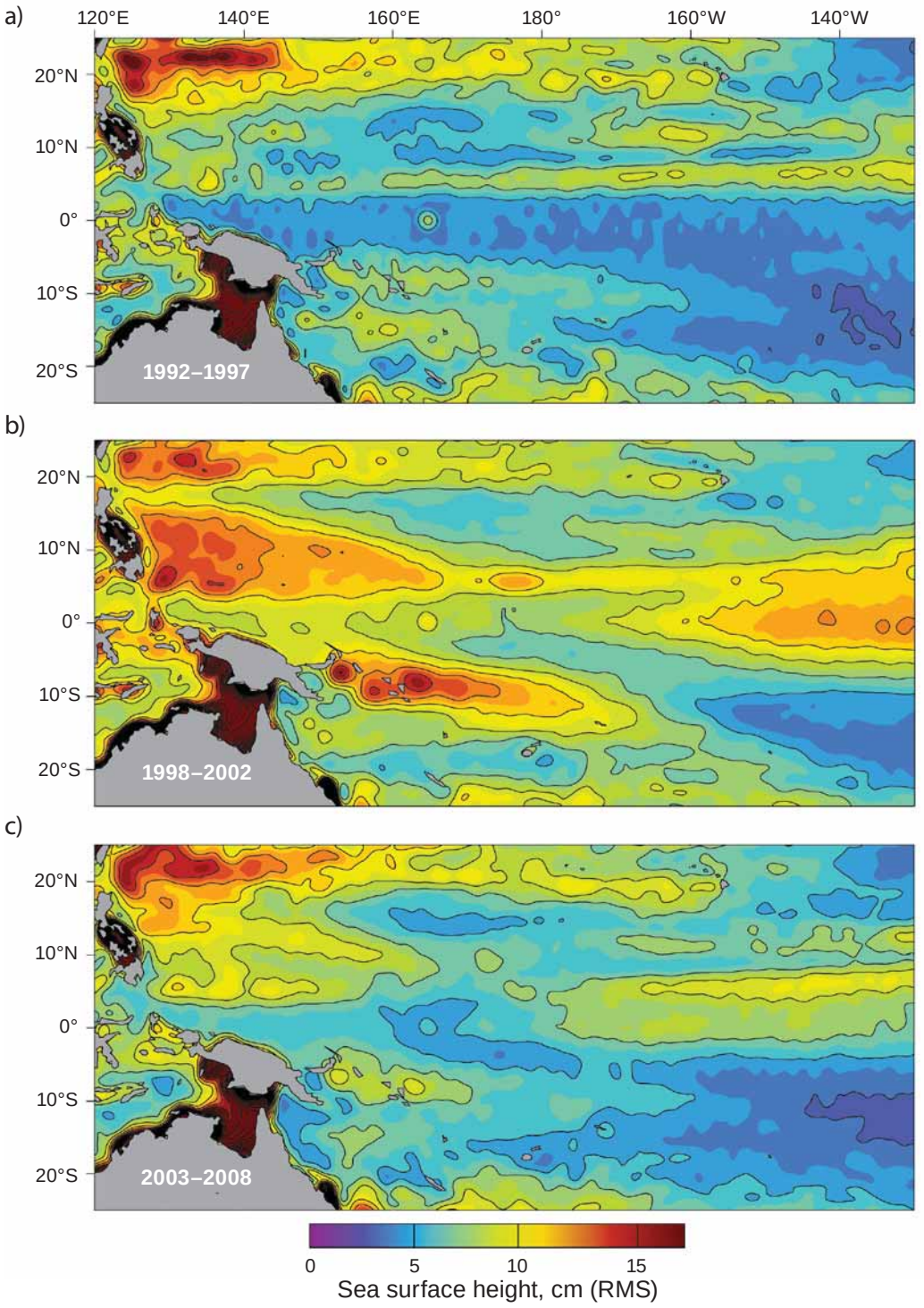

Figure 3.31 Decadal changes in eddy activity, measured from variability in sea surface height (SSH) anomaly for (a) 1992–1997; (b) 1998–2002; and (c) 2003–2008. Each map was obtained using the same procedures as described for Figure 3.12.

The observed decreases in nutrient supply appear to be related to the increased stratification of tropical surface waters (Section 3.3.2) over the past 50 years (**Figure 3.32**). Low-nutrient surface waters are warming and high-nutrient deeper waters are cooling south of 8°N. This may have reduced the efficiency of nutrient transfer into the photic zone (Box 3.2) over broad regions of the tropical Pacific Ocean. North of 8°N, increased stratification is also apparent as the upper waters are warming faster than the waters near and below the pycnocline.

Frequently repeated observations in the western part of the North Pacific Subtropical Gyre Province also demonstrate a decline in nutrient concentration in the mixed layer over the past 30 years. This decline has also been attributed to enhanced stratification acting as a barrier to the transfer of nutrients from the deeper ocean[144]. Below the mixed layer, and down to a depth of 750 m, a comparison of hydrographic data taken ~ 20 years apart in the northern Pacific shows an increase in nitrate. This is attributed to variations in advective transport of nutrients from remote locations rather than changes in the local intensity of remineralisation[145].

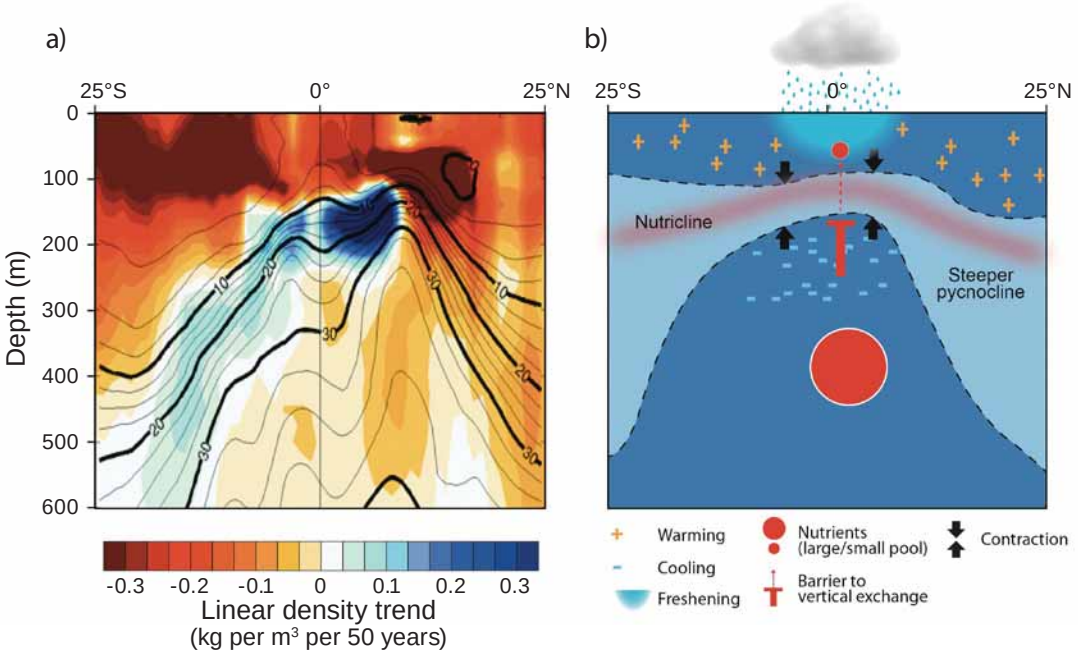

Figure 3.32 (a) Contraction of the pycnocline (shading: zone of maximum vertical density gradient, see Box 3.2) from 1960 to 2008 at 160°W with the mean nitrate concentration overlaid (contour interval = 2.5 μmol per kg) (source: Durack and Wijffels 2010, Ridgway et al. 2003)[190,194]; (b) consequences for nutrient supply: as the surface waters warm and the subsurface waters either cool or warm at lower rates, the vertical density differences increase so that the pycnocline becomes steeper. This limits the vertical exchange that transports nutrients from deeper waters to the surface.

The Hawaii Ocean Time-Series (HOT) station provides the longest continuous records of physical and biogeochemical data throughout the water column for the North Pacific Subtropical Gyre[146]. Although a strong upward trend in primary productivity is evident

over the 26 years of records at the HOT station, there is no such trend in the availability of nutrients[147]. The response of the ecosystem there is complex, and the increase in primary production at the HOT station may be linked to nitrogen fixation in the upper layers – a process that does not require a large increase in nitrate supply (Chapter 4). The corresponding productivity may be supplemented by enhanced eddy mixing to provide the necessary phosphate[59]. The larger-scale processes driving the observations at the HOT station are not yet clear, although they appear to be strongly influenced by ENSO and the PDO (Chapter 2). However, the time-series is not yet sufficient to separate the influence of ENSO and the PDO from global warming trends[147].

A 10-year time-series of satellite data shows a steady decrease in integrated primary production for the tropical Pacific Ocean, after a large intensification during the 1997–1998 El Niño[148]. These data also show an increase of 20% in the area of waters with low productivity over 10 years[149] (Chapter 4). However, the relatively short satellite time-series precludes attributing the observed changes to global warming, even though changes in productivity due to the PDO[143] have been detected in the satellite time-series.

3.3.4.2 Projected changes

A series of model projections from the IPCC Third Assessment Report suggested that under the A2 scenario in 2050 (the effects of which approximates B1 in 2100, see Chapter 1), the area of the oligotrophic North Pacific Tropical Gyre is projected to expand by 16% and the South Pacific Subtropical Gyre by 7% due to increased stratification[60]. Climate change could also decrease export production relative to total production (Chapter 4), thereby modifying the vertical structure of the ecosystem (Figure 3.6) and the transfer of nutrients to deeper layers of the ocean[150]. From the close links between nutrients, ocean circulation and stratification (Section 3.2.4, Chapter 4), it is clear that the projected changes to the ocean are likely to cause significant variation in future levels of biological production. However, rather than relying on projections for the levels of nutrients themselves, we concentrate mainly on the changes that are likely to occur to the physical features that demarcate the five ecological provinces of the region defined in Section 3.2.2.4, and control the potential supply of nutrients[60]. Accordingly, we have used multi-model-mean projections for stratification, maximum depth of the mixed layer during winter (as a measure of vertical mixing), upwelling or downwelling at a depth of 50 m, and the regions of convergence as defined by the main currents from the selected IPCC-AR4 models. These changes are closely related to the projected changes in vertical temperature structure and the position of the Warm Pool (Section 3.3.2).

- **Stratification:** The contrast in density of waters between the surface and a depth of 200 m is projected to increase with time and CO_2 emissions, with the most pronounced increase in stratification occurring in the Warm Pool (**Figure 3.33**).

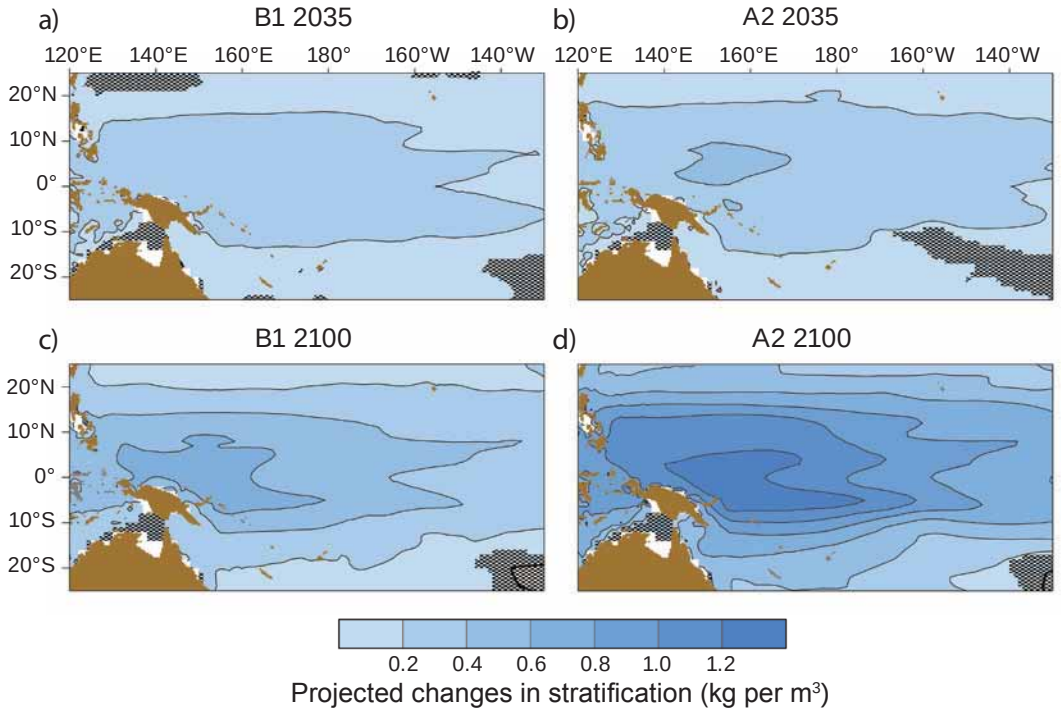

Figure 3.33 Projected changes in stratification (kg per m^3), as defined in Figure 3.14, for (a) the B1 scenario in 2035; (b) A2 in 2035; (c) B1 in 2100; and (d) A2 in 2100, relative to 1980–1999. Shaded areas indicate where the models do not project a consistent trend at the 90% confidence level.

In 2035, the overall increase is expected to be ~ 10% for both scenarios, compared with the average stratification between 1980 and 1999. In 2100, the increase is projected to be 10% to 20% for the B1 scenario, and 20% to 30% for A2, with the greatest changes in the Warm Pool.

- **Mixed layer depth in winter:** Most climate models used in our analysis projected that the maximum depth of the mixed layer during winter will be shallower in the future. This shoaling is projected to be more pronounced with time, and for the higher CO_2 emissions scenario (**Figure 3.34**). It is also most pronounced for the Warm Pool and in the Northern Pacific Tropical Gyre Province. In these regions, a shoaling of at least 5 m is projected under the B1 and A2 scenarios in 2035. By 2100, the mixed layer is projected to be 10 to 15 m shallower under the B1 scenario and 10 to 25 m shallower under the A2 scenario in the Warm Pool[151]. Weak shoaling is projected for the South Pacific Subtropical Gyre Province (SPSG) and the far eastern Pacific between 10°S and 20°S. However, there is considerable disagreement among the models for these regions due to their general failure to represent the SPCZ accurately (Chapter 2).

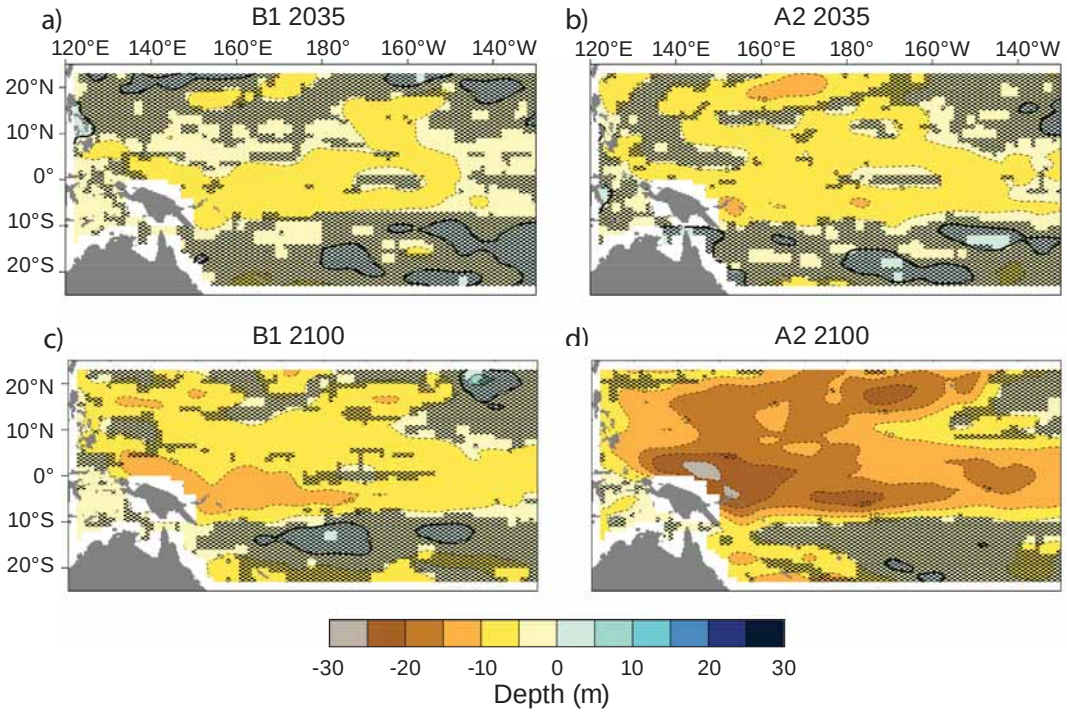

Figure 3.34 Projected changes to the annual maximum mixed layer depth in winter for (a) the B1 scenario in 2035; (b) A2 in 2035; (c) B1 in 2100; and (d) A2 in 2100, relative to 1980–1999. The maximum mixed layer depth is based on the average seasonal cycle from 20-year time-series of AR4 models. Shaded areas indicate where models do not project a consistent trend at the 90% confidence level.

- **Upwelling:** The upwelling in the Pacific Equatorial Divergence Province, integrated between 9°S and 9°N, is very poorly simulated by most IPCC models over the past 50 years, so that projections remain uncertain[152]. Average projected vertical velocity at 50 m is shown in **Figure 3.35**. The multi-model mean suggests that equatorial upwelling at 50 m will decrease over time as atmospheric concentrations of CO_2 increase (**Figure 3.35**). But the vertical velocity at the equator does not result in upwelling of large quantities of nutrient-rich water because it represents a small-scale shallow recirculation ('tropical cell')[153].

  The downwelling regions that flank the equatorial upwelling close to this cell are also projected to decrease in concert with the equatorial upwelling. As a result, net upwelling between 9°N–9°S, which is believed to be more relevant to equatorial SST, climate and possibly nutrient supply, is not projected to change significantly. Downwelling is not expected to change significantly in SPSG for either scenario by 2035. However, it is likely to increase by 20% with respect to the 1980 to 1999 average under the B1 scenario in 2100, and by 55% for A2 in 2100. There is little projected change in the North Pacific Subtropical Gyre Province.

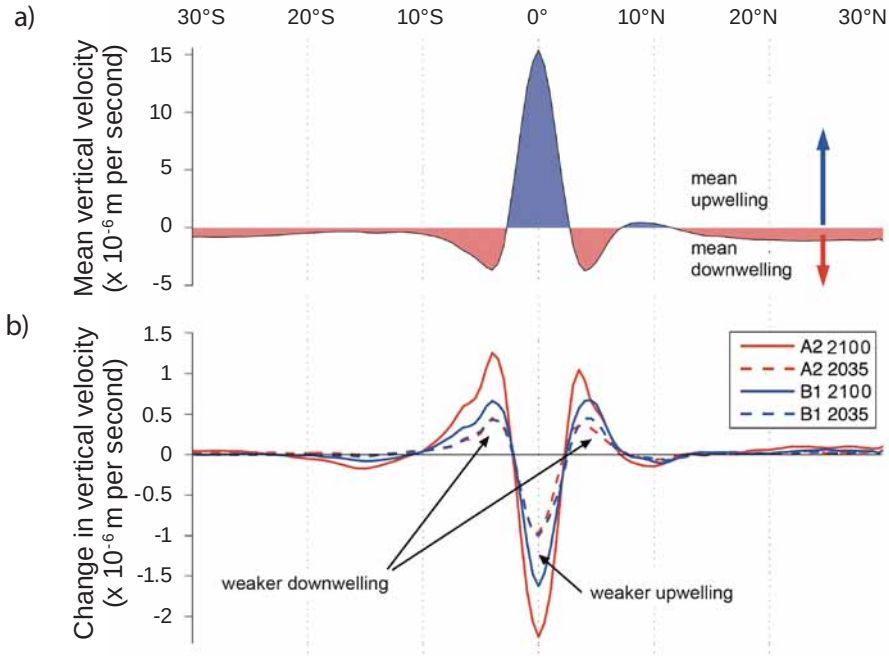

Figure 3.35 (a) Vertical velocities of water (x 10^{-6} m per second) at a depth of 50 m, for 1990 (mean 1980–1999), averaged between 170°E and 110°W, where a positive velocity corresponds to upwelling and a negative velocity to downwelling; and (b) climate driven changes to vertical velocities. The strong equatorial upwelling shows decreases that are immediately balanced by strong downwelling near 4°N–4°S so that net upwelling between 9°N–9°S (which is more relevant to nutrient supply) does not change.

- **Currents and fronts:** In addition to the changes projected for currents (Section 3.3.1), the separation between the westward equatorial flow and the eastward off-equatorial flow, which defines the latitudinal boundaries of the Pacific Equatorial Divergence Province, show little change for either emissions scenario for 2035 or 2100 (**Figure 3.36**). The major projected change occurs in the region of the SECC (around 8°S in the western half of the basin), where the area of eastward flow near the surface is expected to retract west by about 1500 km in 2100 under the A2 scenario (**Figure 3.36**).

These projected changes suggest a general decrease in nutrient supply. Their effects on each ecological province are discussed in Chapter 4, based on a specific simulation (IPSL-CM4 coupled climate carbon model) that includes projections for changes in both the physical and chemical features of the ocean.

Attempting direct modelling of biological production is a major challenge because the model needs to integrate the projected changes in the physical and chemical features of the ocean with the effects of these variables on the biology of organisms. A comparison of 12 climate-ocean biogeochemical cycle model simulations with modern data showed that estimates of average biological production varied by ~ 60% among models,

with a high dependence on the realistic simulation of ocean circulation[154]. One such biogeochemical model (which has been coupled to two different climate models) has provided projections for ~ 2080. Export production is estimated to reduce by 20% in the tropics if atmospheric CO_2 concentration increases to 700 ppm under the A2 scenario by ~ 2080[155,156]. This occurs as a result of projected decreases in upwelling and mixed layer depth; the direct effects of higher temperatures on the biology of organisms in oceanic food webs (Chapter 4) appear to be of lesser influence in this simulation.

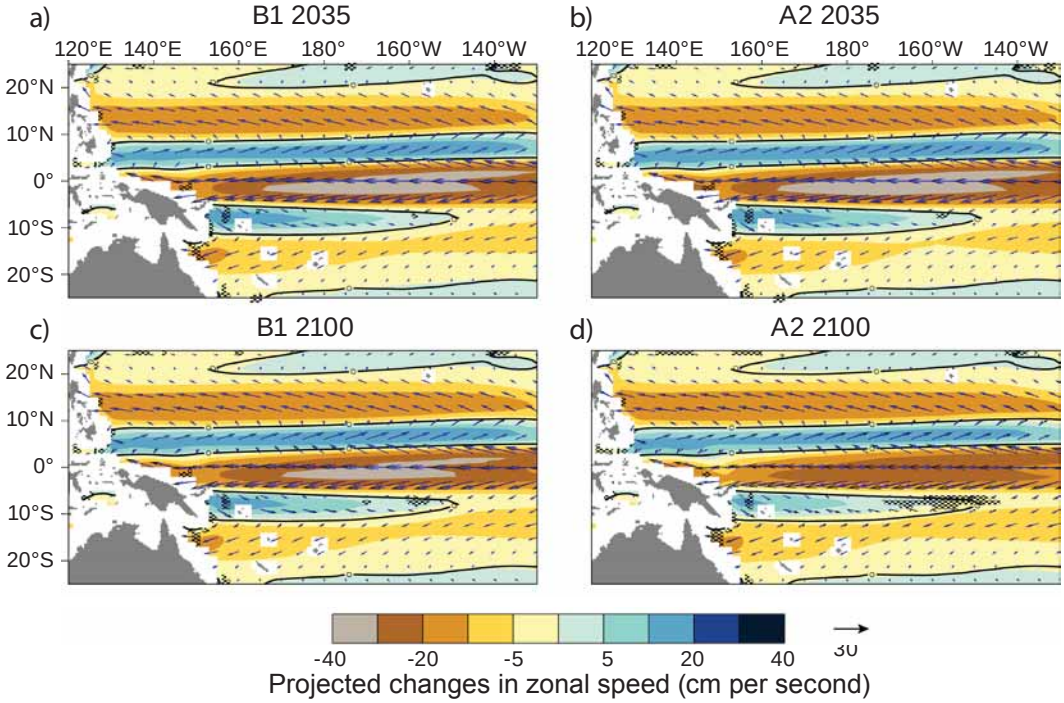

Figure 3.36 Projected changes in the speed of currents in the upper ocean to a depth of 50 m for (a) the B1 scenario in 2035; (b) A2 in 2035; (c) B1 in 2100 and (d) A2 in 2100. Black arrows show the multi-model mean for 1980–1999; blue arrows are projected velocities. The size of arrows reflects velocity; colour shading reflects the zonal component. To help distinguish changes in the extent of the ecological provinces, zero-zonal-velocities (1980–1999) are contoured in all panels. All values are 20-year averages. Shaded areas indicate where models do not project a consistent trend at the 90% confidence level.

3.3.5 Dissolved oxygen

3.3.5.1 Observed changes

Until recently, levels of dissolved oxygen in the tropical Pacific Ocean showed no clear trend[157,158], or decreased with time in regions away from the subtropics at the thermocline level due to decreased water renewal[159]. However, recent data from autonomous profiling floats[iv] have allowed reconstruction of usable time-series at

iv Argo, www.argo.ucsd.edu

selected locations. By comparing these data with historical observations, a major westward expansion of the oxygen-minimum waters in the eastern Pacific basin over the past 50 years has been detected[160] (**Figure 3.37**). The thickness of the oxygen-poor layer has also increased over this time in the Pacific Equatorial Divergence Province at 170°W, and in other tropical oceans[160]. This result is consistent with climate projections (see below) and is of concern because low oxygen concentrations can have dramatic consequences for ecosystems (Chapter 4) and the distribution of tuna (Chapter 8).

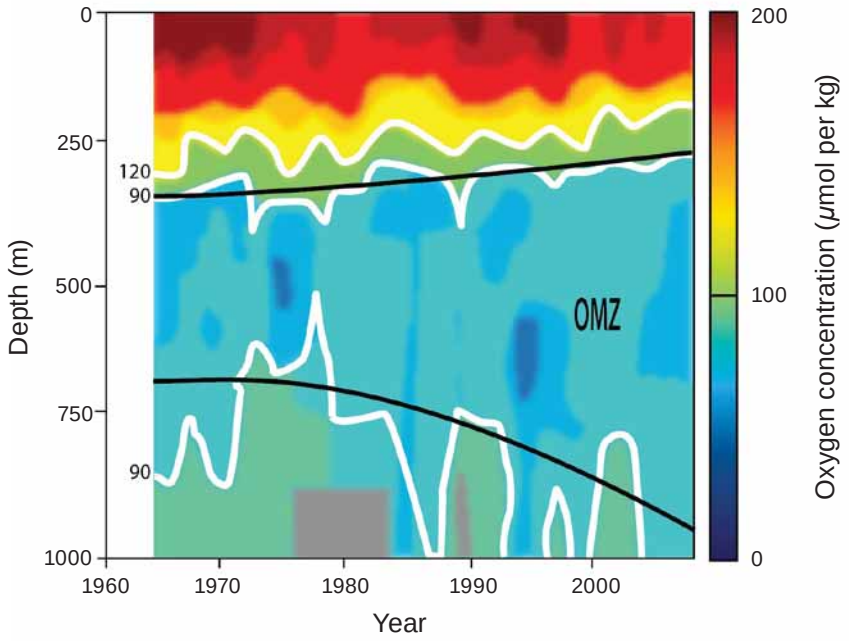

Figure 3.37 Time-series (since 1960) of dissolved oxygen concentrations near 170°W at the equator (5°N–5°S). Measurements were taken between 0 and 1000 m, and show a steady increase in the depth range of low-oxygen waters (< 90 µmol per kg, white line). Black lines denote the Oxygen Miminum Zone (OMZ), superimposed over interannual and decadal variability; grey areas correspond to gaps in the time-series (source: Stramma et al. 2008)[160].

3.3.5.2 Projected changes

Oxygen concentration is not calculated in the CMIP3 climate models and only a small number of biogeochemical models are available to make projections of future levels of O_2 in the tropical Pacific Ocean. Dissolved oxygen is expected to decline in many parts of the region due to larger-scale processes occurring at higher latitudes.

In particular, the increasing temperature and stratification of the ocean at higher latitudes are projected to lead to decreased transfer of O_2 from the atmosphere to the ocean, resulting in lower concentrations of O_2 in the tropical thermocline[156,161,162]. By 2100 under the A2 scenario, average concentrations of O_2 are projected to decrease by 0.2 ml per litre for the subtropical Pacific thermocline[161], where the observed concentrations are ~ 3 ml per litre (**Figure 3.16**) (projections for the other scenarios

are not available). The existing low levels of O_2 and suboxic areas in the eastern Pacific are also expected to intensify. In contrast, increased concentrations of O_2 are projected to occur in the equatorial thermocline due to reduced biological production (and therefore remineralisation/oxidation) within the water masses flowing to the equator[162].

3.3.6 Ocean acidification

3.3.6.1 Observed changes

The best estimates of the recent build-up of anthropogenic CO_2 in the ocean come from an indirect approach that uses (1) *in situ* measurements of total carbon and related variables made during a world-wide survey in the 1990s, and (2) a method to remove the natural (non-anthropogenic) component of CO_2. These data-based estimates of dissolved anthropogenic CO_2 show that its accumulation has not been uniform across the world's oceans. The largest inventories (the concentration of CO_2 summed over the full water depth) are found in the northern Atlantic Ocean and in the southern Pacific Ocean.

In the southern Pacific Ocean, the highest inventories of anthropogenic CO_2 are found between 40°S and 50°S, and the lowest inventories occur close to the equator and in the eastern upwelling regions (**Figure 3.38**). This distribution reflects where anthropogenic CO_2 enters the ocean from the atmosphere (the air-sea flux), and where it is transported by ocean currents. The air-to-sea flux of anthropogenic CO_2 is larger in regions where there is enhanced exchange between surface and deep waters. This facilitates the storage of anthropogenic CO_2 in the deeper ocean and keeps surface CO_2 concentrations relatively low, allowing a continued flux of anthropogenic CO_2 from the atmosphere to the ocean. Away from the equator, surface and subsurface currents generally move dissolved CO_2 towards the subtropics, where the inventory is generally greatest (**Figure 3.38**).

In the subtropical Pacific, the anthropogenic CO_2 penetrates to greater depths as a result of downwelling associated with convergence zones. Anthropogenic CO_2 in the deeper ocean reaches a peak at 50°S, where cold surface waters loaded with this gas sink to depths exceeding 1000 m in winter. Conversely, in the Pacific Equatorial Divergence Province, anthropogenic CO_2 is confined to the upper ocean because of upwelling, so that the inventory over the full depth range is small (**Figure 3.38**).

The ocean currently absorbs about 25% of the additional anthropogenic CO_2 emitted by human activity into the atmosphere each year[164] (**Figure 3.17**). As a direct consequence of emissions during the industrial era, and the uptake of a substantial fraction of this CO_2 by the oceans, the pH of sea water has decreased by ~ 0.06 pH units in the tropics and subtropics and ~ 0.12 units at high latitudes compared with a pre-industrial level of about 8.2. The current rate of decrease is ~ 0.02 units each decade[126]. Due to the log scale used to define pH, a 0.1 decrease in pH corresponds to a 30% change in H^+ ion concentration (Box 3.3).

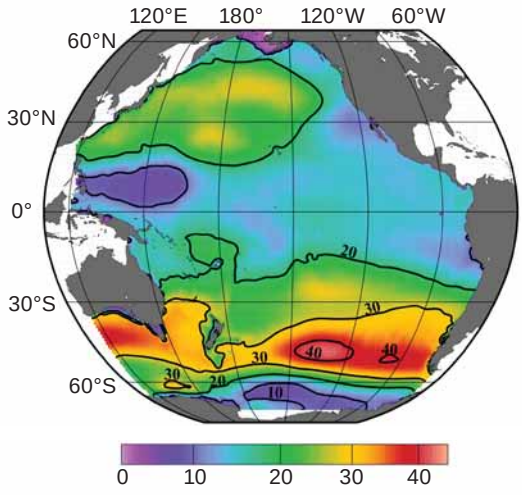

Figure 3.38 Anthropogenic component of depth-integrated, dissolved inorganic carbon concentration in the ocean (mol per m^2), known as the 'Anthropogenic CO_2 Column Inventory'. By the 1990s, dissolved anthropogenic CO_2 had invaded the first 1000 m of the water column near latitudes 30°N–50°S and 30°N–50°S. The largest inventories were found in these regions because the surface waters there sink quickly after taking up atmospheric CO_2. At lower latitudes, stronger stratification and equatorial upwelling limited the penetration of anthropogenic CO_2 to depths of about 500 m. Such measurements are now being repeated to document recent changes (source: Sabine et al. 2002, 2008)[195,196].

The current rate of change in pH is unprecedented in the climate record – changes to ocean pH are unlikely to have exceeded 0.6 units over the past 300 million years[165], despite large changes in atmospheric concentrations of CO_2. This stability is ensured by ocean chemistry, which buffers any changes in pH due to increases in CO_2 that occur over time scales > 1000 years[166]. The unprecedented rate at which CO_2 has accumulated over recent decades means that the buffering capacity of the ocean (Box 3.3) has been unable to keep pH levels stable[167].

3.3.6.2 Projected changes

The projected increase in atmospheric CO_2 (Chapter 1) will drive increased levels of dissolved anthropogenic CO_2 into the tropical Pacific Ocean. This change will cause further acidification of the water column (Box 3.3), and decrease the availability of carbonate ions. It will also promote increased dissolution of carbonate substrates at shallower depths in coral reef ecosystems[68,69,78]. The median projection of future changes in pH and CO_3^{2-} from 13 ocean carbon cycle models shows that the average aragonite saturation state in surface waters is expected to drop from 3.9 (350% saturation) in 1994 to 2.4 in 2100 in the surface waters for the A2 scenario (Figure 3.39). Under the more conservative S650 emissions scenario[v], the average surface aragonite saturation in the tropical Pacific Ocean is projected to be 3.0 in 2100 (**Figure 3.40**).

v The S650 scenario is similar to B2 and slightly above B1. Under this scenario, atmospheric CO_2 concentration would reach 562 ppm in 2100.

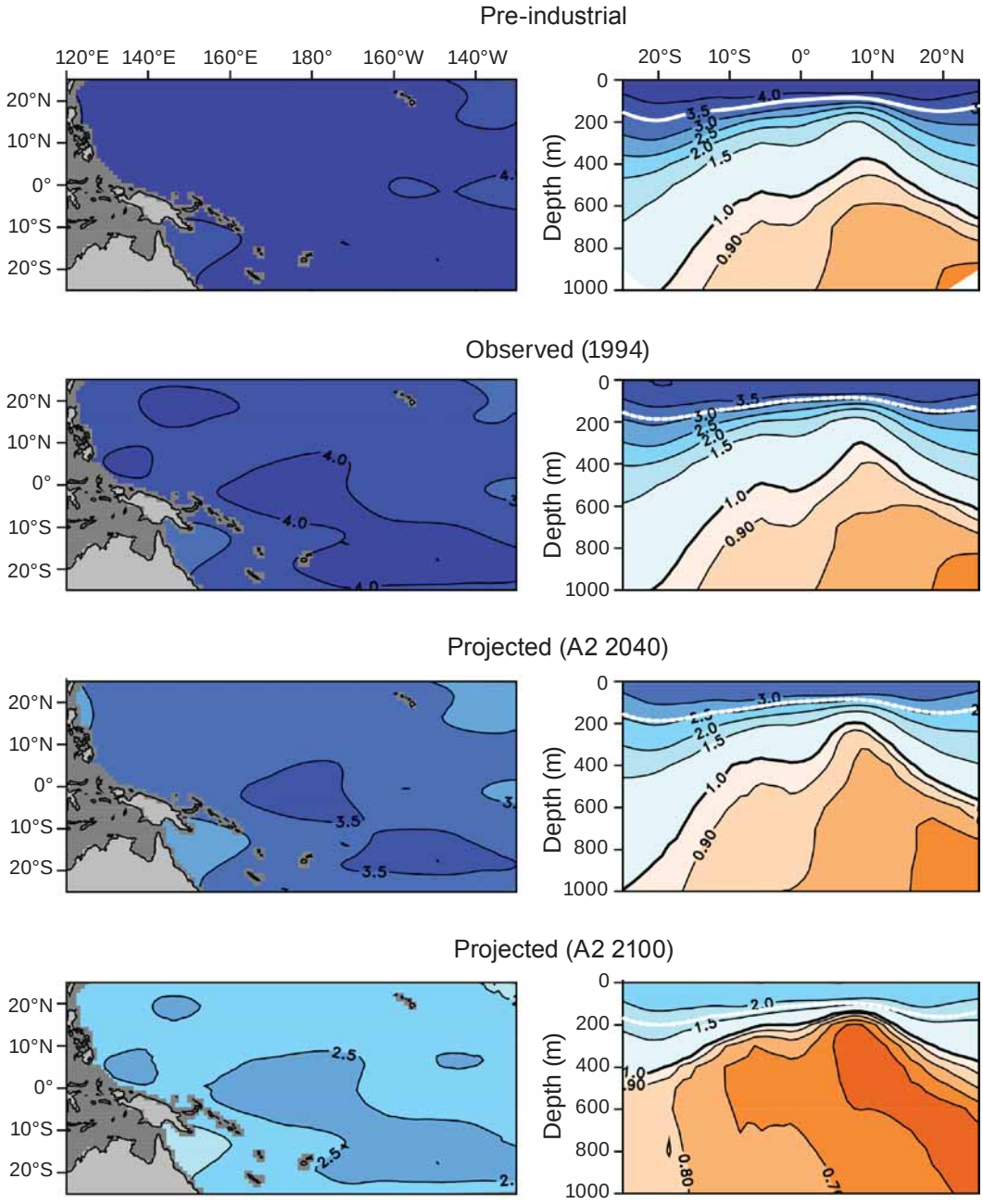

Figure 3.39 Aragonite saturation levels in the tropical Pacific Ocean at the surface (left panels) and to a depth of 1000 m (zonal averages) (right panels) during pre-industrial times and 1994, together with median projected values for the A2 scenario around 2035 (2040) and 2100. The thick white line on the upper right panel is reproduced as a dashed white line on the other three depth sections below. It indicates the depth level where pre-industrial waters have a saturation state that is 3.5 times the value where pure aragonite begins to dissolve, which is indicated by the 1.0 contour (thick black line), known as the aragonite saturation horizon (source: Orr et al. 2005, Key et al. 2004)[77,197].

Average sections to a depth of 1000 m across the domain (**Figure 3.39**) show that although the declines in aragonite saturation are greatest near the surface, there are also noticeable changes at greater depths. In particular, there is a shoaling of the aragonite saturation horizon, below which aragonite dissolves (Box 3.3). In 1994, the aragonite saturation horizon zonal average was at a depth of 300 m at 8°N, and deeper to the south and to the north. It is projected to become shallower over time, reaching 150 m in 2100 under the A2 scenario.

These projections do not account for the physical effects of global warming on ocean acidification: they only simulate geochemical changes due to increases in atmospheric CO_2. However, some feedback effects may be expected due to changes in temperature, ocean stratification, biological production, and remineralisation. Projected increases in SST, for example, would reduce CO_2 solubility and increase CO_3^{2-} near the surface. Overall, the combined physical effects of climate change on ocean acidification are projected to be small, i.e. < 10% of the change directly due to the increase in atmospheric CO_2[77]. Changes in concentrations of CO_3^{2-} associated with natural interannual climate variability are also projected to be small compared with projected long-term changes[77].

Declining aragonite saturation levels have significant implications for coral reefs (Chapter 5). In particular, sustained coral reef accretion and structural density is expected to be jeopardised if the aragonite saturation drops below 3.25[72] and/or when the atmospheric CO_2 concentration exceeds 450 ppm[168]. This threshold is likely to be reached in average surface waters of the tropical Pacific Ocean shortly after 2035 (2040) under the A2 scenario (**Figure 3.39**).

Future decreases in pH due to anthropogenic emissions of CO_2 under the B1 and A2 scenarios are projected to be 0.2 to 0.3 pH units below present levels by the end of this century. Under a worst case scenario, if all known fossil-fuel reserves (~ 5000 Pg C) were combusted, the reduction in pH could reach 0.7 units[165].

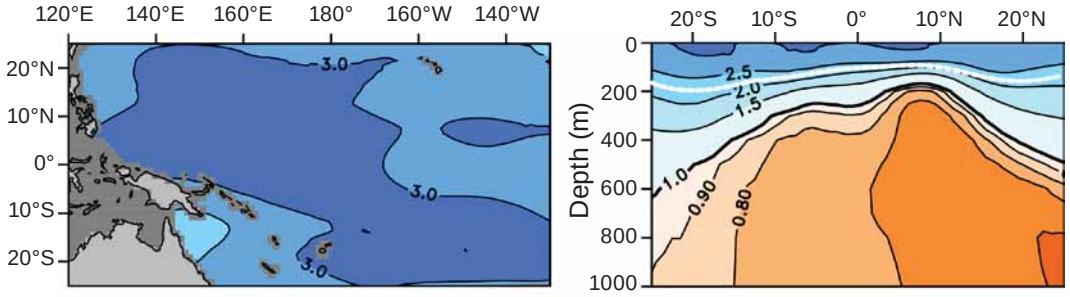

Figure 3.40 Projected levels of aragonite saturation in the tropical Pacific Ocean in 2100 for the S650 scenario. Projections for the B1 scenario in 2100 are expected to be slightly higher than those for S650 (see text for details). Other details as per Figure 3.39.

3.3.7 Wave height

3.3.7.1 Observed changes

Around the world, visual reports from shipping show an increase in significant wave heights (SWH) at mid- and high-northern latitudes since 1950[169]. However, in the far western part of the Warm Pool, SWH has decreased at a rate of 8 cm per decade. Unfortunately, there are insufficient data from other parts of the tropical Pacific Ocean to determine whether SWH has changed over recent decades[169].

Regardless of any changes in SWH, it is plausible that the current wave climate may result in more frequent damage to coastal fish habitats. The combined effects of reductions to the structural complexity of coral reefs, due to more frequent bleaching and increased ocean acidification (Chapter 5), and sea-level rise, means that the force of waves on the shoreline is unlikely to dissipate to the same extent as in the past. The increased wave force is likely to reduce the complexity of coral reefs further; it is also expected to affect mangrove and seagrass habitats (Chapter 6).

3.3.7.2 Projected changes

The CMIP3 climate models do not include wave projections. However, estimated changes can be derived from an empirical relationship between sea-level pressure and SWH. Based on multi-model means from three climate models, an increase in SWH of 8 to 10 cm in the southern tropical Pacific is projected for 2100 under the A2 emissions (**Figure 3.41**), and is expected to be most pronounced in the east. No change or a decrease of about 4 cm is expected by 2100 in the northern tropical Pacific[170,171]. An estimated decrease of 6 to 8 cm for the B2 scenario, which is intermediate between B1 and A2, is projected for 2100[170]. The 20-year return SWH (the value that significant wave height exceeds at least once over a 20-year period) is projected to increase by about 30 cm in the eastern half of the southern tropical Pacific under A2 in 2100.

In general terms, interannual variability of SWH is strongly linked to ENSO. As such, future changes in the wave climate of the tropical Pacific Ocean would also be expected to depend on future changes in ENSO. However, although ENSO events are projected to continue, there is little agreement about how they may change in amplitude or frequency (Chapter 2). Thus, it is only possible to state that waves will continue to be influenced strongly by El Niño and La Niña episodes.

There is more certainty about projections for the SAM. Almost all CMIP3 climate models project a continued southward intensification of the mid-latitude westerly winds, causing the associated increase in storm activity outside the tropics to intensify. Observational studies indicate an increase in SWH, as measured by satellite altimeters, associated with positive SAM phases[172]. Because of the projected southward shift of the extra-tropical storm tracks associated with SAM, however, the

distance that swells have to travel to the tropics increases, which could counteract any influence that the increased storm intensity may have. As a result, little increase in SWH related to SAM is expected in the tropical Pacific Ocean.

Projections for SWH remain at their early stages, and uncertainties are still large. It is likely, however, that application of outputs from a greater range of climate models, using extensions of statistical wave projections[170], and regional dynamical wave projections[173], will soon improve our knowledge.

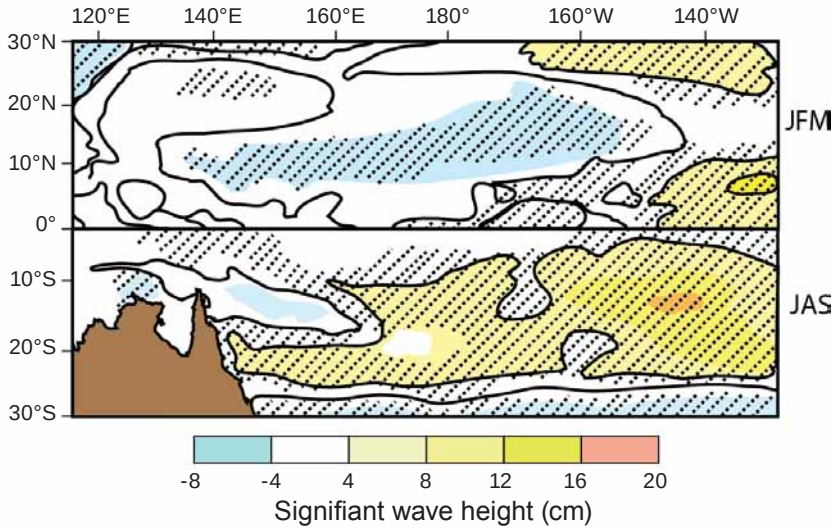

Figure 3.41 Projected increase in significant wave height under the A2 emissions scenario in 2100 for winter months north and south of the equator, relative to levels in 1990. The shaded area corresponds to statistically significant changes from an average over three climate models. JFM = January to March; JAS = July to September (source: Wang and Swail 2006)[170].

3.3.8 Sea level

3.3.8.1 Observed changes

Global sea level has risen ~ 6 cm since 1960 (**Figure 3.42b**) and ~ 17 cm since the industrial revolution[174]. In the past 15 years, the water released from glaciers is estimated to make up 60% of the contribution of melting ice to present-day sea-level rise[175] (**Figure 3.42a**). However, major fluctuations, i.e. periods of a few years with unusually large positive or negative trends, are evident in the record. A good example is the fall in sea level during 1982–1985 as a result of ocean cooling caused by aerosols from the Chichon Volcano eruption (**Figure 3.42**). This temporary reduction in sea level was compensated for within 2 to 3 years as the aerosols were removed from the atmosphere and sea-level rise continued unabated over the longer term. More recently, the rise in sea level has accelerated. More than 60% (~ 4 cm) of the total rise of ~ 6 cm since 1960 has occurred since 1993, and the rate of sea-level rise is now 2.5 cm per decade[176,177]. The rate of sea-level rise varies across the region, as discussed in Section 3.2.8 (**Figure 3.23**).

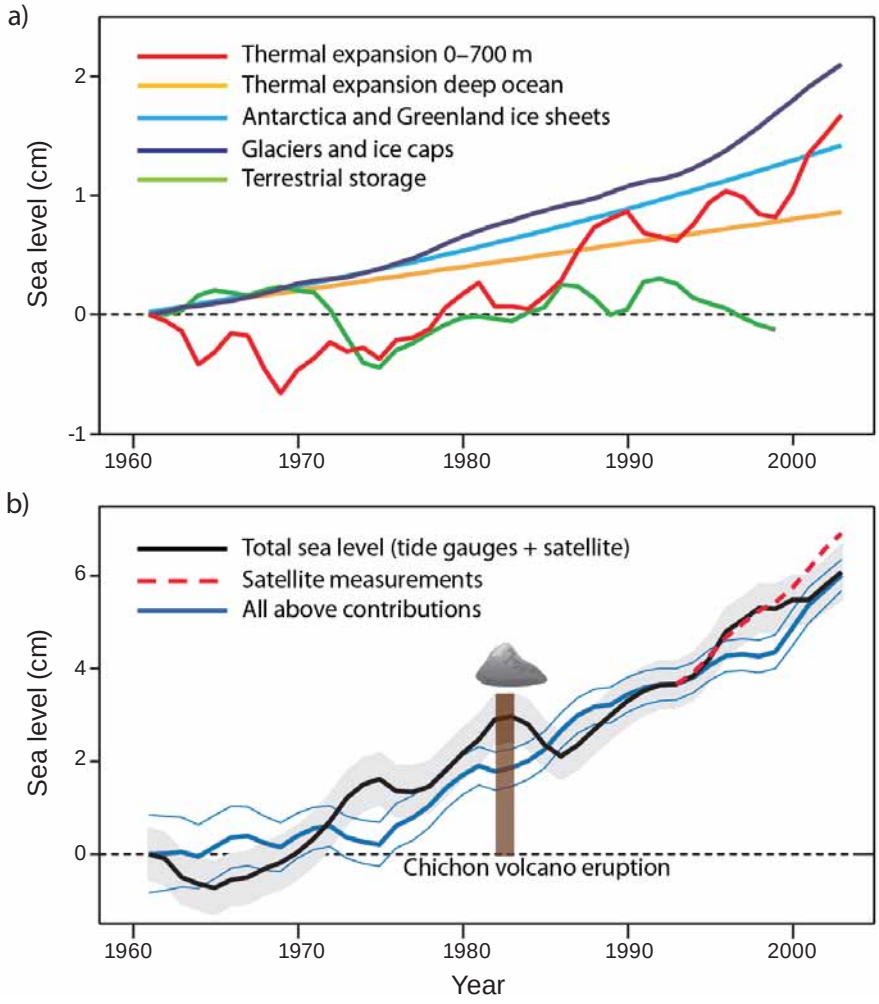

Figure 3.42 (a) Contribution of the different components of global sea-level rise since around 1960; and (b) observed total sea-level rise estimated by tide gauges and satellite data (black) and satellite-only data (dashed red line). Combined contributions of the main factors listed in (a) are shown by the thick blue line (95% confidence limits are indicated by the thin blue lines). Major climate fluctuations are evident in the record, e.g. the drop in sea level during 1982–1985 due to short-term ocean cooling caused by aerosols from the Chichon Volcano eruption (source: Domingues et al. 2008)[177].

3.3.8.2 Projected changes

Short-term drivers of sea level are not expected to change substantially in the next 100 years. Tidal forcing will remain the same and eddies have no clear projected trend in the tropical Pacific (Section 3.3.3). The possibility of stronger tropical cyclones (Chapter 2) would be associated with higher storm surges. The primary drivers of long-term sea-level rise are still expected to be melting of land ice and thermal expansion of sea water.

A comparison of the global sea-level rise simulated over recent decades in the IPCC-AR4 models with recent observations shows that the models generally under-estimate global sea-level rise[178,179]. Nevertheless, projections for the ice melt contributions are recognised as the most important component of future sea-level rise (IPCC-AR4)[180]. Much uncertainty remains, however, because of the limited understanding of mechanisms that control the dynamics of land ice flow into the ocean. With enhanced melting, the flow can accelerate more than expected from classical ice dynamics, as suggested by the most recent observations[175,181].

Indeed, paleo-climatic records suggest that during the last interglacial period (130,000 years ago) when global temperatures exceeded present temperatures by a few degrees, sea level was 3 to 6 m higher than it is today[182,183]. The melting of the Greenland ice sheet contributed about 3.4 m to the total rise that occurred then. According to 2100 projections of surface temperatures in Greenland, similar increases in sea level might be possible[182]. Alternative views are that ice dynamics would limit sea-level rise to between 0.8 and 2.0 m by 2100, regardless of the temperature increase[184]. Extrapolation of present-day acceleration in melting rates suggests that glacier melt alone could cause a sea-level rise of 17–56 cm by 2100[175]. This broad range of estimates in the ice melt component of sea-level rise is expected to narrow in the coming years as understanding of the underlying ice dynamics improves.

Thermal expansion of the water column, which is the second largest factor affecting sea level after ice melt, is diagnosed directly in IPCC-AR4 climate models. The models provide estimates of global sea-level rise due to thermal expansion for B1 and A2 in 2035 of between 5 and 8 cm, compared with the 1980–1999 level. By 2100, the estimates rise to 18–24 cm under the B1 scenario, and between 23 and 31 cm for A2[180]. This component has a much narrower range of estimates than ice melt.

Given the present lack of knowledge about ice dynamics, estimates based on historical reconstructions for global sea-level rise, which include the effects of ice melt and thermal expansion, have been used to provide independent assessments without requiring a detailed understanding of the underlying dynamics. In general, these techniques suggest sea-level rise will exceed the estimates of the IPCC. Using one such empirical estimate, projections are that sea-level rise will be 20 to 30 cm under the B1 and A2 scenarios in 2035, 70 to 110 cm under B1 in 2100 and 90 to 140 cm under A2 in 2100 (**Figure 3.43a**)[185]. Although a rise of almost 2 m by 2100 cannot be ruled out[184], this empirical estimate should be used with caution until the limitations of these projections are more fully understood[vi].

The IPCC-AR4 models project relatively modest regional deviations from the average trend throughout the tropical Pacific Ocean due to differential warming of the water columns. These deviations are projected to be within 5 to 10 cm of the global average rise, based on the multi-model mean (**Figure 3.43b**).

vi See 'Climate Change in the Pacific: Scientific Assessment and New Research' (www.cawcr.gov.au/projects/PCCSP) for more information.

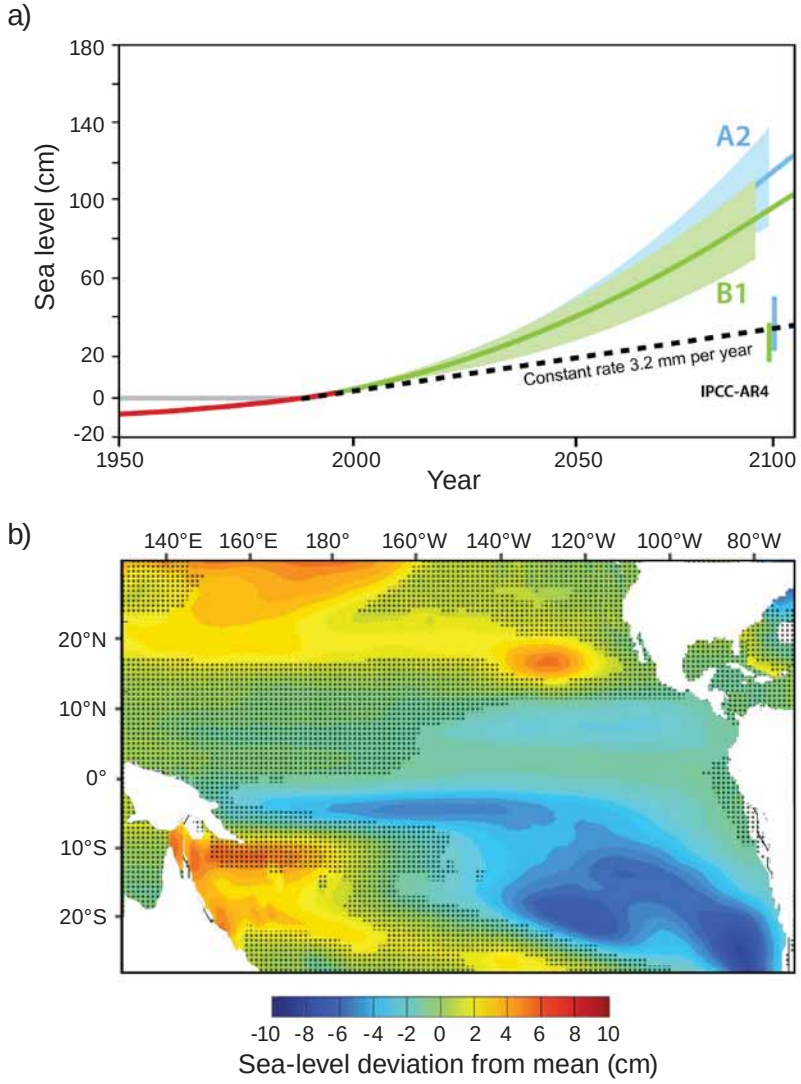

Figure 3.43 (a) Observed and estimated global sea-level rise. The thick dashed black line shows the constant rate hypothesis used by IPCC-AR4. The green (B1) and blue (A2) curves (with uncertainty ranges) show estimates for 2100 from an empirical model based on palaeo-climatic data calibrated against modern data (see text for details) (source: Vermeer and Rahmstorf 2009)[185]; (b) deviations in sea-level rise from global mean sea-level rise within the Pacific basin for A2 in 2100. Shaded areas are regions where model projections do not agree at 90% confidence. At any point, absolute sea-level rise would be the sum of estimates for components in (a) and (b).

3.3.9 Coastal circulation and island effects

3.3.9.1 Observed changes

In the eastern Pacific, recent variations in upwelling systems have been attributed to changes in the wind field and/or the oceanic thermal structure[186,187]. Although the effects of such changes to islands in the Archipelagic Deep Basins Province in

the western Pacific have received much less attention than in the Pacific Equatorial Divergence Province, observed changes in the large-scale wind field, ocean currents, and the thermocline depth described above are expected to have affected island and coastal systems to some extent. This change has not yet been quantified.

3.3.9.2 Projected changes

Projecting future changes at the scale of individual islands is a considerable challenge. To a large extent, the climate models used to project future changes are too coarse to resolve small islands and the processes important for delivering nutrients to the photic zone. However, changes to the productivity of inshore waters depend to some extent on the projected changes to large-scale features that can be resolved in the models, particularly those for ocean currents, wind patterns, and depth of the mixed layer. Changes to these and other oceanic features are expected to interact with coastlines and islands to produce distinct local responses, which would need to be assessed on a case by case basis. The discussion that follows, therefore, makes only general qualitative statements.

Island ecosystems in areas with strong projected changes to the large-scale surface currents, i.e. within 15°N–15°S of the equator (**Figure 3.26**), are likely to be the most affected. Areas of increased current strength are likely to have more local eddies and greater associated nutrient supply (**Figure 3.24**). Conversely, areas of decreased current strength are likely to have fewer local eddies and a reduced supply of nutrients. Changes in wind direction will also alter the island wake position and structure. The IPCC-AR4 projections show (1) relatively stable wind stress in the southwest Pacific, with stronger and more southerly winds occurring in the southeastern part of the region; and (2) weakened equatorial and north trade winds. French Polynesia in particular is likely to be subject to such expected changes.

Regional climate models embedded in IPCC class models have been used in the California upwelling system, suggesting a future increase in strength[188], but similar downscaled investigations are not yet available for the area of the Pacific Community. Paleo-climatic records suggest that upwelling activity in New Caledonia has been ongoing for at least 6000 years[85] and the slight change in projected winds suggest that water motion is unlikely to change dramatically in the future. However, the upwelling system in New Caledonia barely reaches the deep nutrient-rich layers[110], so the projected strengthening of the stratification would lower the already weak mechanisms for transferring nutrients to the photic zone.

There is little reason to expect changes in the formation of internal waves as this depends on the interaction between tides and ocean bathymetry. However, the characteristics of these waves, their propagation patterns and impact could be affected by changes in the thermal structure of the water column.

In summary, climate change is expected to have localised effects on the waters surrounding different islands through interactions between large-scale oceanic and atmospheric processes and island topography. However, the necessary local projections are scarce and there is a need for specific studies to downscale future climate simulations (Section 3.5).

3.4 Summary of present-day ocean features, and observed and projected changes

The circulation of the central and western tropical Pacific Ocean is dominated by two broad westward currents, the North Equatorial Current and the South Equatorial Current. These are separated by two eastward counter currents underneath the atmospheric convergence zones (ITCZ and SPCZ) at latitudes 5°–10°N and 5°N–10°S. As the broad flows encounter islands and coasts, they form narrow and powerful currents that can transport heat, nutrients, particles and larval fish and invertebrates over large distances. Because of their strong relation with winds and SSTs, these ocean currents vary substantially with season and with ENSO.

In the central and eastern equatorial region, where the trade winds drive an upwelling of deep water and create the Pacific Equatorial Divergence Province, the surface waters are relatively rich in nutrients (Chapter 4). Most of the rest of the western tropical Pacific Ocean is nutrient-poor (oligotrophic) because warm surface water is piled up by the trade winds, pushing down the deep layers that are rich in nutrients. Wind-induced mixing, oceanic eddies, internal waves and island upwellings all act to reduce this natural stratification barrier supplying the upper layers of the ocean with the nutrients necessary for biological production. In the western equatorial Pacific, an immense pool of warm, nutrient-poor water moves back and forth along the equator according to the phase of the ENSO cycle. The eastern edge of the Warm Pool in the western Pacific defines the limit of the nutrient-rich Pacific Equatorial Divergence Province.

In addition to the substantial natural variability in the position and size of the Warm Pool, the following long-term changes in the other major oceanographic features of the region have been observed over the past 30 to 50 years (**Table 3.2**).

- The South Pacific gyre has increased in strength, driven by a southward intensification of extra-tropical wind. This has altered the complex current system of the southwest Pacific and changed the structure of water temperatures in the region.
- The upper ocean has warmed by 0.6°C to 1.0°C down to a depth of 100 to 200 m, depending on latitude, with cooling in some regions at greater depths. This has resulted in an increase in stratification, which limits the vertical exchange of water and has major implications for nutrient supply (Chapter 4).

- The two longest existing time-series of oceanographic data in the tropical northern Pacific indicate that there has been no increase or decrease in nutrient supply, consistent with increased stratification. The data are insufficient to establish whether a basin-scale trend is occurring. Trends in nutrient supply to the upper layers and biological activity are difficult to gauge with certainty because high-quality long-term observations are not available. Natural variability generally exceeds any possible long-term trends.
- Subsurface concentrations of dissolved oxygen have been decreasing and there has been an expansion of oxygen-depleted waters. This could have some detrimental effects on biological production (Chapter 4).
- Absorption of increasing amounts of CO_2 have decreased the pH of the tropical Pacific Ocean by ~ 0.06 pH units, making the ocean more acidic (or strictly speaking less basic). The acidification of the ocean is close to the point where calcareous organisms, such as corals and a number of planktonic species, could experience a weakening in their shells or skeletal structure, reducing their fitness and resistance to predation.
- Sea level has risen by about 17 cm globally since pre-industrial times, and 6 cm since 1960. The rate of increase appears to be increasing due to accelerated ice melt and thermal expansion of the upper ocean and is currently ~ 2.5 cm per decade.

Projected changes to the major features of the tropical Pacific Ocean under the B1 and A2 emissions scenarios in 2035 and 2100 have been assessed using selected CMIP3 models from the IPCC-AR4 climate simulations. This analysis shows that substantial changes in ocean circulation and temperature structure are expected to occur, which are likely to impact biological productivity (**Table 3.2**). The major projected changes are summarised below.

- Alteration in speed and direction of some major ocean currents: the tropical part of the South Equatorial Current (SEC) is expected to weaken progressively (18% by 2100 under A2) and become more confined to the surface layers. The Equatorial Undercurrent is likely to strengthen in the western Pacific and become shallower directly beneath the SEC. South of the equator, the near-surface South Equatorial Counter Current is expected to retract and weaken dramatically (60%) by 2100.
- Ocean temperature is expected to continue rising substantially, with higher warming rates near the surface, especially in the first 100 m. The salinity of the tropical western Pacific Ocean is projected to decrease in line with an intensified hydrological cycle (Chapter 2). The salinity front associated with the Warm Pool will extend further east by ~ 1000 km, while the 29°C isotherm will move much further east at the equator.

Table 3.2 General summary of observed and projected changes to the main features of the tropical Pacific Ocean. Observed changes are relative to the period 1950–1960. Projected changes are relative to 1980–1999. Estimates of confidence are provided for each projection (see key below). Details of currents are provided in Figure 3.1; see Table 3.1 for more detailed observed and projected changes for selected key ocean features.

Ocean feature	Observed changes	2035		2100		
		B1	A2	B1	A2	
Currents	South Pacific gyre has strengthened	SEC decreases at the equator; EUC becomes shallower; SECC decreases and retracts westward in the upper 50 m				
Sea surface temperature		Projected to increase significantly over the entire region				
		+0.6 to +0.8°C	+0.7 to +0.8°C	+1.2 to +1.6°C	+2.2 to +2.7°C	
Ocean temperature at 80 m	+0.6 to 1°C since 1950	+0.4 to +0.6°C		+1.0 to +1.3°C	+1.6 to +2.8°C	
Warm Pool	Warmer and fresher	Extends eastward; water warms and becomes fresher, and area of warmest waters increases				
Equatorial upwelling	Decreased	Integral transport 9°S–9°N remains unchanged				
Eddy activity	No measurable changes	Probable variations in regions where major oceanic currents change				
Nutrient supply	Decreased slightly in two locations	Decrease due to increased stratification and shallower mixed layer, with a possible decrease of up to 20% under A2 by 2100				
Dissolved oxygen	Expansion of low-oxygen waters	Possible decrease due to lower oxygen intake at high latitudes				
		Possible increase near the equator due to decreased remineralisation				
Ocean acidification		Aragonite saturation (Ω) projected to continue to decrease significantly				
	➢ Ω decreased from 4.3 to 3.9	n/a	Ω ~ 3.3	Ω ~ 3.0	Ω ~ 2.4	
	➢ Ω horizon rises from 600 to 560 m	n/a	~ 456 m	n/a	~ 262 m	
	➢ pH decreased from 8.14 to 8.08	n/a	~ 7.98	n/a	~ 7.81	
Waves	Decreased in far west Pacific; no data elsewhere	Slight increase (up to 10 cm) in swell wave height; patterns depend on ENSO and tropical cyclones				
Sea level	+6 cm since 1960	Projected to rise significantly				
		*	+8 cm	+18 to +38 cm	+23 to +51 cm	
		**	+20 to +30 cm	+70 to +110 cm	+90 to +140 cm	
Island effects	Not observed	Probable; undocumented				

* Projections from the IPCC-AR4, not including any contribution due to dynamical changes of ice sheets; ** projections from recent empirical models (Section 3.3.8.2); SEC = South Equatorial Current; EUC = Equatorial Undercurrent; SECC = South Equatorial Counter Current; ENSO = El Niño-Southern Oscillation; n/a = estimate not available.

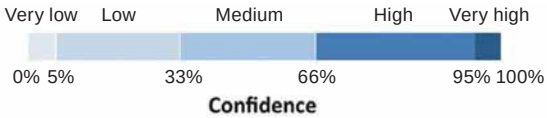

- Stratification of the upper layers of the ocean – a major factor influencing the supply of nutrients from the deep ocean to the photic surface zone – is expected to increase.
- Increases in atmospheric CO_2 are projected to lead to substantial additional acidification of the ocean, reducing the pH of the ocean by 0.2–0.3 units under the B1 and A2 scenarios by 2100, relative to 2000. At such rates of change, aragonite saturation levels in the tropical Pacific Ocean are expected to fall below 3.25 by 2035 to 2040 under the A2 scenario, jeopardising the growth of some corals. The aragonite saturation level is expected to decrease to 2.4 in 2100 under A2, with severe consequences for coral reefs (Chapter 5).
- As a consequence of continued ice melt, and thermal expansion of the upper oceanic layers, the rate of sea-level rise is expected to accelerate. The projections from IPCC-AR4, that sea level will rise between 18 cm under B1 to 51 cm under A2 by 2100, are now considered to be conservative because they underestimate the acceleration of ice sheet melt. More recent empirical estimates based on temperature/sea level relationships based on past records, indicate that sea-level rise could be in the range of 70 to 140 cm by 2100. Even the minimum estimate of 70 cm would mean a profound change for coastal habitats.

3.5 Recommendations to reduce uncertainties in projecting future changes to the tropical Pacific Ocean

3.5.1 SPCZ and ENSO

Much effort during the past decade has been devoted to improving numerical climate simulations and projections. This research has culminated in 22 state-of-the-art climate models (the CMIP3 models used for the 2007 IPCC-AR4 report), which are used to reproduce present conditions and project future changes to the ocean, atmosphere, and sea ice. To test the fidelity of these models, comparisons have been made between observations from the past 20 to 50 years and model simulations forced with historical greenhouse gas concentrations, aerosol concentrations (in some cases) and changes to solar radiation.

A number of important systematic biases are evident in the CMIP3 models that are of particular importance for the tropical Pacific Ocean. These include the position of the SPCZ and the spatial and temporal structure of the ENSO. The overly zonal orientation of the SPCZ in many numerical simulations limits our confidence in projections of the rainfall and wind fields of the central-southern Pacific. ENSO, which acts as a metronome for the ocean-atmosphere system, has a simulated warming (in the case of El Niño events) that is generally situated too far to the west and often occurs too frequently in the models. Both SPCZ and ENSO are the focus of intense research programmes[vii]. A better understanding of the physical mechanisms driving

vii CLIVAR, www.clivar.org, and the Pacific Climate Change Science Programme www.pacificclimatechangescience.org

these characteristics, leading to improved physical parameterisations, combined with higher model resolutions, is expected to help reduce these biases in the new generation of climate models to be used for the 5th IPCC assessment.

3.5.2 Integrating biogeochemical and physical models

Estimating the extent to which climate change is likely to alter nutrients and oxygen concentrations requires the integration of biogeochemistry with physical models. This may be achieved in two ways. Either a biogeochemical model can use the stored output of a physical ocean model (i.e. an 'offline' simulation), or a physical and biogeochemical model can be coupled together so that the components interact throughout a simulation. Such simulations have been used in Chapters 4 and 8 but remain relatively rare, and the results are subject to uncertainties of the physical model. To increase confidence in biogeochemical simulations and their projections, most climate simulations should be supplemented by offline or online biogeochemical simulation.

3.5.3 Dynamical downscaling

Because islands and reefs act as obstacles to wind and water flow, the key features of the tropical Pacific Ocean of significance to fisheries, such as SST, currents and nutrient supply, can all be altered locally. These localised effects are not represented in most of the present climate models due to a lack of model resolution stemming from limited computational power. To overcome this limitation, regional high-resolution numerical models are sometimes used. For example, **Figure 3.25** shows a high-resolution, regional ocean simulation around New Caledonia. This regional simulation relies on a low-resolution global ocean simulation to obtain the information it needs for conditions at the boundary of the region. This technique is referred to as dynamical downscaling. To investigate future changes at these high resolutions, boundary conditions based on projections from the coupled climate models can be used. While downscaling is an economical way of producing high-resolution regional projections, great care must be taken in using such projections. Biases in the low-resolution model will generally be propagated to the high-resolution model, compromising the fidelity of the simulation. Considerable effort is needed to determine how best to implement such downscaling approaches.

3.5.4 Long-term observations and monitoring

High quality, long-term observational datasets with sufficient spatial coverage are vital to understanding climate change and its effects. Such data allow us to distinguish between anthropogenic effects and natural variability, and to validate climate and biogeochemical simulations. The physical state of the tropical Pacific Ocean is now monitored reasonably well over large areas, both by satellite and with *in situ* data

systems[viii]. Specific programmes are being developed to monitor highly energetic boundary currents that transport large amounts of heat and other climatically important properties over large distances. On the other hand, measurements of nutrients, oxygen, and ocean pH have relatively poor data coverage and little reliable monitoring. The Hawaiian Ocean Time-Series programme provides the only complete long-term time-series in the region. The replication of such a monitoring system in other parts of the tropical Pacific would be extremely valuable. Such an initiative is presently underway under the auspices of the GOPS[ix]. Ocean acidification, which is expected to be a major perturbation to marine ecosystems in addition to global warming, requires improved and continuous monitoring. This effort must be supplemented by appropriate field-based studies to improve our understanding of the impact of acidification on ecosystems. Sustained field studies, including measurements of physical and chemical variables, such as those initiated for the Great Barrier Reef[x], must be expanded to other sites in the tropical Pacific Ocean.

viii CLIVAR, www.clivar.org

ix Grand Observatoire de l'Environnement et de la Biodiversité Terrestre et Marine du Pacifique Sud (South Pacific integrated Observatory for environment and terrestrial and marine biodiversity, www.observatoire-gops.org)

x Great Barrier Reef Ocean Observing System, www.imos.org.au/gbroos.html

References

1. Zhang Y, Wallace J and Battisti D (1997) ENSO-like interdecadal variability: 1900–1993. *Journal of Climat*e 10, 1004–1020.
2. Mantua N, Wallace J and Francis R (1997) A Pacific interdecadal climate oscillation with impacts on salmon production. *Bulletin of the American Meteorological Society* 78, 1069–1079.
3. Garreaud R and Battisti D (1999) Interannual (ENSO) and interdecadal (ENSO-like) variability in the Southern Hemisphere tropospheric circulation. *Journal of Climate* 12, 2113–2123.
4. Power S, Casey T, Folland C, Colman A and Mehta V (1999) Inter-decadal modulation of the impact of ENSO on Australia. *Climate Dynamics* 15, 319–332.
5. Folland CK, Renwick JA, Salinger MJ and Mullan B (2002) Relative influence of the Interdecadal Pacific Oscillation and ENSO on the South Pacific Convergence Zone. *Geophysical Research Letters* 29, doi:10.1029/2001GL014201
6. Solomon S, Qin D, Manning M, Chen Z and others (2007) *Climate Change 2007: The Physical Science Basis. Contribution of Working Group I to the Fourth* Assessment *Report of the Intergovernmental Panel on Climate Change*. Cambridge University Press, Cambridge, United Kingdom, and New York, United States of America.
7. Van Oldenborgh G, Philip S and Collins M (2005) El Niño in changing climate: A multi-model study. *Ocean Science* 1, 81–95.
8. Guilyardi E (2006) El Niño-mean state-seasonal cycle interactions in a multi-model ensemble. *Climate Dynamics* 26, 329–348.
9. Guilyardi E, Wittenberg A, Fedorov A, Collins M and others (2009) Understanding El Niño in ocean-atmosphere general circulation models: Progress and challenges. *Bulletin of the American Meteorological Society* 90, 325–340.
10. Leloup J, Lengaigne M and Boulanger J-P (2007) Twentieth century ENSO characteristics in the IPCC database. *Climate Dynamics* 30, 277–291.
11. Reichler T and Kim J (2008) How well do coupled models simulate today's climate? *Bulletin of the American Meteorological Society*, 303–311, doi:10.1175/BAMS-89–3-303
12. Reid JL (1997) On the total geostrophic circulation of the South Pacific Ocean: Flow patterns, tracers and transports. *Progress in Oceanography* 39, 263–352.
13. Qu T and Lukas R (2003) The bifurcation of the North Equatorial Current in the Pacific. *Journal of Physical Oceanography* 33, 5–18.
14. Gouriou Y and Toole J (1993) Mean circulation of the upper layers of the western equatorial Pacific Ocean. *Journal of Geophysical Research* 98, 22,495–22,520.
15. Qu T and Lindstrom E (2002) A climatological interpretation of the circulation in the western South Pacific. *Journal of Physical Oceanography* 32, 2492–2508.
16. Kessler WS and Gourdeau L (2007) The annual cycle of circulation of the south-west subtropical Pacific, analyzed in an ocean GCM. *Journal of Physical Oceanography* 37, 1610–1627.
17. Webb D (2000) Evidence for shallow zonal jets in the South Equatorial Current region of the southwest Pacific. *Journal of Physical Oceanography* 30, 706–720.
18. Gourdeau L, Kessler WS, Davis RE, Sherman J and others (2008) Zonal jets entering the Coral Sea. *Journal of Physical Oceanography* 38, 715–725.
19. Ganachaud A, Gourdeau L and Kessler W (2008) Bifurcation of the subtropical south equatorial current against New Caledonia in December 2004 from a hydrographic inverse box model. *Journal of Physical Oceanography* 38, 2072–2084.

20. Lindstrom E, Lukas R, Rine R, Firing E and others (1987) The western equatorial Pacific Ocean circulation study. *Nature* 330, 533–537.
21. Gordon A and Fine R (1996) Pathways of water between the Pacific and Indian oceans in the Indonesian seas. *Nature* 379, 146–149.
22. Wijffels S, Meyers G and Godfrey S (2008) A 20-year average of the Indonesian throughflow: Regional currents and the interbasin exchange. *Journal of Physical Oceanography* 38, 1965–1978.
23. Fine R, Lukas R, Bingham FM, Warner MJ and Gammon RH (1994) The western equatorial Pacific is a water mass crossroads. *Journal of Geophysical Research* 99, 25,063–25,080.
24. Johnson G, Sloyan B, Kessler W and McTaggart K (2002) Direct measurements of upper ocean currents and water properties across the tropical Pacific during the 1990s. *Progress in Oceanography* 52, 31–61.
25. Reid JL (1959) Evidence of a South Equatorial Countercurrent in the Pacific Ocean. *Nature* 184, 209–210.
26. Qiu B, Chen S and Kessler W (2009) Source of the 70-day mesoscale eddy variability in the Coral Sea and the North Fiji Basin. *Journal of Physical Oceanography* 39, 404–420.
27. Martinez E and Maamaatuaiahutapu K (2004) Island mass effect in the Marquesas Islands: Time variation. *Geophysical Research Letters* 31, doi:10.1029/2004GL020682
28. Martinez E, Ganachaud A, Lefevre J and Maamaatuaiahutapu K (2009) Central South Pacific thermocline water circulation from a high-resolution ocean model validated against satellite data: Seasonal variability and El Niño 1997–1998 influence. *Journal of Geophysical Research* 114, C05012, doi:10.1029/2008JC004824
29. Qiu B, Koh D, Lumpkin C and Flament P (1997) Existence and formation mechanism of the North Hawaiian Ridge Current. *Journal of Physical Oceanography* 27, 431–444.
30. Calil PHR, Richards KJ, Yanli J and Bidigare RR (2008) Eddy activity in the lee of the Hawaiian Islands. *Deep-Sea Research II* 55, 1179–1194.
31. Reverdin G, Frankignoul C, Kestenare E and McPhaden M (1994) Seasonal variability in the surface currents of the equatorial Pacific. *Journal of Geophysical Research* 99, 20,323–20,344.
32. Cravatte S, Picaut J and Eldin G (2003) Second and first baroclinic Kelvin modes in the equatorial Pacific at intraseasonal timescales. *Journal of Geophysical Research* 108, doi:10.1029/2002JC001511
33. Lagerloef G, Mitchum G, Lukas R and Niiler P (1999) Tropical Pacific near-surface currents estimated from altimeter, wind, and drifter data. *Journal of Geophysical Research* 104, 23,313–23,326.
34. Holbrook NJ and Bindoff NL (1999) Seasonal temperature variability in the upper southwest Pacific Ocean. *Journal of Physical Oceanography* 29, 366–381.
35. De Boyer Montégut C, Madec G, Fischer A, Lazar A and Iudicone D (2004) An examination of profile data and a profile-based climatology. *Journal of Geophysical Research* 109, C12003, doi:10.1029/2004JC002378
36. Longhurst AR (2006) *Ecological Geography of the Sea*. Academic Press, New York, United States of America.
37. Picaut J, Ioualalen M, Menkes C, Delcroix T and McPhaden MJ (1996) Mechanism of the zonal displacements of the Pacific warm pool: Implications for ENSO. *Science* 274, 1486–1489.
38. Picaut J, Masia F and du Penhoat Y (1997) An advective-reflective conceptual model for the oscillatory nature of the ENSO. *Science* 277, 663–666.

39. Maes C, Picaut J, Kuroda Y and Ando K (2004) Characteristics of the convergence zone at the eastern edge of the Pacific warm pool. *Geophysical Research Letters* 31, L11304, doi:10.1029/2004GL019867
40. Rodier M, Eldin G and Le Borgne R (2000) The western boundary of the equatorial Pacific upwelling: Some consequences of climatic variability on hydrological and planktonic properties. *Journal of Oceanography* 56, 463–471.
41. Lukas R and Lindstrom E (1991) The mixed layer of the western equatorial Pacific Ocean. *Journal of Geophysical Research* 96 (suppl), 3343–3357.
42. Eldin G, Delcroix T and Rodier M (2004) The frontal area at the eastern edge of the western equatorial Pacific warm pool in April 2001. *Journal of Geophysical Research* 109, doi:10.1029/2003JC002088
43. Maes C, Picaut J and Belamari S (2002) Salinity barrier layer and onset of El Niño in a Pacific coupled model. *Geophysical Research Letters* 29, 2206, doi:10.1029/2002GL016029
44. Maes C, Picaut J and Belamari S (2005) Importance of salinity barrier layer for the buildup of El Niño. *Journal of Climate* 18, 104–118.
45. Ryan JP, Polito PS, Strutton PG and Chavez FP (2002) Unusual large-scale blooms in the equatorial Pacific. *Progress in Oceanography* 55, 263–285.
46. Jones GP, Almany GR, Russ GR, Sale PF and others (2009) Larval retention and connectivity among populations of corals and reef fishes: History, advances and challenges. *Coral Reefs* 28, 307–325.
47. Stammer D (1997) Global characteristics of ocean variability estimated from regional TOPEX/POSEIDON altimeter measurements. *Journal of Physical Oceanography* 27, 1743–1769.
48. Chelton DB, DeSzoeke RA, Schlax MG, El Naggar K and Siwertz N (1998) Geographical variability of the first baroclinic Rossby radius of deformation. *Journal of Physical Oceanography* 28, 433–460.
49. Polito P and Liu T (2003) Global characterization of Rossby waves at several spectral bands. *Journal of Geophysical Research* 108, 3018, doi:10.1029/2000JC000607
50. Barron C, Kara A and Jacobs G (2009) Objective estimates of westward Rossby wave and eddy propagation from sea surface height analyses. *Journal of Geophysical Research* 114, doi:10.1029/2008JC005044
51. Maharaj AM, Holbrook NJ and Cipollini P (2009) Multiple westward propagating signals in South Pacific sea level anomalies. *Journal of Geophysical Research* 114, 1–14.
52. Qiu B and Chen S (2004) Seasonal modulations in the eddy field of the South Pacific Ocean. *Journal of Physical Oceanography* 34, 1515–1527.
53. Uz BM, Yoder JA and Osychny V (2001) Pumping of nutrients to ocean surface waters by the action of propagating planetary waves. *Nature* 409, 597–600.
54. Stammer D and Wunsch C (1999) Temporal changes in eddy energy of oceans. *Deep-Sea Research II* 46, 77–108.
55. Bowen MM, Wilkin JL and Emery WJ (2005) Variability and forcing of the East Australian Current. *Journal of Geophysical Research* 110, doi:10.1029/2004JC002533
56. Mata MM, Wijffels SE, Church JA and Tomczak M (2006) Eddy shedding and energy conversions in the East Australian Current. *Journal of Geophysical Research* 111, C09034, doi:10.1029/2006JC003592
57. Qiu B (1999) Seasonal eddy field modulation of the North Pacific Subtropical Countercurrent: TOPEX/POSEIDON observations and theory. *Journal of Physical Oceanography* 29, 2471–2486.

58. Hwang C, Wu CR and Kao R (2004) TOPEX/Poseidon observations of mesoscale eddies over the subtropical countercurrent: Kinematic characteristics of an anticyclonic eddy and a cyclonic eddy. *Journal of Geophysical Research* 109, C08013, doi:10.1029/2003JC002026
59. Emerson S, Mecking S and Abell J (2001) The biological pump in the subtropical north Pacific Ocean: Nutrient sources, Redfield ratios, and recent changes. *Global Biogeochemical Cycles* 15, 535–554.
60. Sarmiento JL, Slater R, Barber R and Bopp L (2004) Response of ocean ecosystems to climate warming. *Global Biogeochemical Cycles* 18, GB3003, doi:10.1029/2003GB002134
61. Seki MP, Polovina JJ, Brainard RE, Bidigare RR and others (2001) Biological enhancement at cyclonic eddies tracked with GOES Thermal Imagery in Hawaiian waters. *Geophysical Research Letters* 28, 1583–1586.
62. Vaillancourt R, Marra J, Seki M, Parsons M and Bidigare R (2003) Impact of a cyclonic eddy on phytoplankton community structure and photosynthetic competency in the subtropical North Pacific Ocean. *Deep-Sea Research Part II: Topical Studies in Oceanography* 50, 1393–1414.
63. McGillicuddy D, Robinson A, Siegel Jannasch H, Johnson R and others (1998) Influence of mesoscale eddies on new production in the Sargasso Sea. *Nature* 394, 263–266.
64. McGillicuddy DJ, Anderson LA, Bates NR and Bibby T (2007) Eddy/wind interactions stimulate extraordinary mid-ocean plankton blooms. *Science* 316, 1021–1026.
65. Mahadevan A, Thomas LN and Tandon A (2008) Comment on 'Eddy/wind interactions stimulate extraordinary mid-ocean plankton blooms'. *Science* 320, 448, doi:10.1126/science1152111
66. Calil PHR and Richards KJ (2010) Transient upwelling hot spots in the oligotrophic North Pacific. *Journal of Geophysical Research* 115, doi:10.1029/2009JC005360
67. Ryan JP, Ueki I, Chao Y, Zhang H and others (2006) Western Pacific modulation of large phytoplankton blooms in the central and eastern equatorial Pacific. *Journal of Geophysical Research* 111, G02013, doi:10.1029/2005JG000084
68. Andersson A, Mackenzie F and Lerman A (2006) Coastal ocean CO_2 – carbonic acid – carbonate sediment system of the Anthropocene. *Global Biogeochemical Cycles* 20, doi:10.1029/2005GB002506
69. Andersson A, Bates N and Mackenzie F (2007) Dissolution of carbonate sediments under rising pCO_2 and ocean acidification: Observations from Devil's Hole, Bermuda. *Aquatic Geochemistry* 13, 237–264.
70. Feely R, Sabine C, Lee K, Berelson W and others (2004) Impact of anthropogenic CO_2 on the $CaCO_3$ system in the oceans. *Science* 305, 362–366.
71. Doney SC (2006) The dangers of ocean acidification. *Scientific American* 294, 58–65.
72. Hoegh-Guldberg O, Mumby PJ, Hooten AJ, Steneck RS and others (2007) Coral reefs under rapid climate change and ocean acidification. *Science* 318, 1737–1742.
73. Guinotte J and Fabry V (2008) Ocean acidification and its potential effects on marine ecosystems. *Annals of the New York Academy of Science* 1134, 320–342.
74. Martin S, Gazeau F, Orr JC, and Gattuso J-P (2008) Ocean acidification and its Consequences. *Lettre PIGB-PMRC France* 21, 5–16.
75. Zeebe R, Zachos J, Caldeira K and Tyrrell T (2008) Carbon emissions and acidification. *Science* 321, 51–52.
76. Fabry VJ, Seibel BA, Feely RA and Orr JC (2008) Impacts of ocean acidification on marine fauna and ecosystem processes. *ICES Journal of Marine Science* 65, 414–432.
77. Orr JC, Fabry VJ, Aumont O, Bopp L and others (2005) Anthropogenic ocean acidification over the twenty-first century and its impact on calcifying organisms. *Nature* 437, 681–686.

78. Tribollet A, Godinot C, Atkinson M and Langdon C (2009) Effects of elevated pCO_2 on dissolution of coral carbonates by microbial euendoliths. *Global Biogeochemical Cycles,* doi:10.1029/2008GB003286

79. Andersson A, Mackenzie F and Lerman A (2005) Coastal ocean and carbonate systems in the high CO_2 world of the anthropocene. *American Journal of Science* 305, 875–918.

80. Hinga KR (2002) Effects of pH on coastal marine phytoplankton. *Marine Ecology Progress Series* 238, 281–300.

81. Rascle N, Ardhuin F, Queffeulou P and Croize-Fillon D (2008) A global wave parameter database for geophysical applications. Part 1: Wave-current-turbulence interaction parameters for the open ocean based on traditional parameterizations. *Ocean Modelling* 25, 154–171.

82. Ogston AS, Storlazzi CD, Field ME and Presto MK (2004) Sediment resuspension and transport patterns on a fringing reef flat, Molokai, Hawaii. *Coral Reefs* 23, 559–569.

83. Storlazzi CD, Logan JB and Field ME (2003) Quantitative morphology of a fringing reef tract from high-resolution laser bathymetry: Southern Molokai, Hawaii. *Geological Society of America Bulletin* 115, 1344–1355.

84. Storlazzi CD and Field ME (2005) A model for wave control on coral breakage and species distribution in the Hawaiian Islands. *Coral Reefs* 24, 43–55.

85. Montaggioni L, Le Cornec F, Corrège T and Cabioch G (2006) Coral barium/calcium record of mid-Holocene upwelling activity in, New Caledonia, South-West Pacific. *Palaeogeography, Palaeoclimatology, Palaeoecology* 237, 436–455.

86. Sterl A and Caires S (2005) Climatology, variability and extrema of ocean waves: The web-based KNMI/ERA-40 wave atlas. *International Journal of Climatology* 25, 963–977.

87. Hemer M, Church J and Hunter J (2010) Variability and trends in the directional wave climate of the southern hemisphere. *International Journal of Climatology*, doi:10.1002/joc.1900

88. Madin JS, Black KP and Connolly SR (2006) Scaling water motion on coral reefs: From regional to organismal scales. *Coral Reefs* 25, 635–644.

89. Masselink G and Hughes MG (2003) *Introduction to Coastal Processes and Geomorphology.* Arnold Publishers, London, United Kingdom.

90. Callaghan DP, Nielsen P, Cartwright N, Gourlay MR and Baldock TE (2006) Atoll lagoon flushing forced by waves. *Coastal Engineering* 53(8), 691–704.

91. Goodwin ID and Harvey N (2008) Subtropical sea-level history from coral microatolls in the southern Cook Islands, since 300 AD. *Marine Geology* 253, 14–25.

92. Smithers SG and Woodroffe CD (2000) Microatolls as sea-level indicators on a mid-ocean atoll. *Marine Geology* 168, 61–78.

93. Nielsen P, Guard PA, Callaghan DP and Baldock TE (2008) Observations of wave pump efficiency. *Coastal Engineering* 55(1), 69–72.

94. Kruger J and Damlamain H (2010) *Numerical Model of Aitutaki: Water Circulation and Applications.* EU EDF/SOPAC Project Report ER 157.

95. Marshall GJ (2003) Trends in the Southern Annular Mode from observations and reanalyses. *Journal of Climate* 16, 4134–4143.

96. Aucan J (2006) Directional wave climatology for the Hawaiian Islands from buoy data and the influence of ENSO on extreme wave events from model hindcast. *Ninth International Workshop on Wave Hindcasting and Forecasting*, JCOMM Technical Report 34/WMO-TD 1368, www.waveworkshop.org/9thWaves/Papers/Aucan.pdf

97. Jansen E, Overpeck J, Briffa KR, Duplessy J-C and others (2007) Palaeoclimate. In: S Solomon, D Qin, M Manning, Z Chen, M Marquis, KB Averyt, M Tignor and HL Miller (eds) *Climate Change 2007: The Physical Science Basis. Contribution of Working Group I*

to the Fourth Assessment Report of the Intergovernmental Panel on Climate Change. Cambridge University Press, Cambridge, United Kingdom, and New York, United States of America, pp. 433–497.

98. Lemke P, Ren J, Alley RB, Allison I and others (2007) Observations: Changes in snow, ice and frozen ground. In: S Solomon, D Qin, M Manning, Z Chen, M Marquis, KB Averyt, M Tignor and HL Miller (eds) *Climate Change 2007*: *The Physical Science Basis*. *Contribution of Working Group I to the Fourth Assessment Report of the Intergovernmental Panel on Climate Change*. Cambridge University Press, Cambridge, United Kingdom, and New York, United States of America, pp. 347–383.
99. Church J, White N and Hunter J (2006) Sea-level rise at tropical Pacific and Indian Ocean islands. *Global and Planetary Change* 53, 155–168.
100. Church JA, White NJ, Coleman R, Lambeck K and Mitrovica JX (2004) Estimates of the regional distribution of sea-level rise over the 1950 to 2000 period. *Journal of Climate* 17, 2609–2625.
101. Roemmich D, Gilson J, Davis R, Sutton P and others (2007) Decadal spinup of the South Pacific subtropical gyre. *Journal of Physical Oceanography* 37, 162–173.
102. Firing YL and Merrifield MA (2004) Extreme sea level events at Hawaii: Influence of mesoscale eddies. *Geophysical Research Letters* 31L24306, doi:10.1029/2004GL021539
103. Allain V, Kernadel A-J, Andréfouët S, Magron F and others (2008) Enhanced seamount location database for the western and central Pacific Ocean: Screening and cross-checking of 20 existing datasets. *Deep-Sea Research I* 55, 1035–1047.
104. Steinberg C (2007) Impacts of climate change on the physical oceanography of the Great Barrier Reef. In: JE Johnson and PA Marshall (eds) *Climate Change and the Great Barrier Reef: A Vulnerability Assessment*. 1st edition, Great Barrier Reef Marine Park Authority and Australian Greenhouse Office, Townsville, Australia, pp. 51–74.
105. Heywood KJ, Barton ED and Simpson JH (1990) The effect of flow disturbance by an oceanic island. *Journal of Marine Research* 48, 55–73.
106. Holland C and Mitchum GT (2001) Propagation of big island eddies. *Journal of Geophysical Research* 106, 935–944.
107. Wolanski E, Richmond RH, Davis G, Deleersnijder E and Leben RR (2003) Eddies around Guam, an island in the Mariana Islands group. *Continental Shelf Research* 23, 991–1003.
108. Hasegawa D, Lewis MR and Gangopadhyay A (2009) How islands cause phytoplankton to bloom in their wakes. *Geophysical Research Letters* 36, L20605, doi:10.1029/2009GL039743
109. Alory G, Vega A, Ganachaud A and Despinoy M (2006) Influence of upwelling, subsurface stratification, and heat fluxes on coastal sea surface temperature off southwestern New Caledonia. *Journal of Geophysical Research* 111, C07023, doi:10.1029/2005JC003401
110. Ganachaud A, Vega A, Rodier M, Dupouy C and others (2010) Observed impact of upwelling on water properties and biological activity off the southwest coast of New Caledonia. *Marine Pollution Bulletin* 61(7–12), 449–464.
111. Marchesiello P, Lefèvre J, Vega A, Couvelard X and Menkes C (2010) Coastal upwelling, circulation and heat balance around New Caledonia's barrier reef. *Marine Pollution Bulletin* 61(7–12), 432–448.
112. Egbert G and Ray R (2000) Significant dissipation of tidal energy in the deep ocean inferred from satellite altimeter data. *Nature* 405, 775–778.
113. Wolanski EJ, Colin PL, Naithani J, Deleersnijder E and Golbuu Y (2004) Large amplitude, leaky, island-generated, internal waves around Palau, Micronesia. *Estuarine Coastal and Shelf Science* 60, 705–716.

114. Qiu B and Durland T (2002) Interaction between an island and the ventilated thermocline: Implications for the Hawaiian Lee Countercurrent. *Journal of Physical Oceanography* 32, 3408–3426.

115. Yang Y, Xie S-P and Hafner J (2008) Cloud patterns lee of Hawaii Island: A synthesis of satellite observations and numerical simulation. *Journal of Geophysical Research* 113, D15126, doi:10.1029/2008JD009889

116. Lefevre J, Marchesiello P, Jourdain N, Menkes C and Leroy A (2010) Weather regimes and orographic circulation around New Caledonia. *Marine Pollution Bulletin* 61(7–12), 413–431.

117. Cai W (2006) Antarctic ozone depletion causes an intensification of the Southern Ocean super-gyre circulation. *Geophysical Research Letters* 33, doi:10.1029/2005GL024911

118. Ridgway KR (2007) Long-term trend and decadal variability of the southward penetration of the East Australian Current. *Geophysical Research Letters* 34, L13613, doi:10.1029/2007GL030393

119. Roemmich D and Gilson J (2009) The 2004–2007 mean and annual cycle of temperature, salinity and steric height in the global ocean from the Argo Program. *Progress in Oceanography* 82, 81–100.

120. Vecchi G, Soden B, Wittenberg A, Held M and others (2006) Weakening of tropical Pacific atmospheric circulation due to anthropogenic forcing. *Nature* 441, 73–76.

121. Cai W, Shi G, Cowan T, Bi D and Ribbe J (2005) The response of Southern Annular Mode, the East Australian Current, and the southern mid-latitude ocean circulation to global warming. *Geophysical Research Letters* 32, doi:1029/2005GL024701

122. Sen Gupta A, Santoso A, Taschetto A, Ummenhofer CC and others (2009) Projected changes to the Southern Hemisphere Ocean and sea ice in the IPCC-AR4 climate models. *Journal of Climate* 22, 3047–3078.

123. Munday PL, Leis JM, Lough JM, Paris CB and others (2009) Climate change and coral reef connectivity. *Coral Reefs,* doi:10.1007/s00338-008-0461-9

124. Mackay DJ, O'Sullivan JE and Watson RJ (2002) Iron in the western Pacific: A riverine or hydrothermal source for iron in the Equatorial Undercurrent? *Deep-Sea Research I* 49, 877–893.

125. Levitus S, Antonov J and Boyer T (2005) Warming of the world ocean, 1955–2003, *Geophysical Research Letters* 32, L02604, doi:10.109/2004GL021592

126. Bindoff NL, Willebrand J, Artale V, Cazenave A and others (2007) Observations: Oceanic climate change and sea level. In: S Solomon, D Qin, M Manning, Z Chen, M Marquis, KB Averyt, M Tignor and HL Miller (eds) *Climate Change 2007: The Physical Science Basis. Contribution of Working Group I to the Fourth Assessment Report of the Intergovernmental Panel on Climate Change*. Cambridge University Press, Cambridge, United Kingdom, and New York, United States of America, pp. 385–428.

127. Chen JY, Del Genio AD, Carlson BE and Bosilovich MG (2008) The spatiotemporal structure of twentieth-century climate variations in observations and reanalyses. Part I: Long-term trend. *Journal of Climate* 21, 2611–2633.

128. Cravatte S, Delcroix T, Zhang D, McPhaden M and Leloup J (2009) Observed freshening and warming of the western Pacific warm pool. *Climate Dynamics* 33, 565–589, doi:10.1007/s00382-009-0526-7

129. Chen JY, Del Genio AD, Carlson BE and Bosilovich MG (2008) The spatiotemporal structure of twentieth-century climate variations in observations and reanalyses. Part II: Pacific pan-decadal variability. *Journal of Climate* 21, 2634–2650.

130. Barnett T, Pierce D, AchutaRao K, Glecker P and others (2005) Penetration of human-induced warming into the World's Ocean. *Science* 309, 284–285.

131. Wijffels SE, Willis J, Domingues CM, Barker P and others (2008) Changing expendable bathythermograph fall rates and their impact on estimates of thermosteric sea-level rise. *Journal of Climate* 21, 5657–5672.

132. Levitus S, Antonov J, Boyer T, Locarnini R and others (2009) Global ocean heat content 1955–2008 in light of recently revealed instrumentation problems. *Geophysical Research Letters* 36, doi:10.1029/2008GL037155

133. Han W, Meehl GA and Hu A (2006) Interpretation of the tropical cooling in the Indian and Pacific oceans during recent decades. *Geophysical Research Letters* 33, L23615, doi:10.1029/2006GL027982

134. Wang H and Mehta VM (2008) Decadal variability of the Indo-Pacific warm pool and its association with atmospheric and oceanic variability in the NCEP-NCAR and SODA reanalyses. *Journal of Climate* 21, 5545–5565.

135. Delcroix T, Cravatte S and McPhaden MJ (2007) Decadal variations and trends in tropical Pacific sea surface salinity since 1970. *Journal of Geophysical Research* 112, C03012, doi:10.1029/2006JC003801

136. Randall DA, Wood RA, Bony S, Colman R and others (2007) Climate Models and Their Evaluation. In: S Solomon , D Qin, M Manning, Z Chen, M Marquis, KB Averyt, M Tignor and HL Miller (eds) *Climate Change 2007: The Physical Science Basis. Contribution of Working Group I to the Fourth Assessment Report of the Intergovernmental Panel on Climate Change*. Cambridge University Press, Cambridge, United Kingdom, and New York, United States of America, pp. 589–661.

137. Zhang GJ and Wang H (2006) Toward mitigating the double ITCZ problem in NCAR CCSM3. *Geophysical Research Letters* 33, L06709, doi:10.1029/2005GL025229

138. Misra V, Marx L, Brunke M and Zeng X (2008) The equatorial Pacific cold tongue bias in a coupled climate model. *Journal of Climate* 21, 5852–5869.

139. Misra V, Marx L, Fennessy M, Kirtman B and Kinter III JL (2008) A comparison of climate prediction and simulation over the tropical Pacific. *Journal of Climate* 21, 5852–5869.

140. Stammer D, Wunsch C and Ueyoshi K (2006) Temporal changes in ocean eddy transports. *Journal of Physical Oceanography* 36, 543–550.

141. Qiu B and Chen S (2006) Decadal variability in the large-scale sea surface height field of the south Pacific Ocean: Observations and causes. *Journal of Physical Oceanography* 36, 1751–1762.

142. Fyfe JC and Saenko OA (2007) Anthropogenic speed-up of oceanic planetary waves. *Geophysical Research Letters* 34, L10706, doi:10.1029/2007GL029859

143. Martinez E, Antoine D, D'Ortienzio F and Gentili B (2009) Climate-driven basin-scale decadal oscillations of oceanic phytoplankton. *Science* 326, 1253–1256.

144. Watanabe YW, Ishida H, Nakano T and Nagai N (2005) Spatiotemporal decreases of nutrients and chlorophyll-*a* in the surface mixed layer of the western North Pacific from 1971 to 2000. *Journal of Oceanography* 61, 1011–1016.

145. Keller K, Slater RD, Bender M and Key R (2002) Possible biological or physical explanations for decadal scale trends in north Pacific nutrient concentrations and oxygenutilization. *Deep-Sea Research II* 49, 345–362.

146. Karl DM and Lukas R (1996) The Hawaii Ocean Time-series (HOT) program: Background, rationale and field implementation. *Deep-Sea Research II* 43, 129–156.

147. Corno G, Karl DM, Church MJ, Letelier RM and others (2007) Impact of climate forcing on ecosystem processes in the North Pacific subtropical gyre. *Journal of Geophysical Research* 112, C04021, doi:10.1029/2006JC003730

148. Behrenfeld MJ, O'Malley RT, Siegel DA and McClain CR (2006) Climate-driven trends in contemporary ocean productivity. *Nature* 444, 752–755.

149. Polovina JJ, Howell EA and Abecassis M (2008) Ocean's least productive waters are expanding. *Geophysical Research Letters* 35, L03618, doi:10.1029/2007GL031745

150. Bopp L, Aumont O, Cadule P, Alvain S and Gehlen M (2005) Response of diatoms distribution to global warming and potential implications: A global model study. *Geophysical Research Letters* 32, L19606, doi:10.1029/2005GL023653

151. Yeh S-W, Yim B, Noh Y and Dewitte B (2009) Changes in mixed layer depth under climate change projections in two CGCMs. *Climate Dynamics* 33, 199–213.

152. Zhang D and McPhaden MJ (2006) Decadal variability of the shallow Pacific meridional overturning circulation: Relation to tropical sea surface temperatures in observations and climate change models. *Ocean Modelling* 15, 250–273.

153. Lu P, McCreary J and Klinger B (1998) Meridional circulation cells and the source waters for the Pacific Equatorial Undercurrent. *Journal of Physical Oceanography* 28, 62–84.

154. Najjar RG, Jin X, Louanchi F, Aumont O and others (2007) Impact of circulation on export production, dissolved organic matter, and dissolved oxygen in the ocean: Results from Phase II of the Ocean Carbon-cycle Model Intercomparison Project (OCMIP-2). *Global Biogeochemical Cycles* 21, GB3007, doi:10.1029/2006GB002857

155. Bopp L, Monfray P, Aumont O, Dufresne JL and others (2001) Potential impact of climate change on marine export production. *Global Biogeochemical Cycles* 15, 81–99.

156. Schmittner A, Oschlies A, Matthews H and Galbraith E (2008) Future changes in climate, ocean circulation, ecosystems, and biogeochemical cycling simulated for a Business-as-usual CO_2 emission scenario until year 4000 AD. *Global Biogeochemical Cycles* 22, GB1013, doi:10.1029/2007GB002953

157. Emerson S, Watanabe YW, Ono T and Mecking S (2004) Temporal trends in apparent oxygen utilization in the upper pycnocline of the north Pacific: 1980–2000. *Journal of Oceanography* 60, 139–147.

158. Mecking S, Warner M and Bullister J (2006) Temporal changes in pCFC-12 ages and AOU along two hydrographic sections in the eastern subtropical North Pacific. *Deep-Sea Research I* 53, 169–187.

159. Doney SC, Bullister JL and Wanninkhof R (1998) Climatic variability in upper ocean ventilation rates diagnosed using chlorofluorocarbons. *Geophysical Research Letters* 25, 1399–1402.

160. Stramma L, Johnson G, Sprintall J and Mohrholz V (2008) Expanding oxygen-minimum zones in the tropical oceans. *Science* 320, 655–658.

161. Bopp L, Le Quere C, Heimann M, Manning AC and Monfray P (2002) Climate-induced oceanic oxygen fluxes: Implications for the contemporary carbon budget. *Global Biogeochemical Cycles* 16, 1022, doi:10.1029/2001GB001445

162. Matear RJ and Hirst AC (2003) Long-term changes in dissolved oxygen concentrations in the ocean caused by protracted global warming. *Global Biogeochemical Cycles* 17, 1125, doi:10.1029/2002GB001997

163. Sabine CL, Feely RA, Gruber N and Key RM (2004) The oceanic sink for anthropogenic CO_2. *Science* 305, 367–371.

164. Global Carbon Project (2008) *Carbon Budget and Trends 2007*. www.globalcarbonproject.org

165. Caldeira K and Wickett E (2003) Anthropogenic carbon and ocean pH. *Nature* 424, 365.

166. Zondervan I, Zeebe RE, Rost B and Riebesell U (2001) Decreasing marine biogenic calcification: A negative feedback on rising atmospheric pCO_2. *Global Biogeochemical Cycles* 15, 507–516.

167. The Royal Society (2005) *Ocean Acidification Due to Increasing Atmospheric Carbon Dioxide Contents*. The Royal Society, Policy Document 12/05. www.royalsoc.ac.uk

168. Veron JEN, Hoegh-Guldberg O, Lenton T, Lough J and others (2009) The coral reef crisis: The critical importance of < 350 ppm CO_2. *Marine Pollution Bulletin* 58, 1428–1436.

169. Gulev SK and Grigorieva V (2004) Last century changes in ocean wind wave height from global visual wave data. *Geophysical Research Letters* 31, L24302, doi:10.1029/2004GL021040

170. Wang XL and Swail VR (2006) Climate change signal and uncertainty in projections of ocean wave heights. *Climate Dynamics* 26, 109–126.

171. Mori N, Ysuda T, Mase H, Tom T and Oku Y (2010) Projection of extreme wave climate change under global warming. *Hydrological Research Letters* 4, 15–19.

172. Hemer MA, Simmonds I and Kea K (2008) A classification of wave generation characteristics during large wave events on the southern Australian margin. *Continental Shelf Research* 28, 634–652.

173. Grabemann I and Weisse R (2008) Climate change impact on extreme wave conditions in the North Sea: An ensemble study. *Ocean Dynamics* 58, 199–212, doi:10.1007/s10236-008-0141

174. Church JA and White NJ (2006) A 20th century acceleration in global sea-level rise. *Geophysical Research Letters* 33, L01602, doi:10.1029/2005GL024826

175. Meier MF, Dyurgerov MB, Rick UK, O'Neel S and others (2007) Glaciers dominate eustatic sea-level rise in the 21st century. *Science* 317, 1064.

176. Church JA, White N and Arblaster J (2005) Significant decadal-scale impact of volcanic eruptions on sea level and heat content. *Nature* 438, 74–77.

177. Domingues CM, Church JA, White NJ, Gleckler PJ and others (2008) Improved estimates of upper-ocean warming and multi-decadal sea-level rise. *Nature* 453, 1090–U6.

178. Rahmstorf S (2007) Response to comments on a semi-empirical approach to projecting future sea-level rise. *Science* 317, 1866d.

179. Rahmstorf S (2007) A semi-empirical approach to projecting future sea-level rise. *Science* 315, 368–370.

180. Meehl GA, Stocker TF, Collins WD, Friedlingstein P and others (2007) Global Climate Projections. In: S Solomon, D Qin, M Manning, Z Chen, M Marquis, KB Averyt, M Tignor M and HL Miller (eds) *Climate Change 2007: The Physical Science Basis. Contribution of Working Group I to the Fourth Assessment Report of the Intergovernmental Panel on Climate Change*. Cambridge University Press, Cambridge, United Kingdom, and New York, United States of America, pp. 747–845.

181. Van den Broeke M, Bamber J, Ettema J, Rignot E and others (2009) Partitioning recent Greenland mass loss. *Science* 326, 984–986.

182. Overpeck JT, Otto-Bliesner BL, Miller GH, Muhs DR and others (2006) Paleoclimatic evidence for future ice-sheet instability and rapid sea-level rise. *Science* 311, 1747–1750.

183. Blanchon P, Eisenhauer A, Fietzke J and Leibetrau V (2009) Rapid sea-level rise and reef back-stepping at the close of the last interglacial highstand. *Nature* 458, 881–884

184. Pfeffer WT, Harper JT and O'Neel S (2008) Kinematic constraints on glacier contributions to 21st Century Sea-Level Rise. *Science* 321, 1340–1343.

185. Vermeer M and Rahmstorf S (2009) Global sea level linked to global temperature. *Proceedings of the National Academy of Science of the USA,* doi:10.1073/pnas.0907765106

186. Bakun A (1990) Coastal ocean upwelling. *Science* 247, 198–201.

187. Roemmich D and McGowan J (1995) Climatic warming and the decline of zooplankton in the California Current. *Science* 267, 1324–1326.

188. Snyder MA, Sloan LC, Diffenbaugh NS and Bell JL (2003) Future climate change and upwelling in the California Current. *Geophysical Research Letters* 30, 1823, doi:10.1029/2003GL017647

189. Sudre J and Morrow R (2008) Global surface currents: A high-resolution product for investigating ocean dynamics. *Ocean Dynamics,* doi:10.1007/s10236-008-0134-9

190. Ridgway KR and Dunn JR (2003) Mesoscale structure of the East Australian Current System and its relationship with topography. *Progress in Oceanography* 56, 189–222.

191. Carton JA, Chepurin GA , Cao X and Giese B (2000) A simple ocean data assimilation retrospective analysis of the global ocean 1950–1995. Part I: Methodology. *Journal of Physical Oceanography* 30, 294–309.

192. Ridgway KR (2007) Seasonal circulation around Tasmania: An interface between eastern and western boundary dynamics. *Journal of Geophysical Research* 112, C10016, doi:10.1029/2006JC003898

193. Canadell JG, Le Quéré C, Raupach M, Field C and others (2007) Contributions to accelerating atmospheric CO_2 growth from economic activity, carbon intensity, and efficiency of natural sinks. *Proceedings of the National Academy of Science of the USA* 104, 18,866–18,870.

194. Durack P and Wijffels S (2010) Fifty-year trends in global ocean salinities and their relationship to broad-scale warming. *Journal of Climate* 23, 4342–4362.

195. Sabine CL, Feely RA, Key RM, Bullister JL and others (2002) Distribution of anthropogenic CO_2 in the Pacific Ocean. *Global Biogeochemical Cycles* 16, doi:10.1029/2001GB001639

196. Sabine CL, Feely RA, Millero FJ, Dickson AG and others (2008) Decadal changes in Pacific carbon. *Journal of Geophysical Research* 113, C07021, doi:10.1029/2007JC004577

197. Key RM, Kozyr A, Sabine CL, Lee K and others (2004) A global ocean carbon climatology: Results from global data analysis project (GLIDAP). *Global Biogeochemical Cycles* 18, 4031, doi:10.1029/2004GB002247

198. Gent PR and McWilliams JC (1990) Isopycnal mixing in ocean circulation models. *Journal of Physical Oceanography* 20, 150–155.

199. Griffies SM (1998) The Gent-McWilliams skew flux. *Journal of Physical Oceanography* 28, 831–841.

200. Bryan K and Lewis LJ (1979) A water mass model of the world ocean. *Journal of Geophysical Research* 84, 347–376.

201. Pacanowski RC and Philander SGH (1981) Parameterization of vertical mixing in numerical models of tropical oceans. *Journal of Physical Oceanography* 11, 1443–1451.

202. Noh Y and Kim H-J (1999) Simulations of temperature and turbulence structure of the oceanic boundary layer with the improved near-surface process. *Journal of Geophysical Research* 104, 15,621–15,634.

203. Blanke B and Delecluse P (1993) Variability of the tropical Atlantic Ocean simulated by a general circulation model with two different mixed-layer physics. *Journal of Physical Oceanography* 23, 1363–1388.

204. Visbeck M, Marshall J and Haine T (1997) Specification of eddy transfer coefficients in coarse-resolution ocean circulation models. *Journal of Physical Oceanography* 27, 381–402.

205. Large W, McWilliams JC and Doney SC (1994) Oceanic vertical mixing: A review and a model with a nonlocal boundary mixing parameterization. *Review of Geophysics* 32, 363–403.

206. Nakano H and Suginohara N (2002) Effects of bottom boundary layer parameterization on reproducing deep and bottom waters in a world ocean model. *Journal of Physical Oceanography* 32, 1209–1227.

207. Beckmann A and Doscher R (1997) A method for improved representation of dense water spreading over topography in geopotential-coordinate models. *Journal of Physical Oceanography* 27, 581–591.

208. Furevik T, Bentsen M, Drange H, Kindem IKT and others (2003) Description and evaluation of the bergen climate model: ARPEGE coupled with MICOM. *Climate Dynamics* 21, 27–51.

209. Salas-Mélia D (2002) A global coupled sea ice-ocean model. *Ocean Modelling* 4, 137–172.

210. Gordon HB, Rotstayn D, McGregor JL, Dix MR and others (2002) *The CSIRO Mk3 Climate System Model*. Commonwealth Scientific and Industrial Research Organisation Atmospheric Research Technical Paper 60, Aspendale, Australia.

211. Delworth TL, Broccoli AJ, Rosati A, Stouffer RJ and others (2006) GFDL's CM2 global coupled climate models. Part I: Formulation and simulation characteristics. *Journal of Climate* 19, 643–674.

212. Marti O, Braconnot P, Bellier J, Benshila R and others (2005) *The New IPSL Climate System Model: IPSL-CM4c*. dods.ipsl.jussieu.fr/omamce/IPSLCM4/DocIPSLCM4/FILES/DocIPSLCM4.pdf

213. K-1 model developers (2004) *K-1 Coupled Model (MIROC) Description*. K-1 Technical Report 1, Center for Climate System Research, University of Tokyo, Japan. www.ccsr.u-tokyo.ac.jp/kyosei/hasumi/MIROC/tech-repo.pdf

214. Min S-K, Legutke S, Hense A and Kwon W-T (2005) Internal variability in a 1000-yr control simulation with the coupled climate model ECHO-G – I: Near-surface temperature, precipitation, and mean sea level pressure. *Tellus* 57A, 605–621.

215. Yukimoto S, Noda A, Kitoh A, Sugi M and others (2001) The New Meteorological Research Institute coupled GCM (MRI-CGCM2) – Model climate and variability. *Papers in Meteorology and Geophysics* 51(2), 47–88.

216. Collins WD, Bitz CM, Blackmon ML, Bonan GB and others (2006) The community climate system model version 3 (CCSM3). *Journal of Climate* 19, 2122–2143.

217. Washington WM, Weatherly JM, Meehl GA, Semter AJ Jr and others (2000) Parallel climate model (PCM) control and transient simulations. *Climate Dynamics* 16, 755–774.

218. Gordon C, Cooper C, Senior CA, Banks HT and others (2000) The simulation of SST, sea ice extents and ocean heat transports in a version of the Hadley Centre coupled model without flux adjustments. *Climate Dynamics* 16, 147–168.

219. Johns TC, Durman CF, Banks HT, Roberts MJ and others (2006) The new Hadley Centre climate model HadGEM1: Evaluation of coupled simulations. *Journal of Climate* 19, 1327–1353.

Appendix 3.1 CM1P3 models

Details of the 13 CMIP3 models from IPCC-AR4 used to make projections for the main features of the tropical Pacific Ocean, as shown below. **Vertical coordinate (VC):** RHO = isopycnal; H = hybrid; Z = depth. **Mixing parameterisation (MP):** GM (Gent and McWilliams 1990)[198]; GM* (Griffies 1998)[199] implementation of GM; BL (Bryan and Lewis 1979)[200] depth varying vertical mixing; PP (Pacanowski and Philander 1981)[201] vertical eddy viscosity and diffusion; NK (Noh and Kim 1999)[202] vertical diffusion and viscosity; EVD = convective mixing parameterisation; TKE (Blanke and Delecluse 1993)[203]; V (Visbeck et al. 1997)[204] controls eddy-induced transport coefficient; KT = Kraus-Turner, wind-generated turbulent kinetic energy; KPP = mixed-layer scheme (Large et al. 1994)[205]. **Bottom boundary layer (BBL):** BBL-NS (Nakano and Suginohara 2002)[206]; BBL-BD (Beckmann and Doscher 1997)[207]; NO-BBL. **Flux correction (FC):** N = none; H = heat; F = fresh water; M = momentum. **Forcing (anthropogenic):** ALL = greenhouse gases, ozone, and sulfate aerosols; -O = no anthropogenic ozone. Further details and references are available at PCMDI website (www.pcmdi.llnl.gov)

Model	Oceanic model	Oceanic resolution	VC	MP	Atmospheric resolution	FC	Forcing	Reference
BCCR BCM2.0	MICOM2.8	1.5° x 1.5°(0.5°) L35	RHO	KT, KPP	T63 L31	N	ALL -O	208
CNRM CM3	OPA8.1	2°(0.5°) x 2° L31	Z	GM, TKE	T63 L45	N	ALL -O	209
CSIRO Mk3.0	MOM2.2	0.84° x 1.875° L31	Z	GM*, BL, PP	T63 L18	N	-	210
CSIRO Mk3.5	MOM2.2	0.84° x 1.875° L31	Z	GM*, BL, PP, V, KT	T63 L18	N	-	210
GFDL CM2.0	OM3P4	1°(1/3°) x 1° L50	Z	GM*, BL, BBL-BD, KPP	2.5° x 2° L24	N	ALL	211
IPSL CM4	OPA	2° x 2° (1°) L31	Z	GM, BBL-BD, EVD, TKE	2.5° x 3.75° L19	N	ALL -O	212
MIROC Medres	COCO3.3	1.4°(0.5°) x 1.4° L43	H	GM, NK, BBL-NS, EVD	T42 (2.81° x 2.81°) L20	N	ALL	213
MIROC Hires	COCO3.3	0.19° x 0.28° L47	H	GM, NK, BBL-NS, EVD	T106 (1.12° x 1.12°) L56	N	ALL	213
MIUB ECHO-G	HOPE-G	2.8° x 2.8° (0.5°) L20	Z	PP, EVD	T30 (3.75° x 3.75°) L19	HF	ALL	214
MRI CGCM2.3	Bryan-Cox	2.0°(0.5°) x 2.5° L23	Z	GM	T42 L30	HFM	ALL-O	215
NCAR CCSM3	POP	1.1°(0.27°) x 1.1° L40	Z	GM, KPP, NO-BBL	T85 L26	N	ALL	216
NCAR PCM1	POP	2/3°(0.5°) x 2/3° L32	Z	GM, KPP, NO-BBL	T42 L18	N	ALL	217
UKMet HadCM3	Bryan-Cox	1.25° x 1.25° L20	Z	GM*, V, KT, PP	2.75° x 3.75°L19	N	ALL	218, 219

SPC
Secretariat of the Pacific Community

Vulnerability of Tropical Pacific Fisheries and Aquaculture to Climate Change

Edited by Johann D Bell, Johanna E Johnson and Alistair J Hobday

Vulnerability of Tropical Pacific Fisheries and Aquaculture to Climate Change

Edited by Johann D Bell, Johanna E Johnson and Alistair J Hobday

SPC
Secretariat
of the Pacific
Community

© Copyright Secretariat of the Pacific Community 2011

All rights for commercial/for profit reproduction or translation, in any form, reserved. SPC authorises the partial reproduction or translation of this material for scientific, educational or research purposes, provided that SPC and the source document are properly acknowledged. Permission to reproduce the document and/or translate in whole, in any form, whether for commercial/for profit or non-profit purposes, must be requested in writing. Original SPC artwork may not be altered or separately published without permission.

The copyright for individual chapters is held by the respective authors or the institutions to which they are affiliated.

The photographs in this book cannot be reproduced without the permission of the individual photographers or photographic agencies credited.

Original text: English

Secretariat of the Pacific Community Cataloguing-in-publication data

Vulnerability of Tropical Pacific Fisheries and Aquaculture to Climate Change

1. Fishery management – Oceania. 2. Marine ecosystem management – Oceania. 3. Climatic changes – Oceania. 4. Aquaculture – Management – Oceania

I. Bell, Johann D. II. Johnson, Johanna E. III. Hobday, Alistair J. IV. Title. V. Secretariat of the Pacific Community.

639.20995 AACR2
ISBN: 978-982-00-0471-9

Please cite this publication as:

Bell JD, Johnson JE and Hobday AJ (eds) (2011) Vulnerability of Tropical Pacific Fisheries and Aquaculture to Climate Change. Secretariat of the Pacific Community, Noumea, New Caledonia.

Please cite individual chapters as (e.g.):

Lough JM, Meehl GA and Salinger MJ (2011) Observed and projected changes in surface climate of the tropical Pacific. In: JD Bell, JE Johnson and AJ Hobday (eds) Vulnerability of Tropical Pacific Fisheries and Aquaculture to Climate Change. Secretariat of the Pacific Community, Noumea, New Caledonia.

Cover photo: Wave breaking over a coral reef at Wallis Island by Franck Mazeas. Cover design and layout by Carla Appel.

The views expressed in this publication do not necessarily reflect those of the Secretariat of the Pacific Community or other participating organisations. This publication has been made possible in large part by funding from the Australian Agency for International Development (AusAID).

Published by the Secretariat of the Pacific Community, Noumea, New Caledonia
BP D5, 98848 Noumea Cedex, New Caledonia
(Email: spc@spc.int)

Also available at http://www.spc.int/climate-change/fisheries/assessment

Printed in New Zealand by Stredder Print Ltd, Auckland, 2011